ELECTROCHEMISTRY OF PORPHYRINOIDS AND TETRAPYRROLE TRIPLE-DECKER COMPLEXES

A Dissertation Presented to

the Faculty of the Department of Chemistry

University of Houston

In Partial Fulfillment

of the Requirements for the Degree

Doctor of Philosophy

By

Xiaoqin Jiang

December 2016

ELECTROCHEMISTRY OF PORPHYRINOIDS AND TETRAPYRROLE TRIPLE-DECKER COMPLEXES

Xiaoqin Jiang

APPROVED:

Dr. Karl M. Kadish

Dr. Roman S. Czernuszewicz

Dr. Steven Baldelli

Dr. Arnold Guloy

Dr. James Briggs

Dean, College of Natural Sciences and Mathematics

ACKNOWLEDGEMENTS

First and foremost I would like to express my deepest appreciation to my advisor, Dr. Karl M. Kadish. It has been a great honor for me to be his Ph.D. student and have the opportunity to work with such a passionate, knowledgeable and intelligent researcher, a wise and inspiring guide, and a kind and helping friend. He has taught me, both consciously and unconsciously, to come up with innovative and courageous thinking and to pursue scientific professionalism through continuous hard work. I appreciate his contribution of time, ideas and funding to make my Ph.D. experience productive and stimulating. The joy and enthusiasm Dr. Kadish has for research was always motivational for me during my study.

I also want to thank all members of the Dr. Kadish's research group, which have contributed immensely to my personal and professional growth at UH. The group has been a source of friendship as well as a source of good advice and collaboration. Special thanks are to Dr. Zhongping Ou, Dr. John L. Bear and Dr. Eric Van Caemelbecke, for giving me invaluable advice on my research and career. Moreover, I am grateful to all of my scientific collaborators for providing me with interesting-to-study compounds and giving me constructive suggestions; they are Dr. Roger Guilard, Dr. Claude P. Gros and Dr. Teoder Silviu Balaban from France, Dr. Yulia Gorbunova and Dr. Alla Bessmertnykh-Lemeune from Russia, Dr. Hong Wang from North Texas University in US and Dr. Guifen Lu from Jiangsu University in China. My sincere thanks also go to all of the committee members, which are Dr. Roman Czernuszewicz, Dr. Steven Baldelli, Dr. Arnold Guloy and Dr. James M. Briggs, for providing me with their valuable time and constructive comments. Support provided by the Robert A. Welch Foundation is also gratefully acknowledged.

Lastly, I want to give my deepest love and gratitude to my parents, Xicai Jiang and Yinlian Chen, who were always there for me with their strongest love and support, and who gave me the freedom to pursue what I am passionate about. Thank you!

ELECTROCHEMISTRY OF PORPHYRINOIDS AND TETRAPYRROLE TRIPLE-DECKER COMPLEXES

A Dissertation Presented to

the Faculty of the Department of Chemistry

University of Houston

In Partial Fulfillment

of the Requirements for the Degree

Doctor of Philosophy

By

Xiaoqin Jiang

December 2016

ABSTRACT

This dissertation describes the electrochemistry and spectroelectrochemistry of porphyrinoids and tetrapyrrole triple-decker complexes, which were examined in nonaqueous media using electrochemical techniques in combination with spectroelectrochemical analysis as a function of the central metal ions, the axial ligands, the π-conjugated macrocycles, the peripheral substituents as well as solution conditions. Examined macrocyclic compounds in this dissertation are (i) *meso*-nitrophenyl metalloporphyrins; (ii) *meso*-diphosphorylated metalloporphyrins; (iii) unsymmetrical mono-benzoporphyrins; (iv) push-pull *opp*-dibenzoporphyrins; (v) phthalocyanine-corrole and phthalocyanine-porphyrin triple-decker complexes.

In addition to two ring-centered reductions and two ring-centered oxidations, the *meso*-nitrophenyl metalloporphyrins exhibit reductions of the electroactive NO_2Ph groups with a first reversible one-electron-addition followed by one or more irreversible reductions at more negative potentials. The *meso*-diphosphrylated porphyrins exhibit a slow chemical reaction after the second ring-centered reduction, forming a redox-active phlorin anion which can either be re-oxidized back to the initial porphyrin or be further reduced to form the phlorin dianion. The β, β'-fused mono-benzoporphyrin and *opp*-dibenzoporphyrin possess smaller HOMO-LUMO gaps and red-shifted and broadened absorption bands compared to those of the corresponding non-benzo porphyrin derivatives, due to the extension of the π-system. The Pc-M-Cor-M-Pc triple-decker complexes bearing nitrophenyl groups on the corrole unit exhibit 5 oxidations and 3-5 reductions depending on the number of the redox-active NO_2Ph groups. However, the Pc-M-Pc-M-Por triple-deckers exhibit 4 oxidations and 3 reductions with the first oxidation and the first reduction both being assigned as a one-electron-transfer process on the Pc macrocycle.

Table of Contents

List of Abbreviations

Abbreviation	Meaning
A	absorbance
CE	counter electrode
CH_2Cl_2	dichloromethane
CV	cyclic voltammetry
DMF	N, N-dimethylformamide
DMSO	dimethylsulfoxide
$\Delta E_{1/2}$	difference in half-wave potential
$E_{1/2}$	half-wave potential
E_p	peak potential (by cyclic voltammetry)
E_{pa}	anodic peak potential (by cyclic voltammetry)
E_{pc}	cathodic peak potential (by cyclic voltammetry)
ε	molar absorptivity
ESR	electron spin resonance
FTIR	Fourier transform infrared
HOMO	highest occupied molecular orbital
i_{pa}	anodic peak current (by cyclic voltammetry)
i_{pc}	cathodic peak current (by cyclic voltammetry)
LUMO	lowest unoccupied molecular orbital
λ_{max}	wavelength at a specific peak maximum
OEP	2,3,7,8,12,13,17,18-octaethylporphyrin dianion
Py	pyridine
PhCN	benzonitrile
RE	reference electrode
SCE	saturated calomel electrode
TBAP	tetra-*n*-butylammonium perchlorate
TMP	trimestiyltetraphenylporphyrin dianion
TFA	trifluoroacetic acid
TPP	5,10,15,20-tetraphenylporphyrin dianion
WE	working electrode

List of Schemes and Charts

List of Figures

List of Tables

CHAPTER ONE

Introduction

1.1 General Introduction and Scope of this Dissertation

The main long-term research interest of our laboratory has focused on the areas of electrochemistry, spectroelectrochemistry, electrosynthesis and electrochemical reactivity of porphyrins, corroles, phthalocyanines and related macrocycles with different central metal ions. The overall goal was to study the redox properties and electron transfer mechanism of complexes with multiple redox centers, through electrochemical characterization of redox reactions, followed by assignment of site of electron transfer via spectroscopic data or electrochemical criteria, or alternatively through comparisons with the known chemistry and electrochemistry of known systems.

The projects in this dissertation are in line with this interest and multiple related chemical systems were selected and studied, with results described on the following pages. Chapter One provides a general introduction of the investigated compounds, while detailed experimental techniques and methodologies are presented in Chapter Two. Chapters Three and Four focus on porphyrins bearing functional substituents at the *meso* positions of the macrocycle. While Chapters Five and Six report electrochemical studies on the mono- and di-benzoporphyrins with benzo-fusion at the β,β'-pyrrole position. Finally, the redox properties of two types of heteroleptic triple-decker complexes, phthalocyanine-corrole and phthalocyanine-porphyrin sandwiches are described in Chapter Seven and Chapter Eight, respectively.

The electrochemical and spectroscopic data of each chemical system are analyzed as a function of: (1) the nature of the conjugated macrocycles (type and planarity), (2) type and oxidation sate of the central metal ions, (3) type and number of axially ligands, (4) type, number and position of the peripheral substituents o and (5) solution conditions; while also providing supplementary information for applications in the area of chemical catalysis, molecular devices, electrochemical sensors and agents for use in photodynamic therapy.[1]

1.2 Porphyrins

Porphyrins are a class of naturally occurring macrocyclic compounds, which play important roles in various biological processes, including cell respiration, oxygen transport, fatty acid oxidation and light harvesting.[2,3] The study of synthetic porphyrins has gained particular interest due to their potential applications in areas such as catalysis,[4] optical sensors,[5] electronic devices,[6] supramolecular systems,[7] photovoltaic cells,[8] solar energy conversion[9] and photodynamic therapy.[10]

The core structure of a porphyrin consists of four pyrrole units inter-connected by four methane bridges, forming a 16-atom, 18-elctron conjugated p-system (see Figure 1-1). The peripheral of the macrocycle can be substituted by electron-donating groups (EDGs) or electron-withdrawing groups (EWGs) at the *meso* and/or β-pyrrole positions (see labelling system in Figure 1-1a), giving a variety of functional porphyrin derivatives.

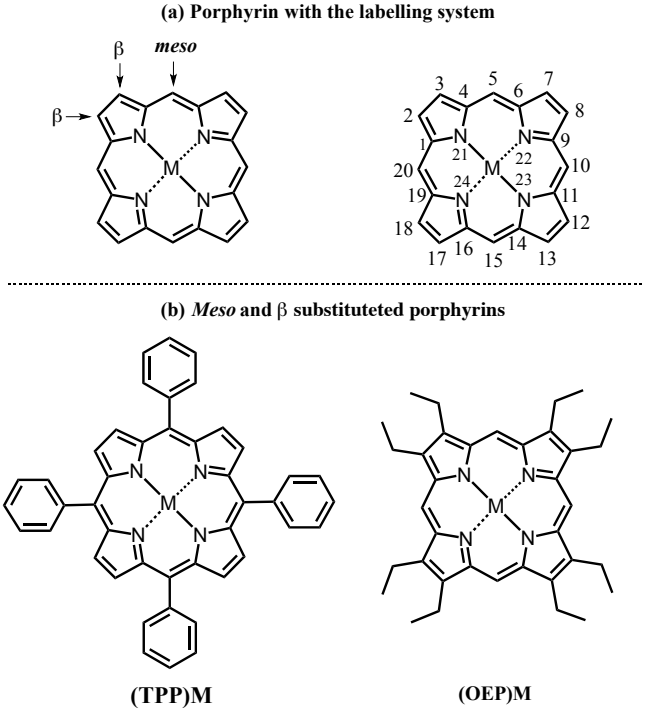

Figure 1-1. Core structure of (a) porphyrin with the labeling system and (b) representative synthetic porphyrins: tetraphenylporphyrin **(TPP)M** and octaethylporphyrin **(OEP)M**.

The best-known porphyrin derivatives are tetraphenylporphyrin (TPP) and octaethylporphyrin (OEP) (see Figure 1-1b). Compounds in these two series of macrocycles have been widely investigated over the last forty years and have long served as reference compounds against which the physiochemical data of newly synthesized metalloporphyrins have been compared.[1, 11-14]

In general, metalloporphyrins containing the OEP or TPP macrocycles can undergo two stepwise ring-centered reductions to give porphyrin π-anion radicals and dianions. The porphyrins can also be oxidized at the conjugated macrocycle by two electrons in nonaqueous media to give π-cation radicals and dications.[1] The potential difference between the first ring-centered oxidation and the first ring-centered reduction (the HOMO-LUMO gap) averages 2.25 ± 0.15 V;[1] in addition, the difference in potential between the first and second reductions of the macrocycle was reported to average 0.29 ± 0.05 V. This result has often been used as an electrochemical "diagnostic criteria" to distinguish between metal-centered and ring-centered reactions of metalloporphyrins.[1] Large deviations from these values have often been used to suggest an electrode reaction which involves the electroactive parts of the molecule other than the conjugated macrocycle. These electroactive parts could be the central metal ion, like in the case of Co, Fe, Ag or Cr derivative,[15,16] or it would be redox-active coordinated axial ligands or redox-active peripheral substituents.[1] The electrochemistry of metalloporphyrins in nonaqueous media have been reported by Kadish and coworkers in Chapters 55 of the Porphyrin Handbook with redox potentials summarized in Chapter 59 of the same Handbook series.[14]

1.3 π-Extended Porphyrins

Porphyrins fused with aromatic units have recently emerged as a hot topic of research, due in part to their unique photophysical and electronic properties. In particular, π-extended porphyrins in which one or more aromatic rings are fused to the porphyrin periphery at the β,

β'-positions (see Figure 1-2), have attracted much attention owing to their unique combination of photophysical, optoelectronic, and physiochemical properties, and their potential applications in various areas such as electronics, optic electronics and photomedicines.[17-25]

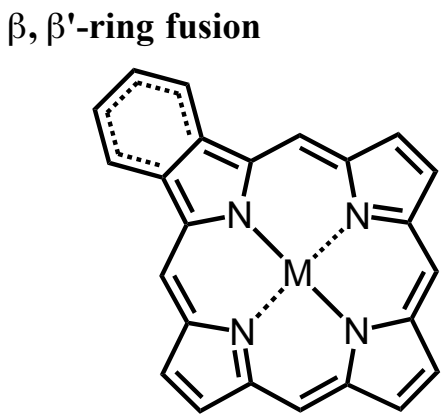

Figure 1-2. Porphyrin ring extension through β, β'-fusion.

In general, benzoporphyrins have a UV-vis absorption spectrum similar to porphyrins; however, as the π-conjugation increases upon going from a porphyrin to benzoporphyrin, the lowest energy Q_{00} transitions increase in intensity and decrease in frequency; thus benzoporphyrins possess a more intense and red-shifted Q-band absorption (600-750 nm) as compared to that of the corresponding non-π-extended porphyrins and the magnitude of the shift in wavelength (nm) depending on the number of the fused benzene rings on the macrocycle.[24, 26-28] This property, coupled with the fact that benzoporphyrins are good single oxygen generators, makes these molecules and analogous compounds of interest with respect to their use in therapeutic applications.[29]

The electrochemical properties of benzoporphyrins are also affected by an extension of the π-ring system. Similar to porphyrins, benzoporphyrins can also undergo two ring-centered reductions and two ring-centered oxidations. However, the first oxidation of a benzoporphyrin is easier (more positive potential) than a non-π-extended porphyrin due to destabilization of the macrocycle-localized HOMO by a fusion of the macrocycle with external

aromatic rings. At the same time, the half-wave potentials for the first reduction of the two compounds are virtually the same and this results in a smaller HOMO-LUMO gap for the benzoporphyrins. [1, 28, 30]

Part of the focus in this dissertation is on the electrochemical and optical properties of unsymmetrically functionalized mono-benzoporphyrins which are expected to display different electronic and photo-physical properties from their symmetrical counterparts due to a splitting of the frontier orbitals and another is on push-pull dibenzoporphyrins with functionalized substituents at the fused benzene ring compound, which demonstrates huge potentials in dye-sensitized solar-cells (DSSCs).

The structures of these two types of benzoporphyrins are shown in Figure 1-3.

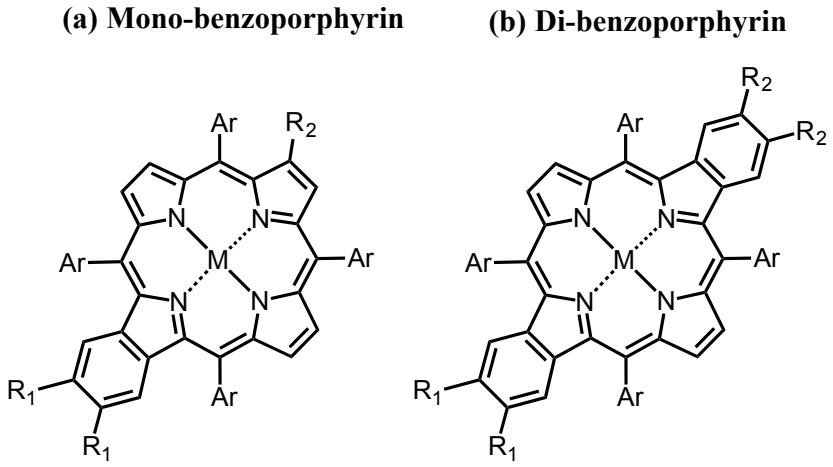

Figure 1-3. Core structure of (a) unsymmetrically functionalized mono-benzoporphyrin and (b) *opp*-dibenzoporphyrin.

1.4 Corroles

Corroles are a class of synthetic tetrapyrrolic macrocycles in the porphyrinoid family. The first synthesis of a corrole was reported in 1965,[31] five years after the macrocycle was introduced by Johnson and Price in 1960 as a tetrahydrocorrin.[32] Corroles (see structures in Figure 1-4) have been closely identified with porphyrins over the last 50 years, with comparisons made to their chemical, electrochemical and spectroscopic properties.

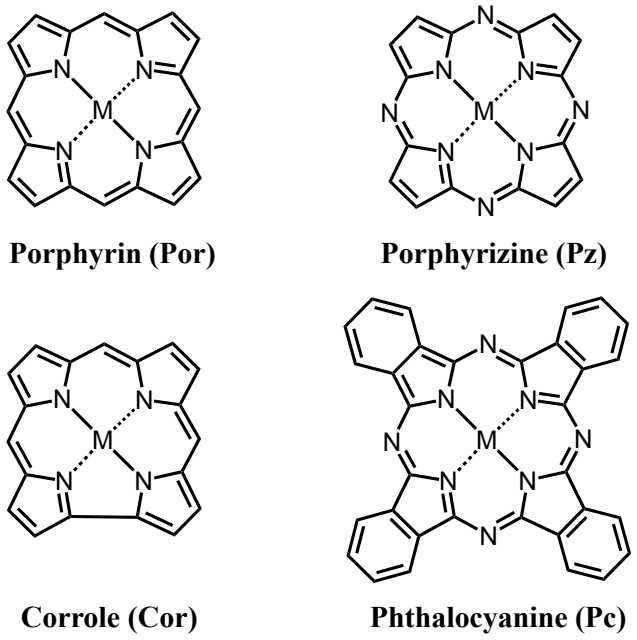

Figure 1-4. Core structure of a porphyrin, porphyrazine, corrole and phthalocyanine.

The structure of a corrole is closely related to that of a porphyrin in that both macrocycles have an 18 π-electron aromatic system (see Figure 1-4), but a direct carbon-carbon bond between two pyrroles in the corrole leads to a smaller cavity size and also to a reduced symmetry than in the case of porphyrins.[33] The lack of the C-20 carbon atom also causes the corrole macrocycle to be trivalent as compared to divalent in that of porphyrins,[33] which enables this macrocycle to stabilize the central metal ion in a higher oxidation state than for the same metal ions incorporate into a porphyrin; the ability of corroles to induce a facile ligand-to-metal electron transfer leads them to generally behave as a "non-innocent" ligand.[34-36] The above unique properties of corroles lead them to be diversely used in areas of chemical sensors, catalysts, solar cells and medicine.[37-40]

Many similarities exists between the redox properties of metallocorroles and metalloporphyrins but there are also many differences due, in part, to the different changes of the two conjugated macrocycles and the non-innocence of the corrole ligand in a variety of

compounds. Because the corrole macrocycle is trivalent,[41] metallocorroles are much harder to reduce and easier to oxidize than the corresponding metalloporphyrins where the ring is divalent.[29, 38] Corroles can undergo up to three ring-centered one-electron oxidations to stepwise produce a corrole π-cation radical, dication and trication; this compares with the analogous porphyrins which can only undergo two ring-centered oxidations.[1] However, due to the increased electron density on the corrole macrocycle, normally only one ring-centered reduction is observed for many metallocorroles in nonaqueous media, and this usually occurs at potentials close to the negative potential limit of the nonaqueous solvent. For an example, $E_{1/2}$ = -1.74 V for (OEC)Sn^{IV}(Ph)[42] and $E_{1/2}$ = -1.58 V (vs SCE) for (OEC)Mn^{III} in PhCN.[43]

The electronic absorption spectrum of a corrole is very similar to that of the analogous porphyrin due to the structural similarity of the two macrocycles. Both macrocycles exhibit an intense Soret band around 400 nm and one or two Q-bands at 500-650 nm. However, the molar absorptivity for the intense Soret band of a metallocorrole is much smaller than in the case of a metalloporphyrin with smaller ring substituents.[44] The spectral features of metallocorroles and metalloporphyrins both depend on the central metal ions and its oxidation state, on the presence of absence of any coordinating axial ligands and specific peripheral electron-withdrawing or electron-donating groups on the macrocycle.

1.5 Phthalocyanines

Metallophthalocyanines, like metalloporphyrins, are well known for their intense color and high thermal stability.[45-47] Moreover, the optical and redox properties of phthalocyanines can be tuned by changing the central metal ions and/or substituents at the peripheral and/or axial positions of the macrocycle.[47, 48] Owing to their increased stability, unique photophysical characteristics, diverse coordination properties and architectural flexibility, these synthetic porphyrin analogues have surpassed porphyrins in diverse fields[45] such as photosensitizers in photodynamic therapy, red or near-infrared light absorbers in optical data storage systems, photoconductors, electrochromic devices, artificial photosynthesis and solar cells;[49] additional

applications include the use of these compounds as analytical (sensor) devices in industrial, environmental or medical areas.[8, 50]

Most applications of M(Pc) species rely critically on their spectroscopic and electrochemical properties. Phthalocyanines are a class of porphyrazine macrocycles with fused benzene rings at the β,β' position of the macrocycle (see structures in Figure 1-4). The extended π-system of phthalocyanines leads to an absorption spectrum with an intense Q-band between 620-700 nm and a weak Soret band near 350 nm; the Soret band of a Pc is much broader and less intense than that in a porphyrin. [49, 51]

The electrochemistry of phthalocyanines has been widely investigated, with their redox properties being summarized in reviews by L'Her and Pondaven[49] and Lever and Leznoff.[52] Monomeric phthalocyanines may be electroxidized in two steps or electroreduced in four steps, each of which is a one-electron-transfer process at the macrocycle. The average HOMO-LUMO gap of phthalocyanines is around 1.6 V,[49] which is smaller than that of porphyrins with TPP or OEP macrocycles (2.25 ± 0.15 V).[1]

The specific redox reactivity and electron transfer mechanism of the phthalocyanine macrocycle may be changed by insertion of redox-active central metal ions, the coordination of axial ligands or the addition of substituents on the periphery of the macrocycle.[49,52] For example, PcZn is reduced at -0.86, -1.30 V (vs. SCE) within the reduction limit of DMF, while $(CN)_6$PcZN can undergo four reductions at -0.15, -0.59, -1.10 and -1.35 V (vs. SCE) in the same solution condition. This is because the eight strong electron-withdrawing CN groups on the macrocycle make the reduction much easier to be observed within the -2.0 V negative limit.[53]

In this dissertation, two Pc macrocycles and one corrole macrocycle are linked by two lanthanide ions to form a triple-decker sandwich complex of the type shown in Figure 1-5. These types of compounds display multiple redox reactions and unique electron absorption

spectra. The electrochemical and spectroscopic properties for this series of compounds are elucidated in Chapter Seven.

1.6 Triple-decker Complexes Containing Phthalocyanine-Corrole or Phthalocyanine-Porphyrin Macrocycles

Tetrapyrrole derivatives such as porphyrins and phthalocyanines, which contain four pyrrole or isoindole nitrogen atoms, are able to complex with most metal ions. Sandwich-type complexes are represented by the double- (A) and triple-decker (B) compounds shown in Figure 1-5.[54-57] They have large metal centers that favor octa-coordination (e.g. rate earth, actinides, group 4 transition metals and several main group elements such as Sn, As, Sb and Bi).

Sandwich-type rare earth complexes represent a unique class of compounds. Apart from their double- and triple-decker structures, these compounds display tunable electron and optical properties and π-π interactions, which have found important applications in material science, such as field effect transistors,[58] molecular magnets,[59] molecular-based multibit information storage materials,[60] and receptors for metal ions, dicarboxylic acids, or saccharides.[61] Early work in this field has focused mainly on the homoleptic unsubstituted phthalocyanine and porphyrin complexes. In the last decade, substantial progress has been made in the area of synthesis and several new synthetic pathways have been developed for the preparation of these compounds. The increasing accessibility of these compounds in large quantities has opened up a way to more easily explore their photophysical properties and applications.

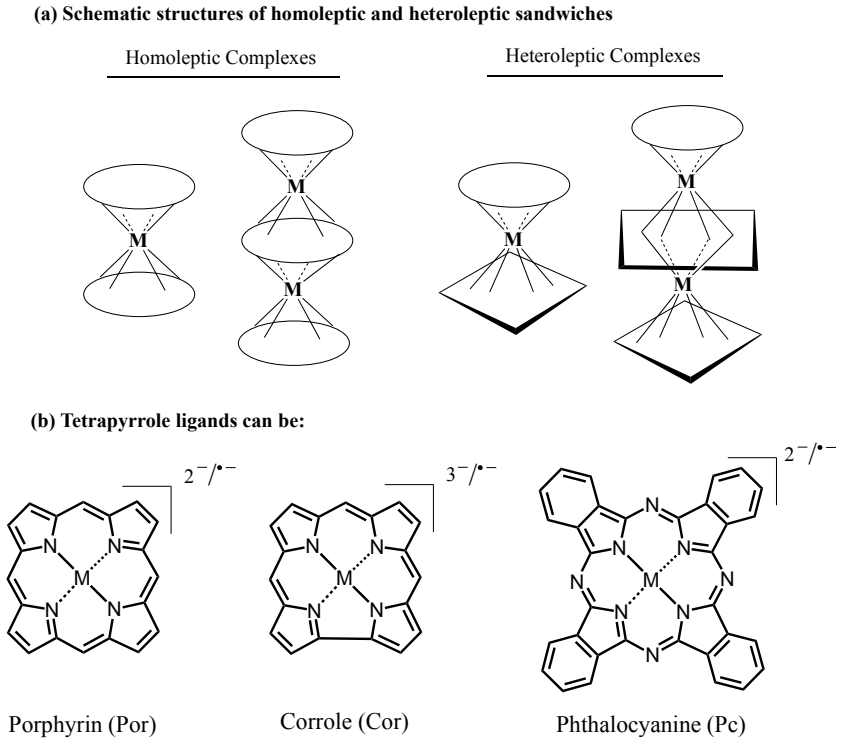

Figure 1-5. Schematic structures of homoleptic and heteroleptic sandwich complexes with tetrapyrrole ligand. Figure is adapted from Ref. 57 with the giving of the tetrapyrrole ligands.

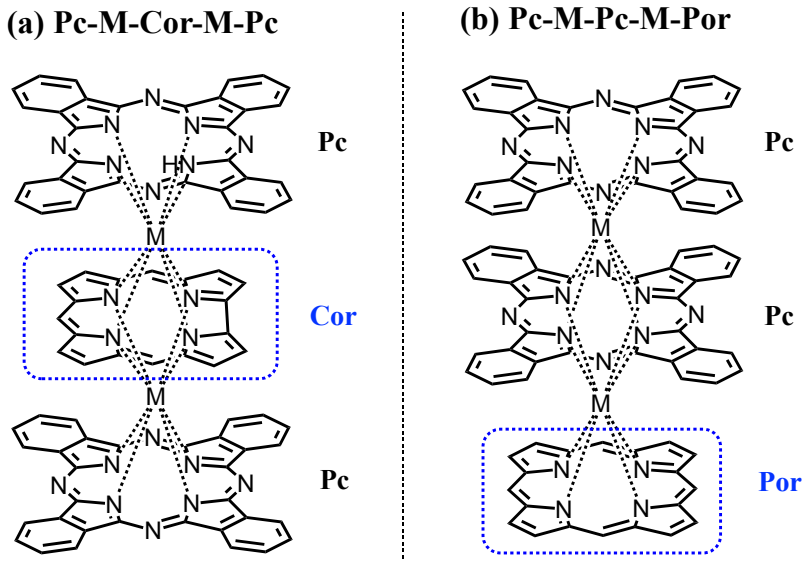

Figure 1-6. Structures of two types of triple-decker complexes: (a) Pc-M-Cor-M-Pc, (b) Pc-M-Pc-M-Por.

1.7 References

(1) Kadish, K. M.; Royal, G.; Van Caemelbecke, E.; Gueletti, L. In *The Porphyrin Handbook*, Kadish, K. M.; Smith, K. M.; Guilard, R. Eds., Academic Press: San Diego, **2000**; Vol. 8, 1-114.

(2) Drain, C. M.; Varotto, A.; Radivojevic, I. *Chem. Rev.* **2009**, *109*, 1630-1658.

(3) Milgrom, L. R. *The Colors of Life: an Introduction to the Chemistry of Porphyrins and Related Compounds.* Oxford University Press, London **1997**.

(4) Che, C. M.; Lo, V.; K. Y.;Zhou, C, Y.; Huang, J. S. *Chem. Soc. Rev.* **2011**, *40*, 1950-1975.

(5) Stich, M. I. J.; Fischer, L. H.; Wolfbeis, O. S. *Chem. Soc. Rev.* **2010***, 39,* 3102-3114.

(6) Senge, M. O.; Fazekas, M.; Nataras, E. G. A.; Blau, W. J.; Zawadzka, M.; Locos, O. B.; Mhuicheartaigh, E. M. N. *Adv. Mater.* **2007**, *19*, 2737-2774.

(7) Drain, C. M.; Russell, K. C.; Lehn, J. M. *Chem. Commun.* **1996**, *3*, 337-339.

(8) Walter, M. G.; Rudine, A. B.; Wamser, C. C. *J. Porphyrins Phthalocyanines* **2010**, *14*, 759-792.

(9) Guldi, D. M. *Chem. Soc. Rev.* **2002**, *31*, 22-36.

(10) Kadish, K. M.; Smith, K. M.; Guilard, R. *The Porpyrin Handbook*. Academic Press: San Diego, **2000**; Vol. 6, 1-346.

(11) Kadish, K. M.;Smith, K. M.; Guilard, R. In *The Porphyrin Handbook*, Academic Press: San Diego, **2000**, Vol. 1-10.

(12) Kadish, K. M.;Smith, K. M.; Guilard, R. In *The Porphyrin Handbook*, Academic Press: San Diego, 2000, Vol. 11-20.

(13) Dolphin, D. *The Porphyrins,* Academic Press: New York, **1978**,Vol. 1-17.

(14) Kadish, K. M.;Smith, K. M.; Guilard, R. In *The Porphyrin Handbook*, Academic Press: San Diego, **2000**, Vol. 9.

(15) Furhop, J. H.; Kadish, K. M.; Davis, D. G. *JACS.* **1973**, *95*, 5140-5147.

(16) Kadish, K. M.; Davis, D. G.; Furhop, J. H. *Angew, Chem. Int. Ed.* **1972**, *11*,1014-1016.

(17) Young, S. W.; Qing, F.; Harriman, A.; Sessler, J. L.; Dow, W. C.; Mody, T. D.; Hemmi, G. W.; Hao, Y.; Miller, R. A. *Proc. Natl. Acad. Sci.***1996***, 93,* 6610-6615.

(18) Lash, T. D.; *J. Porphyrins Phthalocyanines* **2001**, *5*, 267-288.

(19) Ongayi, O.; Gottumulkkala, V.; Fronczek, F. R.; Vicente, M. G. H. *Bioorg. & Med. Chem. Lett.* **2005**, *15*, 1665-1668.

(20) Smith, K. M.; Lee, S. H.; Vicente, M. G. H. *J. Porphyrins Phthalocyanines* **2005,** *9*, 769-778.

(21) Baluschev, S.; Yakutkin, V.; Miteva, T.; Avlasevich, Y.; Chernov, S.; Aleshchenkov, S.; Nelles, G.; Cheprakov, A.; Yasuda, A.; Muellen, K.; Wegner, G. *Angew. Chem.* **2007**, *46*, 7693-7696.

(22) Borek, C.; Hanson, K.; Djurovich, P. I.; Thompson, M. E.; Aznavour, K.; Bau, R.; Sun, Y.; Forrest, S. R.; Brooks, J.; Michalski, L.; Brown, J. *Angew. Chem.* **2007***, 46,* 1109-1112.

(23) Okujima, T.; Hashimoto, Y.; Jin, G.; Yamada, H.; Uno, H.; Ono, N. *Tetrahedron* **2008**, *64*, 2405-2411.

(24) Carvalho, C. M. B.; Brocksom, T. J.; Thiago de Oliveira, K. *Chem. Soc. Rev.* **2013,** *42,* 3302-3317.

(25) Mack, J.; Bunya, M.; Shimizu, Y.; Uoyama, H.; Komobuchi, N.; Okujima, T.; Uno, H.; Ito, S.; Stillman, M. J.; Ono, N.; Kobayashi, N. *Chem.-Eur. J.* **2008**, *14*, 5001-5020.

(26) Rogers, J. E.; Nguyen, K. A.; Hufnagle, D. C.; McLean, D. G.; Su, W.; Gossett, K. M.; Burke, A. R.; Vinogradov, S. A.; Pachter, R.; Fleitz, P. A. *J. Phys. Chem.: A* **2003**, *107*, 11331-11339.

(27) Kim, P.; Sung, J.; Uoyama, H.; Okujima, T.; Uno, H.; Kim, D. *J. Phys. Chem.: B* **2011**, *115*, 3784-3792.

(28) Chen, P.; Finikova, O. S.; Ou, Z.; Vinogradov, S. A.; Kadish, K. M. *Inorg. Chem.* **2012**, *51*, 6200-6210.

(29) Lash, T. D.; Syntheses of Noval Porphyrinoid Chromophores. In *The Porphyrin Handbook*, Kadish, K. M.; Smith, K. M.; Guilard, R., Eds. Academic Press: San Diego, **2000**; Vol. 2, 125-199.

(30) Ono, N.; Hironaga, H.; Ono, K.; Kaneko, S.; Murashima, T.; Ueda, T.; Tsukamura, C.;Ogawa, T. *J. Chem. Soc.* **1996**, 417-423.

(31) Johnson, A. W.; Kay, I.T. *J. Chem. Soc.* **1965**, 1620-1629.

(32) Johnson, A. W.; Price, R. *J. Chem. Soc.* **1960**, 1649-1653.

(33) Erben, C.; Will, S.; Kadish, K. M. Metallocorroles: Molecular Structure, Spectroscopy and Electronic States. In *The Porphyrin Handbook*, Kadish, K. M.; Smith, K. M.; Guilard, R., Eds.; Academic Press: San Diego, **2000**; Vol. 2, 233-300.

(34) Ghosh, A.; Steene, E. *J. Inorg. Biochem.* **2002**, *91*, 423-436.

(35) Thomas, K. E.; Vazquez-Lima, H.; Fang, Y.; Song, Y.; Gagnon, K. J.; Beavers, C. M.; Kadish, K. M.; Ghosh, A. *Chem.-Eur. J.* **2015**, *21*, 16839-16847.

(36) Norheim, H. K.; Capar, J.; Einrem, R. F.; Gagnon, K. J.; Beavers, C. M.; Vazquez-Lima, H.; Ghosh, A. *Dalton Trans.* **2016**, *45*, 681-689.

(37) Aviv, I.; Gross, Z. *Chem. Commun.* **2007**, *20*, 1987-1999.

(38) Aviv-Harel, I.; Gross, Z. *Chem.-Eur. J.* **2009**, *15*, 8382-8394.

(39) Aviv-Harel, I.; Gross, Z. *Coord. Chem. Rev.* **2011**, *255*, 717-736.

(40) Paolesse, R.; Di Natale, C.; Macagnano, A.; Sagone, F.; Scarselli, M. A.; Chiaradia, P.; Troitsky, V. I.; Berzina, T. S.; D'Amico, A. *Langmiur* **1999**, *15*, 1268-1274.

(41) Paolesse, R. Syntheses of Corroles. In *The Porphyrin Handbook*, Kadish, K. M.; Smith, K. M.; Guilard, R., Eds. Academic Press: San Diego, **2000**; Vol. 2, 201-232.

(42) Shen, D.-M.; Liu, C.; Chen, Q.; *J. Org. Chem.* **2006**, *71*, 6508-6511.

(43) Kadish, K. M.; Erben, C.; Ou, Z.; Adamian, V. A.; Will, S.; Vogel, E. *Inorg. Chem.* **2000**, *39*, 3312-3319.

(44) Kadish, K. M.; Shao, J.; Ou, Z.; Zhan, R.; Burdet, F.; Barbe, J. M.; Gros, C. P.; Guilard, R. *Inorg. Chem.* **2005**, *44*, 9023-9038.

(45) Kadish, K. M.; Smith, K. M.; Guilard, R. In *The Porpyrin Handbook*. Academic Press: San Diego, **2003**; Vol. 15-20.

(46) Rio, Y.; Rodriguez-Morgade, M. S.; Torres, T. *Org. Biomol. Chem.* **2008**, *6*, 1877-1894.

(47) Nemykin, V. N.; Lukyanets, E. A. In *The Porphyrin Handbook*, Kadish, K. M.; Smith, K. M.; Guilard, R., Eds. Academic Press: Singapore, **2010**; Vol. 3, 1-323.

(48) Li, R.; Zhang, X.; Zhu, P.; Ng, D. K. P.; Kobayashi, N.; Jiang, J. *Inorg. Chem.* **2006***, 45,* 2327-2334.

(49) L'Her, M.; Pondaven, A. In *The Porphyrin Handbook*, Kadish, K. M.; Smith, K. M.; Guilard, R., Eds. Academic Press: San Diego, **2003**; Vol. 16, 117-169.

(50) Trogler, W. C. *Struct. Bonding* **2012**, *142*, 91-118.

(51) Rawling, T.; McDonagh, A. *Coord. Chem. Rev.* **2007**, *251*, 1128-1157.

(52) Lever, A. B. P.; Milaeva, E. R.; Speier, G. *Phthalocyanines* **1993**, *3*, 5-69.

(53) Giraudeau, A.; Louati, A.; Gross, M.; Andre, J. J.; Simon, J.; Su, C. H.; Kadish, K. M. *JACS.* **1983**, *105*, 2917-2919.

(54) Ng, D. K. P.; Jiang, J. *Chem. Soc. Rev.***1997**, *26*, 433-442.

(55) Jiang, J.; Kasuga, K.; Arnold, D. P. In *Sandwich-type Phthalocyaninato and Porphyrinato Metal Complexes*, Academic Press: **2001**, 113-210.

(56) Jiang, J.; Bao, M.; Rintoul, L.; Arnold, D. P. *Coord. Chem. Rev.* **2006**, *250*, 424-448.

(57) Jiang, J.; Ng, D. K. P. *Acc. Chem. Res.* **2009**, *42*, 79-88.

(58) Chen, Y.; Su, W.; Bai, M.; Jiang, J.; Li, X.; Liu, Y.; Wang, L.; Wang, S. *J. Chem. Soc.* **2005**, *127*, 15700-15701.

(59) Ishikawa, N.;Sugita, M.; Wernsdorfer, W. *Angew. Chem.* **2005**, *44*, 2931-2935.

(60) Liu, Z.; Yasseri, A. A.; Lindsey, J. S.; Bocian, D. F. *Science* **2003**, *302*, 1543-1545.

(61) Takeuchi, M.; Ikeda, M.; Sugasaki, A.; Shinkai, S. *Acc. Chem. Res.* **2001**, *34*, 865-873.

CHAPTER TWO

Experimental Methods

2.1 Electrochemical Techniques

2.1.1 Cyclic Voltammetry

Cyclic voltammetry (CV) is now the most widely used method for measuring redox potentials of metalloporphyrins. The advantages of this technique are numerous when compared to the earlier techniques of potentiometry and polarography. First, the potential of a redox couple may be rapidly determined from the current-voltage curve. Secondly, the chemical stability of the electrogenerated species may be ascertained by reversing the potential sweep and observing the electrode reaction of the product. Furthermore, in the case of the coupled chemical reaction(s), a variation of the potential sweep rate and measurement of the new current-voltage curve might enable determination of the type of the coupled chemical reactions and the mechanism of electron transfer. This has been discussed in detail by Nicholson and Shain,[1] as well as Weissberger and Rossiter.[2] The standard heterogeneous electron-transfer rate constant can be estimated by measuring the difference in anodic and cathodic peak potentials as a function of the scan rate.[3]

The CV experiment involves applying a linearly increasing potential (Figure 2-1) to the working electrode (WE), while recording the resultant current flowing through the WE as a function of the applied potential. The corresponding current-voltage curve is known as a "cyclic voltammogram". The applied potential starts at a value, E_1, typically a potential chosen where the chemical species under investigation is not oxidized or reduced. The potential is then swept in a linear manner to a voltage, E_2, where the direction of the scan is reversed, usually to its original value (Cycle 1). The potential E_2 is normally selected so that the potential interval (E_2 - E_1) contains an oxidation or reduction process of interest. If the product of the electron transfer is not stable and a new chemical species is formed, then the reverse scan may be extended beyond E_1 so as to allow for further characterization of the reaction products and/or a second triangular potential sweep (Cycle 2) may be employed to learn more about the system and its electrochemical reactivity.

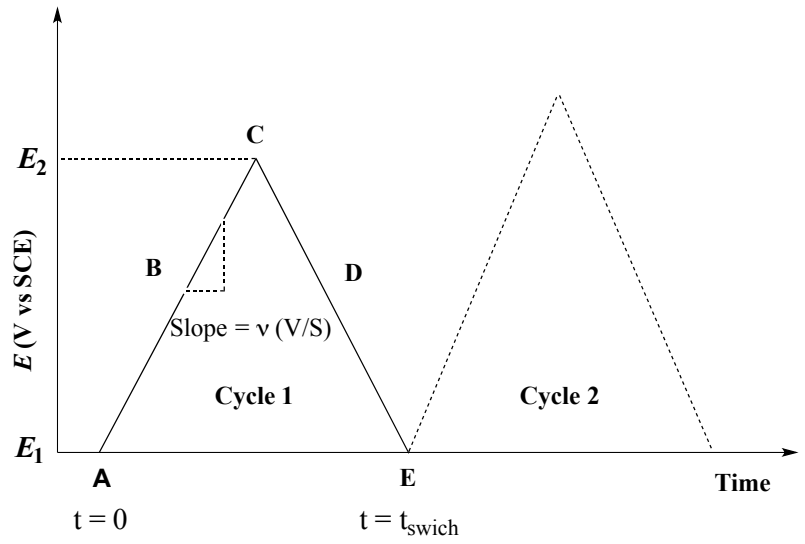

Figure 2-1. The potential waveform applied to the working electrode in a cyclic voltammetric experiment.

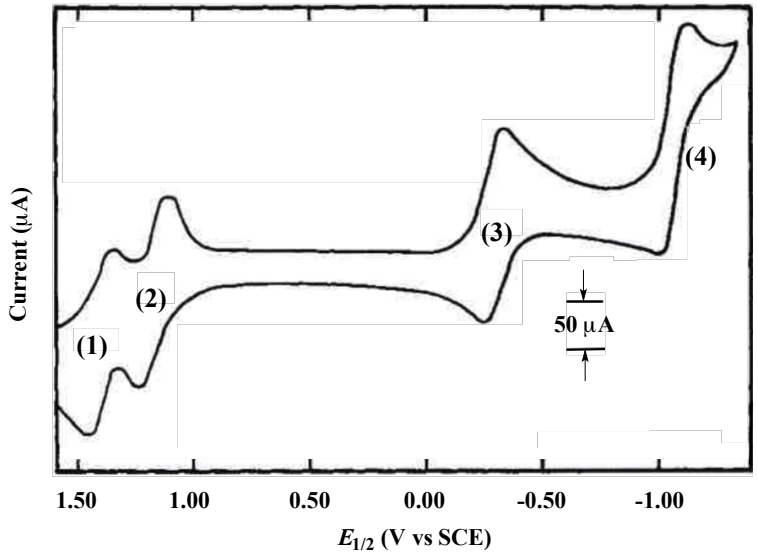

Figure 2-2. Cyclic voltammogram of TPPFeCl in CH_2Cl_2 containing 0.1 M TBAP. Figure adapted from Ref. 4. (1) and (2) oxidations and (3) and (4) are reductions.

Multiple electrode reactions may be seen on a given potential sweep between E_1 and E_2 and back to E_1 (from point A to C and then to E). An example of this is given in Figure 2-2, which illustrates the cyclic voltammogram of TPPFeCl in CH_2Cl_2 containing 0.1 M TBAP. Four sets of reduction and reoxidation peaks are observed; reaction (3) and (4) correspond to the

successive reduction of TPPFeCl and TPPFe, while reactions (2) and (1) are the stepwise oxidations of TPPFeCl via one-electron-transfer steps. To investigate each step of electron-transfer processes (for example, to observe the reductions), the potential is scanned first in a cathodic direction through the standard potential of the Fe(III)/Fe(II) couple (-0.29 V in this case), then reversed at some point between -0.5 V and -0.9 V in order to observed the backward reaction; then, in a second cathodic scan (in this case, to observe the 2nd reduction), the potential is swept even further (-1.50 V in this case) to observe the reduction of TPPFe/[TPPFe]$^-$ couple. For investigating each oxidation process, the potential is scanned in a similar manner.

There are several diagnostic criteria which must be considered when analyzing the current-voltage curves of the type shown in Figure 2-2. These include analysis of both the shaped and the position of the peak, as well as the maximum peak current with respect to the square root of the scan rate. A theoretical cyclic voltammogram for a reversible one-electron-transfer process is shown in Figure 2-3, where the half-wave potential $E_{1/2}$ can be obtained from Eq. 2-1 and are good to ±10 mV.

$$E_{1/2} = (E_{pa} + E_{pc})/2 \qquad (2\text{-}1)$$

Again, assuming that the electroreduction is reversible, the following relationships may be observed,

$$E_{pc} - E_{1/2} = -0.0285/n \text{ V} \qquad (2\text{-}2a)$$

$$E_{pc} - E_{1/2} = -0.0285/n \text{ V} \qquad (2\text{-}2b)$$

Combining Eq. (2-2a) and (2-2b) yields

$$\Delta E_p = E_{pa} - E_{pc} = 0.057/n \qquad (2\text{-}3)$$

Where n is the number of electrons transferred; in addition, the peak current, i_p, should increase with the square root of the scan rate, v, following the Randes-Sevick equation,

$$i_p = 2.69 \times 10^5 n^{3/2} A D^{1/2} v^{1/2} C \qquad (2\text{-}4)$$

Where i_p is the peak current in amperes, n is the number of electrons transferred, A the electrode area in cm^2, D the diffusion constant in cm^2/s, C the bulk concentration of the species in mol/cm^3, and v the scan rate in V/s.

In addition, if the diffusion coefficients of the oxidized and reduced species are equal, *i.e.,* $D_{ox} = D_{red}$, then the anodic current maximum i_{pa} will be equal to the cathodic current maximum i_{pc} and the ratio of i_{pa}/i_{pc} will be equal to 1.

Constancy of $i_p/v^{1/2}$ and a ratio of $i_{pa}/i_{pc} = 1$ indicates diffusion control and that there are no coupled chemical reactions at the scan rate investigated (that is, for the effective time of the experiment). Variation of the values of $i_p/v^{1/2}$ and i_{pa}/i_{pc} with scan rate can be used to prove nonreversible behavior and to probe any coupled chemical reactions which may occur on the time-scale of the experiment.[1]

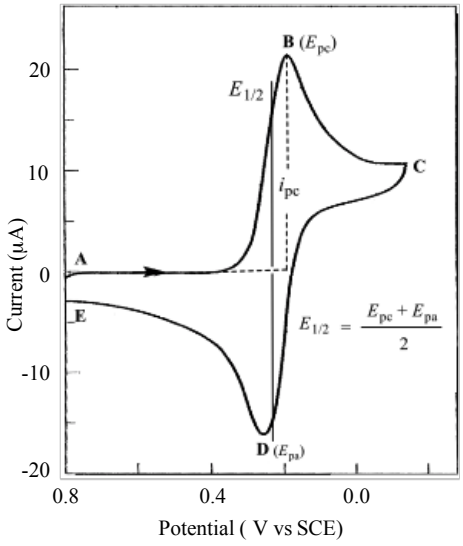

Figure 2-3. Typical current-voltage curve for a reversible one-electron-transfer reduction process. Figure adapted from Ref. 5 with the addition of labeling and equation.

2.1.2 Spectroelectrochemistry

Spectroelectrochemistry combines the technique of electrochemistry and spectroscopy in which *in-situ* generated products of redox reactions are monitored by spectroscopic methods as the reaction proceeds. In this dissertation, I mainly focus on using

thin-layer UV-vis spectroelectrochemistry coupled with routine electrochemical measurements as a powerful tool to analyze electrode reaction mechanisms or to identify intermediates which are formed during redox processes; IR, Raman and EPR spectroscopy can also be combined with electrochemistry,[6, 7] but these spectroelectrochemical techniques are not utilized in our thesis. An example of how the spectroscopic measurements can be obtained is given in Figures 2-4 and 2-5 for the reduction of TPPFeCl in DMSO. First the cyclic voltammogram of the investigated species is recorded in the thin-layer cell. This cyclic voltammogram is shown in Figure 2-4.

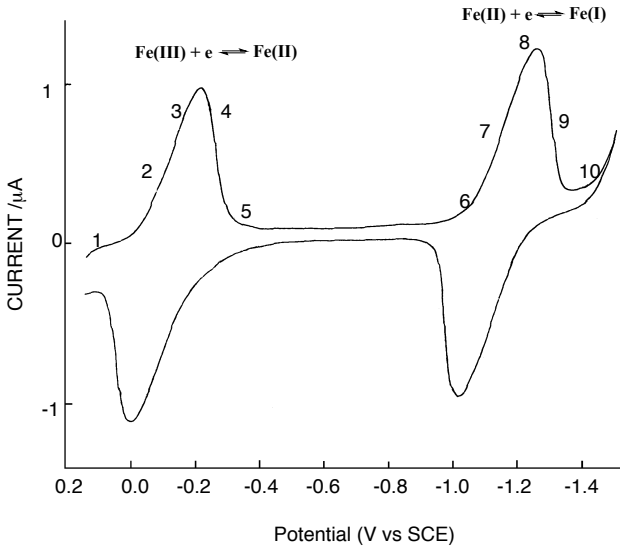

Figure 2-4. Thin-layer cyclic voltammogram of $TPPFeClO_4$ in DMSO, 0.1 M TBAP. Points correspond to potentials where spectra were obtained. Figure adapted from Ref. 4 with addition of labeling of reactions.

UV-vis spectra are taken at the potentials marked as 1 to 10 on the CV and the obtained spectra at each potential are shown in Figure 2-5. As seen in this figure, clean isosbestic points are obtained upon pasing from $[TPPFe(DMSO)_2]^+$ to $TPPFe(DMSO)_2$ (points 1 to 5) as well as from $TPPFe(DMSO)_2$ to $[TPPFe]^-$ (points 6 to 10). If the reaction is reversible, identical spectra will be obtained upon multiple scans, and the starting material can be quantitatively regenerated by returning to an initial potential of -0.15 V. The main advantage of the spectroelectrochemical techniques is that quantative generation of a new

species may be obtained in the absence of oxygen in a matter of seconds without the necessity of chemcal oxidants or reductants. Several complete experiments may be rapidly undertaken as a function of the changing potential without destroying the complex and the reversiblility of the system can be easily determined.

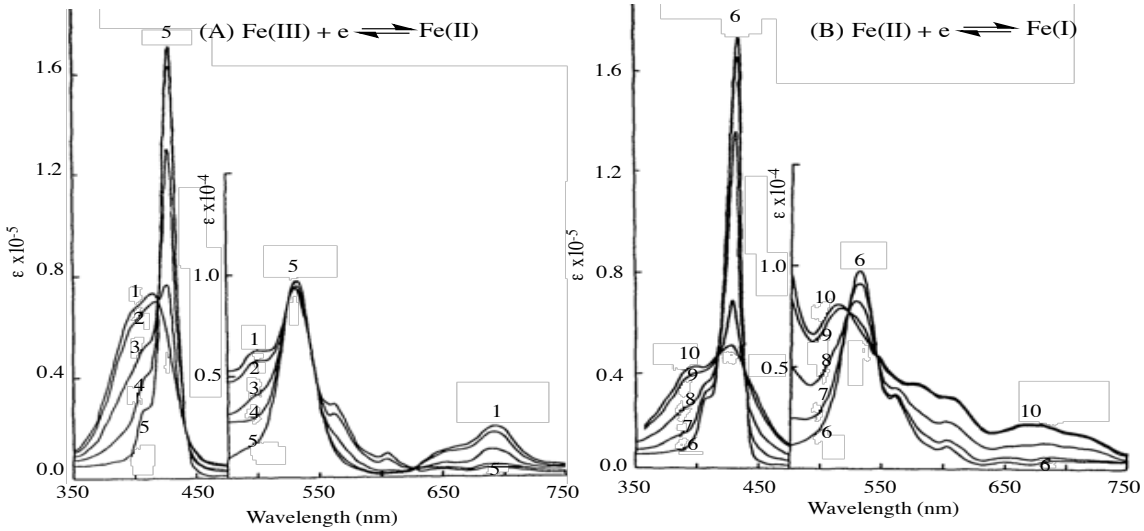

Figure 2-5. Thin-layer spectra obtained during reduction of $TPPFeClO_4$ in DMSO, 0.1 M TBAP. (Numbers correspond to potentials given in Figure 2-4). Figure adapted from Ref. 5 with labeling of reactions.

In our lab, spectroelectrochemucal methods are routinely used to distinguish metal-centered reaction from ring-centered reactions of porphyrins. For example, a metal-centered reaction of a porphyrin is dominated by red or blue shifts of the Soret band which is located between 350-450 nm, while a ring-centered reaction of the conjugated porphyrin ring system leads to a significant decrease in intensity of the Soret band along with the appearance of new broad visible or near IR bands.[8, 9]

2.2 Physical Measurements

2.2.1 Cyclic Voltammetry

In this dissertation, cyclic voltammetric measurements were performed in a three-electrode system using an EG&G Princeton Applied Research (PAR) Model 173 potentiostat. The three-electrode system consists of a platinum/glass-carbon electrode as a

working electrode (WE), a platinum electrode as a counter electrode (CE) and a homemade saturated calomel electrode (SCE) as the reference electrode (RE). The SCE was separated from the bulk of the solution by a fritted glass bridge of low porosity, containing the solvent/supporting electrolyte mixture. High-purity N_2 gas (99.99% Ultra High Purity) from Matheson Trigas was used to de-oxygenate the solution before conducting the measurement. Ferrrocene (Fc) was used as a common internal standard for the measurement.

2.2 UV-vis Spectroelectrochemisty (SEC)

UV-vis spectroelectrochemisty experiments were performed with an opically transparent platinum thin-layer electrode of the type described in the literature.[10,11] The controlled potentials were applied and mornitored with an EG&G Princeton Applied Research (PAR) Model 173 potentiostat. Time-resolved UV-vis spectra were recorded with a Hewlett-Packard Model 8453 diode-array rapid-scanning spectrophotometer.

2.3 Analytical Methods ---Measurement of Formation Constants

Formation constants for ligand binding were calculated using either UV-vis spectroscopy of electrochemistry to monitor the changes in properties of the examined compound as the ligand was added to solution. A stock solution containing a known concentration of the ligand was quantitatively added to the solution of the compound in a nonaqueous solvent, typically PhCN or CH_2Cl_2. Changes in the UV-vis spectra or in the half-wave potentials for reduction or oxidation were then monitored during the titration. The methods described below were used to calculate the formation constants.

2.3.1 Calculation of Formation Constants by Electrochemical Methods[5, 12, 13]

For a reversible electron-transfer reaction involving the ligand binding reaction shown in Eq. 2-5,

$$M + pL + ne \Leftrightarrow (ML_p)^{n-} \qquad (2\text{-}5)$$

The half-wave potentials will shift with change in the concentration of the free ligand in solution, according to Eq. 2-6,

$$(E_{1/2})_c = (E_{1/2})_s - RT / nF (\log K + p\log[L]) \quad (2\text{-}6)$$

where $(E_{1/2})_c$ and $(E_{1/2})_s$ are half-wave potentials for the electron-transfer reactions of the ligated and unligated compound of interest, respectively, and n is the number of electrons transferred in the redox reaction. The term RT/F is equal to 59 mV at 25 °C. The number of bound ligands is represented by *p* and can be calculated from the slope of the line from the plot of $(E_{1/2})_c$ vs. log[L]. The formation constants (K) can be determined from the intercept of the plot.

If both the oxidized and reduced forms of the compound of interest can bind axial ligands, the electrochemical calculations are more complicated and the relevant equation (at 25 °C) is given by Eq. 2-7,

$$(E_{1/2})_c = (E_{1/2})_s - 0.059\log[K_{ML_p}/K(_{ML_p})^-] - (p - q)0.059\log[L] \quad (2\text{-}7)$$

In this case, *p* and *q* are equal to the number of the ligands bound to the oxidized and reduced forms of the compound, $(E_{1/2})_c$ and $(E_{1/2})_s$ are the half-wave potentials for the electron-transfer reactions of the ligand and un-ligated species, and K_{ML_p} and $K(_{ML_p})^-$ are formation constants of the oxidation and reduction couple, ML_p and $(ML_p)^-$, respectively. When the ligand concentration is equal to 1.0 M or when $p = q$, the difference in half-wave potentials $(E_{1/2})_c$ and $(E_{1/2})_s$ will give directly the ratio of stability constants for ligand binding to the different forms of the redox couple.

2.3.2 Calculation of Formation Constants by UV-vis Spectroscopic Methods[14-16]

For the ligand binding reaction: $M + pL = ML_p$, the relationship between the concentration of the species in solution and the equilibrium constant, logK, is given by Eq. 2-8,

$$\log([ML_p]/[M]) = \log K + p \log [L] \quad (2\text{-}8)$$

Where [M] and $[ML_p]$ are the concentration of the un-ligated and ligated metalloporphyrin species and [L] is the free-ligand concentration in solution. If M and ML_p have different spectra, then we have:

$$A_0 = \varepsilon_M b C_M \quad (2\text{-}9)$$

$$A_f = \varepsilon_{MLp}\, b\, C_{MLp} \quad (2\text{-}10)$$

$$A_i = \varepsilon_M\, b\, [M] + \varepsilon_{MLp}\, b\, [ML_p] \quad (2\text{-}11)$$

Where C_M and C_{MLp} are the total concentration of M or ML_p, ε is the molar absorptivity and b is the path length, A_0 and A_f are the initial and final absorbance at a given wavelength (λ_{max}) for the species M and ML_p and A_i is the absorbance at λ_{max} at any point during the titration as shown in Figure 2-6.

According to the mass balance equation: $C_M = C_{MLp} = [M] + [ML_p]$, we have:

$$\begin{aligned} A_i &= \varepsilon_M\, b\, [M] + \varepsilon_{MLp}\, b\, [ML_p] \\ &= \varepsilon_M\, b\, (C_M - [ML_p]) + \varepsilon_{MLp}\, b\, [ML_p] \\ &= \varepsilon_M\, b\, C_M - \varepsilon_M\, b\, [ML_p] + \varepsilon_{MLp}\, b\, [ML_p] \\ &= A_0 + (\varepsilon_{MLp}\, b - \varepsilon_M\, b)\, [ML_p] \end{aligned}$$

or

$$\begin{aligned} A_i &= \varepsilon_M\, b\, [M] + \varepsilon_{MLp}\, b\, [ML_p] \\ &= \varepsilon_M\, b\, [M] + \varepsilon_{MLp}\, b\, (C_{MLp} - [M]) \\ &= \varepsilon_M\, b\, [M] + \varepsilon_{MLp}\, b\, C_{MLp} - \varepsilon_{MLp}\, b\, [M] \end{aligned}$$

$$[M] = (A_f - A_i)/(\varepsilon_{MLp}\, b - e_M\, b)$$

Substituting the values of [M] and $[ML_p]$ into equation (2-1) gives a useful result:

$$\log((A_i - A_0)/(A_f - A_i)) = \log K + p \log [L] \quad (2\text{-}12)$$

Plot of $\log((A_i - A_0)/(A_f - A_i))$ vs. log [L] should be a straight line whose slope should be equal to the number of ligands (*p*) axially bound to the metalloporphyrin and the intercept will give the formation constant (logK) as shown in Figure 2-6. The multiple step coordination is defined as $\log\beta_n$ which related to logK as: $\log\beta_n = \log K_1 \cdot \log K_2 \ldots \log K_n$.

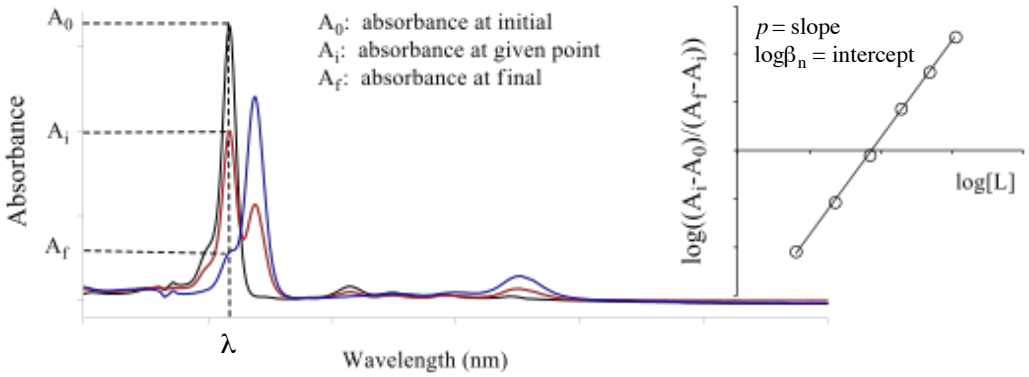

Figure 2-6. Examples of UV-vis spectra change during titration of a compound with ligand (L).

2.4 Other Experimental Methods

2.4.1 Degassing of the Solution

High-purity nitrogen gas (99.99% Ultra High Purity) from Matheson Trigas was used to deoxygenate the solutions for 5-10 minutes before each electrochemical experiment and a positive nitrogen pressure was maintained above the solution throughout the experiment.

2.4.2 Temperature Control

All experiments are performed at room temperature (22 ± 1ºC) unless otherwise noted. A dry ice and acetone mixture was used to obtain low temperatures that varied from room temperature to -75 ºC. The exact temperature was monitored using a mercury thermometer and the cell was centered in a slush bath of the dry ice and acetone.

2.5 Chemicals

2.5.1 Investigated Compounds

All compounds examined and characterized in this dissertation were synthesized by my collaborators. The nitrophenylporphyrins described in Chapter Three were synthesized in the laboratory of Dr. Claude P. Gross from Université de Bourgogne in Dijon, France.[17] The phosphorylated porphyrin compounds were synthesized in the laboratory of Dr. Alla Bessmertnykh-Lemeune from France.[18] The benzoporphyrins described in Chapters Five and

Six were synthesized by Dr. Hong Wang's group from the University of North Texas.[19,20] The corrole/phthalocyanine triple-decker complexes were synthesized by Dr. Guifen Lu from Jiangsu University in China[21] and the phthalocyanine/porphyrin triple-deckers were synthesized by Dr. Silviu Balaban's group From Aix Marseille University in France. All compounds were stored in dark under vacuum condition. The UV-vis spectrum of each compound was measured before I carried out experiments and the obtained spectral data were compared to those provided by my collaborator or published in the literature. If the spectrum of the examined compound I obtained was inconsistent with the result from my collaborator or from the literature, I would identify the reason for the difference and inform my collaborator of the problem so that they would resynthesize and purify the compound if needed. In this way, I could assure that the examined compound was in the same form as provided by my collaborators who had characterized the same compound by a number of standard methods prior to the electrochemical characterization.

2.5.2 Other Chemicals

Benzontrile (PhCN) obtained from Fluka Chemika or Siama-Aldrich Co. was distilled over phosphorous pentoxide (P_2O_5, 99%, Reagent Plus) under vacuum prior to use. Absolute dichloromethane (CH_2Cl_2, 99.8%, GC Purity) and pyridine (Py, Biotech. Grade ≥99.9%) were used as received without further purification. N_2 gas (99.99% Ultra High Purity) from Matheson Trigas was used for deoxygenate the solution before each electrochemical experiment. Tetra-*n*-butylammonium perchlorate (TBAP, for electrochemical analysis, ≥ 99.0%) were purchased form Sigma-Aldrich Chemical or Fluka Chemika Co. and used without further purification. Trifluoroacetic acid (TFA, ChromaSolv., for HPLC, >99.0%) was obtained from Sigma-Aldrich Chemical Co. and used as received.

2.6 Reference

(1) Nicholson, R. S.; Shain, I. *Anal. Chem.* **1964**, *36*, 706-723.

(2) Weissberger, A.; Rossiter, B. W.; Eds. *Physical Methods of Chemistry, Pt. 2A: Electrochemical Methods* **1971**, pp 723.

(3) Nicholson, R. S. *Anal. Chem.* **1965**, *37*, 1351-1355.

(4) Kadish, K. M.; Morrison, M. M.; Constant, L. A.; Dickens, L.; Davis, D. G. *JACS.* **1976**, *98*, 8387-8390.

(5) Murray, P. R.; Yellowlees, L. J. In *EPR spectroelectrochemistry*, **2008**, 207-231.

(6) Kaim, W.; Fiedler, J. *Chem. Soc. Rev.* **2009**, *38*, 3373-3382.

(7) Gouterman, M. *J. Mol. Spectrosc.* **1961**, *6*, 138-163.

(8) Fuhrhop, J. H. *Structu.Bonding* **1974**, *18*, 1-67.

(9) Lin, X. Q.; Kadish, K. M.; *Anal. Chem.* **1985**, *57*, 1498-1501.

(10) Kadish, K. M.; Mu, X. H.; Lin, X. Q.; *Electroanalysis* **1989**, *1*, 35-41.

(11) Lingane, J. J. *Chem. Rev.* **1941**, *29*, 1-35.

(12) Crow, D. R. *Polarography of Metal Complexes* **1969**, p 203.

(13) Lever, A. B. P.; Gray, H. B.; Eds.; *Physical Bioinorganic Chemistry Series, No. 2: Iron Porphyrins, Pt. 2.* **1983**, p 254.

(14) Yoe, J. H.; Jones, A. L. *Ind. Eng. Chem.* **1944***, 16,* 111-115.

(15) Budesinsky, B. W. *Talanta* **1974**, *21*, 323-326.

(16) Ellis, P. E.; Linard, J. E.; Szymanski, T.; Jones. R. D.; Budge, J. R.; Basolo, F. *JACS.* **1980**, *102,* 1889-1896.

(17) Fang, Y.; Jiang, X.; Ou, Z.; Michelin, C.; Desbois, N.; Gros, C. P.; Kadish, K. M. *J. Porphyrins Phthalocyanines* **2014**, *18*, 832-841.

(18) Fang, Y.; Gorbunova, Y. G.; Chen, P.; Jiang, X.; Manowong, M.; Sinelshchikova, A. A.; Enakieva, Y. Y.; Martynov, A. G.; Tsivadze, A. Y.; Bessmertnykh-Lemeune, A.; Stern, C.; Guilard, R.; Kadish, K. M. *Inorg. Chem.* **2015**, *54*, 3501-3512.

(19) Jinadasa, R. G. W.; Fang, Y.; Deng, Y.; Seshpande, R.; Jiang, X.; Kadish, K. M. Wang, H.; *RSC. Adv.* **2015**, *5*, 51489-51492.

(20) Jinadasa, R. G. W.; Fang, Y.; Kumar, S.; Osinshi, A. J.; Jiang, X.; Ziegler, C. J.; Kadish, K. M. Wang, H. *J. Org. Chem.* **2015**, *80*, 12076-12087.

(21) Lu, G.; Li, J.; Jiang, X.; Ou, Z.; Kadish, K. M. *Inorg. Chem.* **2015**, *54*, 9211-9222.

CHAPTER THREE

Redox Properties of Nitrophenylporphyrins and Electrosynthesis of Nitrophenyl-linked Zn Porphyrin Dimers or Arrays

3.1 Introduction

The addition of NO_2 groups to a porphyrin and corrole may significantly modify its chemical and physical properties, with the type and magnitude of the effect being dependent largely on the position of these highly electron-withdrawing substituents.[1-25] Examples of nitro-substituted porphyrins include (i) *meso*-NO_2 substituted octaethylporphyrins, (ii) β-pyrrole nitro substituted tetraphenylporphyrins and triphenylcorroles, (iii) *meso*-nitrophenyl substituted porphyrins and (iv) porphyrins containing one or more NO_2 substituents on β,β'-fused group(s) of the macrocycle, as in the case of nitro-substituted quinoxalinoporphyrins.

Early electrochemical studies of metalloporphyrins have shown that the presence of one or more electron-withdrawing NO_2 groups at the *meso*- or β-pyrrole positions of the macrocycle will have a large effect on the $E_{1/2}$ for electroreduction, shifting the reversible potentials in a positive direction by 230-380 mV per nitro group in the case of β-pyrrole substituted (TPP)M and by 450-550 mV in the case of *meso*-substituted (OEP)M type derivatives.[23] Much smaller positive shifts of potential are seen upon oxidation and the measured shifts of $E_{1/2}$ are generally less than 100 mV per nitro group, with the exact value depending upon the solvent, the position of the nitro substituents and the specific central metal ion in the macrocycle.

The NO_2 group on the phenyl ring of a tetraphenylporphyrin or triphenylcorrole type complex may itself be involved in an electroreduction as was recently shown by our group in two papers which characterized the electoreduction of iron[25] and cobalt[10] triarylcorroles having 1, 2 or 3 nitrophenyl substituents at the *meso* positions of the macrocycle. The examined compounds are represented as $(NO_2Ph)_xPh_{3-x}CorCo(PPh_3)$ **9-12** and $(NO_2Ph)_3CorCoFe(NO)$ **14** whose structures are given in Chart 3-1 and cyclic voltammograms reproduced in Figure 3-1.

(a) Porphyrins

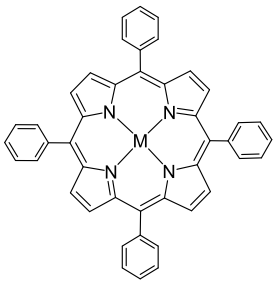

(TPP)H_2 **1**
(TPP)Zn **4**
(TPP)Pd **7**

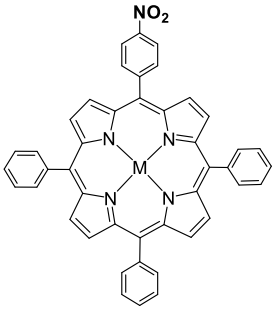

(NO_2Ph)Ph_3PorH_2 **2**
(NO_2Ph)Ph_3PorZn **5**
(NO_2Ph)Ph_3PorPd **8**

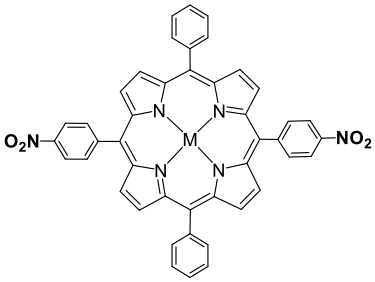

($NO_2Ph)_2Ph_2PorH_2$ **3**
($NO_2Ph)_2Ph_2$PorZn **6**

(b) Corroles

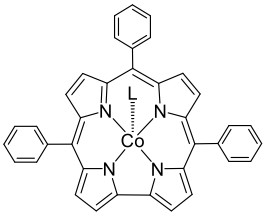

Ph_3CorCo(PPh_3) **9**

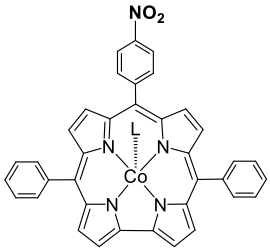

(NO_2Ph)Ph_2CorCo(PPh_3) **10**

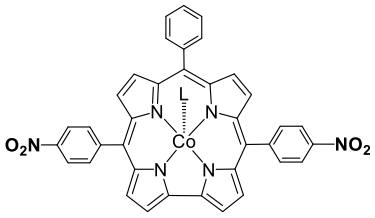

($NO_2Ph)_2$PhCorCo(PPh_3) **11**

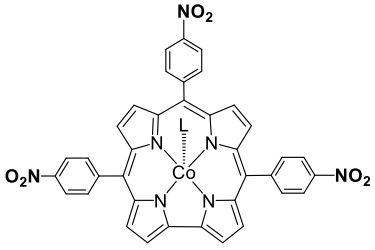

($NO_2Ph)_3$CorCo(PPh_3) **12**

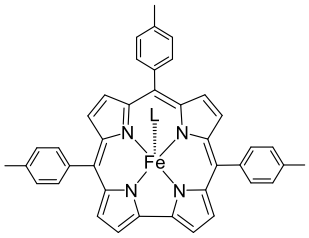

($MePh)_3$CorFe(NO) **13**

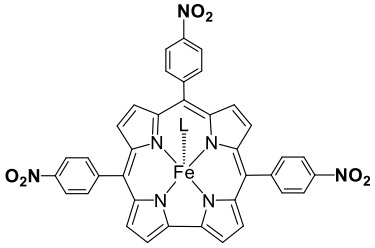

($NO_2Ph)_3$CorFe(NO) **14**

Chart 3-1. Structures of (a) investigated nitrophenylporphyrins in this thesis and (b) previously studied nitrophenylcorroles (Compounds **9-12** from Ref.10 and **13-14** from Ref. 25).

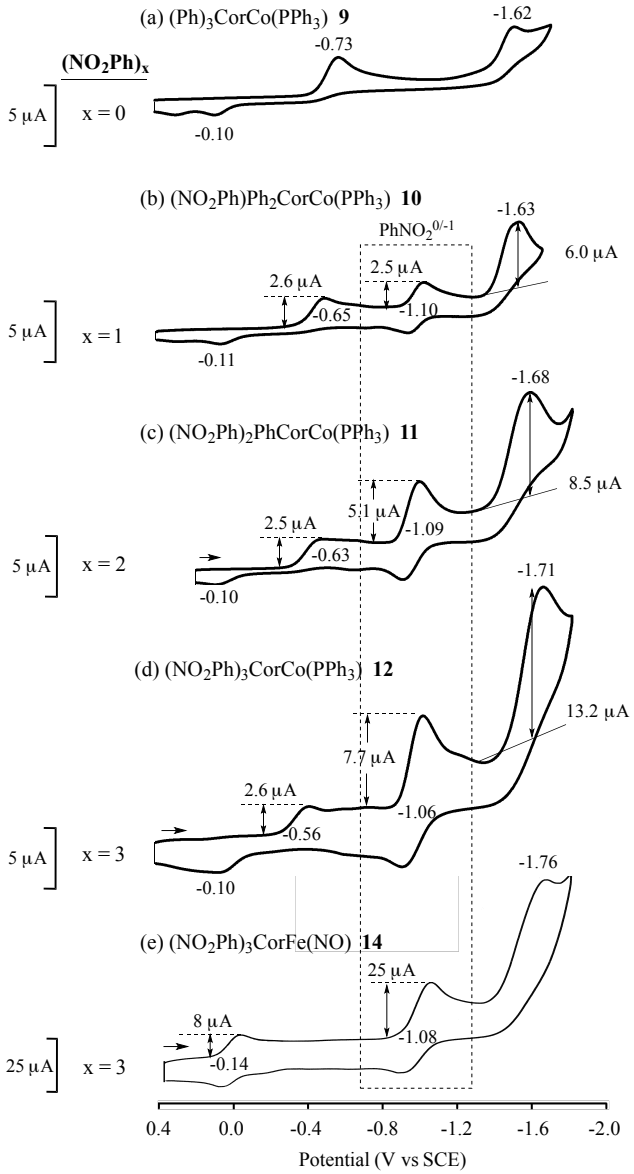

Figure 3-1. Cyclic voltammograms of previously investigated NO_2Ph substituted corroles in CH_2Cl_2 containing 0.1 M TBAP. Data on cobalt corroles (**9-12**) are from Ref. 10 and data on $(NO_2Ph)_3CorFe(NO)$ (**14**) are from Ref. 25.

The examined *meso*-nitrophenyl corroles all undergo an initial metal-centered redox process upon reduction, Co^{III} to Co^{II} in the case of **10-12** and Fe^{III} to Fe^{II} in the case of **14**, and this is then followed at more negative potentials by a reversible one electron reduction of each *meso*-substituted nitrophenyl substituent on the compounds. This reversible reduction is located at $E_{1/2}$ = -1.06 to -1.10 V and followed by further irreversible reductions of the singly reduced nitrophenyl substituent at E_p = -1.63 to -1.76 V. These latter reductions are also overlapped in potential with the first reduction of the conjugated corrole macrocycle.

One key finding in our published studies from Dr. Kadish's lab on nitrophenylcorroles[10, 25] is the fact that the multiple NO_2Ph substituents in compounds **11, 12** and **14** are non-interacting and all were reduced at essentially the same potential with a peak current which was directly proportional to the number of nitrophenyl substituents on the macrocycle. For example, compounds **10**, **11** and **12** with 1, 2 and 3 NO_2Ph substituents exhibited peak currents of 2.5, 5.1 and 7.7 μA respectively, as illustrated in Figure 3-1.

As part of the research described in this dissertation, I wished to know if similar electrochemistry would be observed for *meso*-nitrophenyl substituted porphyrins with different central metal ions as well as for free-base nitrophenylporphyrins, and I also wanted to examine how UV-vis spectra of the singly reduced nitrophenylporphyrins might be affected by the presence of one or more reduced nitrophenyl groups at the *meso*-positions of the macrocycle. This is investigated in the present study where five *meso*-nitrophenyl substituted porphyrins were characterized as to their electrochemical and spectroelectrochemical properties in dichloromethane. The investigated compounds are represented as $(NO_2Ph)_xPh_{4-x}PorM$, where Por represents the dianion of the porphyrin macrocycle, Ph is a phenyl group on the *meso*-position of the macrocycle, NO_2Ph is a *meso*-substituted nitrophenyl group, M = 2H, Pd^{II} or Zn^{II}, and x = 1 or 2. The effect of the *meso*-nitrophenyl groups on the redox potentials of the porphyrin π-ring system are examined and comparisons are made with

non-nitrophenyl-substituted porphyrins with the same central metal ions. Comparisons are also made to the previously studied nitrophenylcorroles.[10, 25]

3.2 Results and Discussion

3.2.1 Electrochemistry of $(NO_2Ph)Ph_3PorPd$

Cyclic voltammograms illustrating the reduction of nitrobenzene (NO_2Ph), (TPP)Pd **7** and $(NO_2Ph)Ph_3PorPd$ **8** in CH_2Cl_2, are shown in Figure 3-2a. As seen in the Figure, the reduction of $PhNO_2$ proceeds in two steps, an initial reversible one electron addition at half wave potential of $E_{1/2}$ = -1.13 V and an irreversible reduction at E_p = -2.00 V for a scan rate of 0.1 V/s. The reduction of (TPP)Pd also proceeds in two one-electron transfer steps, the first at $E_{1/2}$ = -1.34 V and the second at -1.80 V. All four redox processes can be seen in the cyclic voltammogram of $(NO_2Ph)Ph_3PorPd$ **8** (Figure 3-2) where the first two reductions are reversible ($E_{1/2}$ = -1.07 and -1.25 V) and last two irreversible (E_{pc} = -1.78 and -1.91 V) for a scan rate of 0.1 V/s. Moreover, the third irreversible reduction process generates an unknown product which can be re-oxidized at E_{pa} = -1.34 V on the return scan. This peak is not observed when the potential sweep is reserved after the second reduction which formed the porphyrin π-anion radical (see dashed line in Figure 3-2a).

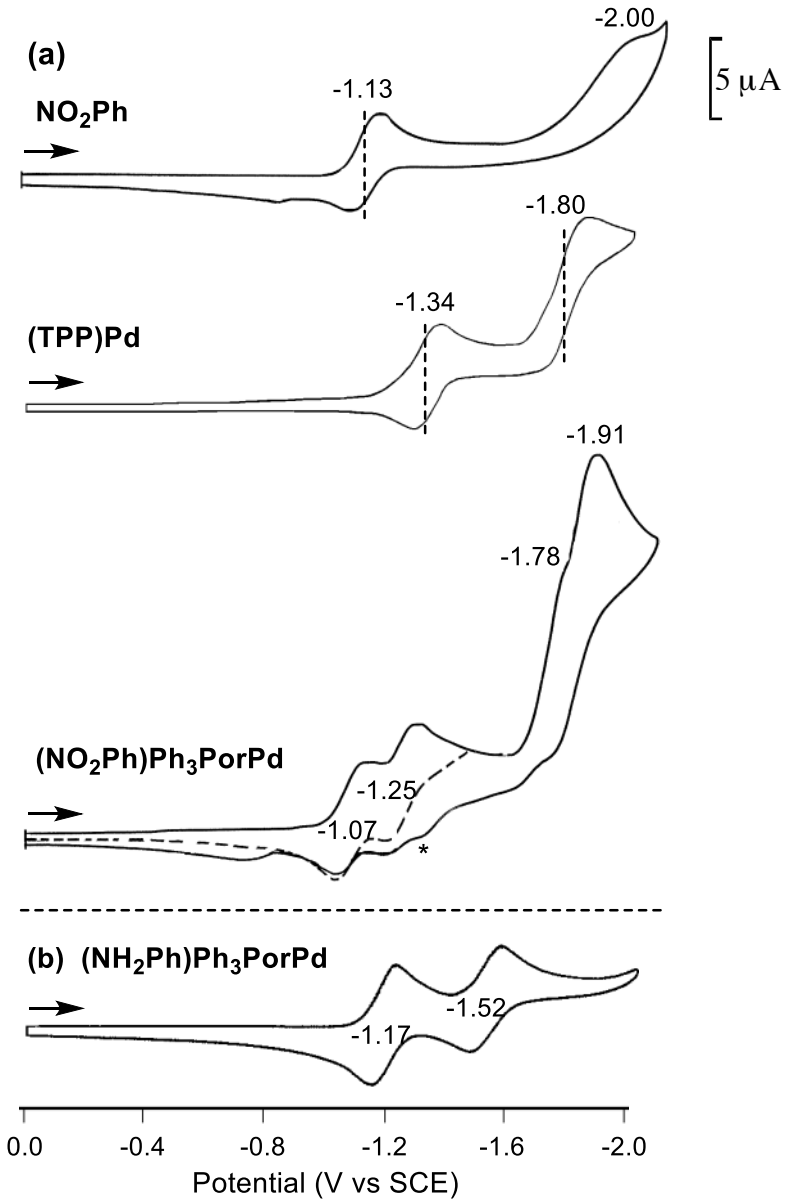

Figure 3-2. Cyclic voltammograms of (a) $(NO_2Ph)Ph_3PorPd$ **8** and its unlinked components, (TPP)Pd **7** and NO_2Ph, and (b) $(NH_2Ph)Ph_3PorPd$ in CH_2Cl_2, 0.1 M TBAP. An uncharacterized electroactive product after the 3rd reduction of **8** occurs at E_{pa} = -1.34 V on the reversed oxidation scan and is indicated by an asterisk.

The $E_{1/2}$ = -1.07 V for the initial reduction of **8** is virtually identical to the half-wave potential for reduction of the nitrophenyl substituent(s) on compounds **10**-**12** and **14** (see Figure 3-1) and is clearly assigned to the nitrophenyl substituent. This process on **8** is shifted positively by 60 mV as compared to $E_{1/2}$ for reduction of nitrobenzene in CH_2Cl_2 ($E_{1/2}$ = -1.13 V) and a similar positive shift in $E_{1/2}$ also occurs for reduction of the porphyrin π-ring system in $(NO_2Ph)Ph_3PorPd$ **8** (-1.25 V) as compared to that of (TPP)Pd (-1.34 V). The third reduction of $(NO_2Ph)Ph_3PorPd$ **8** (E_p = -1.78 V) is located at a similar potential as the second reduction of (TPP)Pd (-1.80 V) while the forth irreversible reduction of **8** at -1.91 V is easier than the irreversible NO_2Ph reduction at E_p = -2.00 V but harder (more negative) than the irreversible NO_2Ph reductions of **10**-**12** and **14**, perhaps because of the added negative charge on the triply reduced nitrophenyl Pd^{II} complex **8**.

The final product or products in the electrochemical reduction of $(NO_2Ph)Ph_3PorPd$ **8** at -1.78 or -1.91 V were not elucidated in the present study but there was no evidence for generation of $(NH_2Ph)Ph_3PorPd$ which is formed upon chemical reduction of compound **8** in protic media. This was ascertained by comparison of the cyclic voltammogram of **8** and that of chemically synthesized $(NH_2Ph)Ph_3PorPd$ which is reversibly reduced and re-oxidized at potentials of -1.17 and -1.52 V under the same solution conditions (see Figure 3-2b).

The UV-vis spectra of the singly and doubly reduced $(NO_2Ph)Ph_3PorPd$ **8** were examined by thin-layer spectroelectrochemistry and this data is discussed in a later section of this chapter.

3.2.2 Electrochemistry of $(NO_2Ph)_xPh_{4-x}PorM$, where M = H_2 or Zn and x = 1, 2.

Cyclic voltammograms illustrating the reduction and oxidation of the Zn^{II} and free-base nitrophenylporphyrins **2, 3, 5** and **6** are illustrated in Figure 3-3 and a summary of half-wave and peak potentials is given in Table 3-1, which also includes data for the related $(TPP)H_2$ **1** and $(TPP)Zn^{II}$ **4** complexes under similar solution conditions.

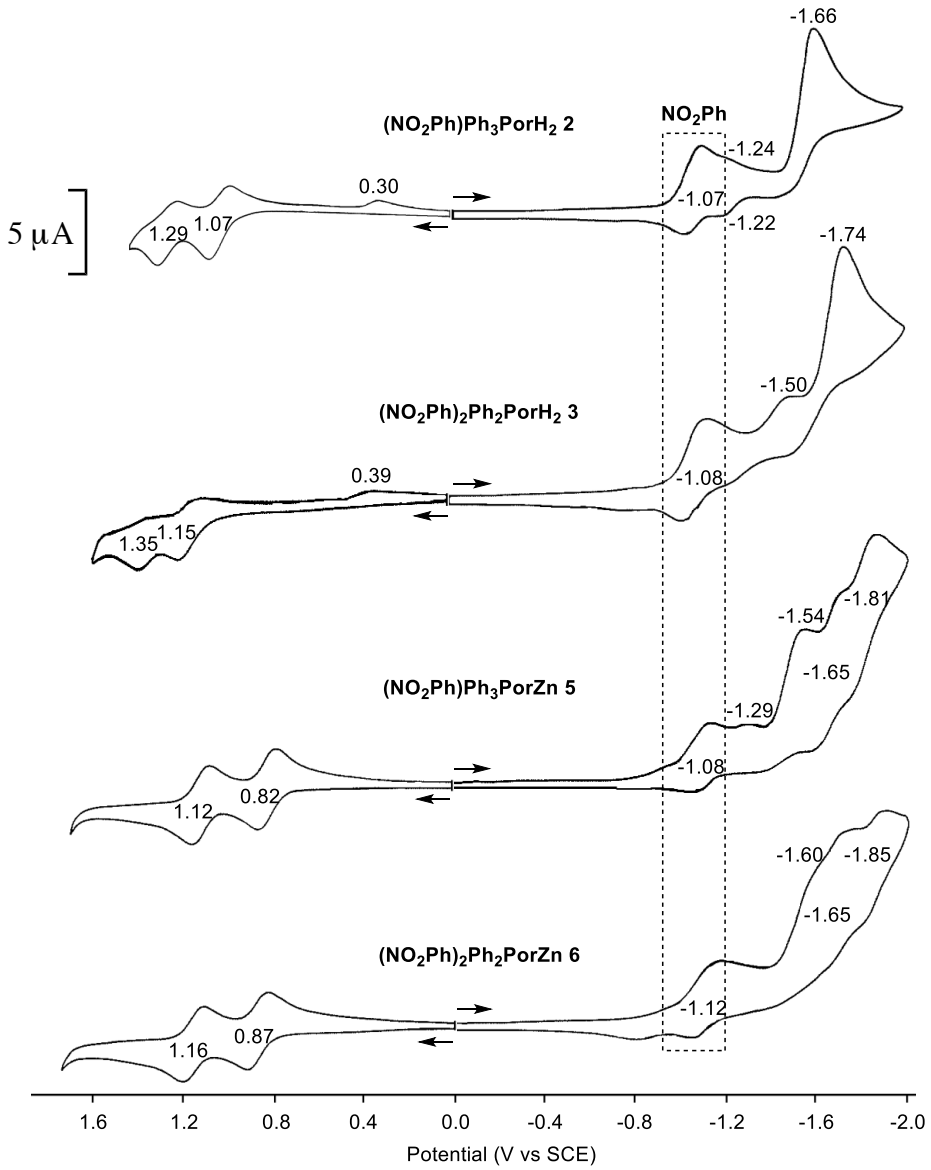

Figure 3-3. Cyclic voltammograms of investigated porphyrins in CH_2Cl_2, 0.1 M TBAP.

Table 3-1. Half-wave potentials (V vs SCE) of investigated porphyrins in CH_2Cl_2, 0.1 M TBAP (Data from this work are good to ±10 mV).

Compound	Oxidation		$M^{III/II}$	Reduction				ref
	ring			$[NO_2Ph]$	ring		nitrophenyl groups	
				0/-1	1^{st}	2^{nd}		
NO_2Ph				-1.13			-2.00[a]	*tw*
$(TPP)H_2$ **1**	1.25	1.00			-1.23	-1.59		*tw*
$(NO_2Ph)Ph_3PorH_2$ **2**	1.29	1.07		-1.07	b	c	-1.66[a]	*tw*
$(NO_2Ph)_2Ph_2PorH_2$ **3**	1.35	1.15		-1.08	b	-1.50[a]	-1.74[a]	*tw*
(TPP)Zn **4**	1.09	0.78			-1.32	-1.71		*tw*
$(NO_2Ph)Ph_3PorZn$ **5**	1.12	0.82		-1.08	-1.29[a]	d	d	*tw*
$(NO_2Ph)_2Ph_2PorZn$ **6**	1.16	0.87		-1.12	b	-1.60[a]	e	*tw*
(TPP)Pd **7**	1.55	1.14			-1.34	-1.80		*tw*
$(NO_2Ph)Ph_3PorPd$ **8**	1.54	1.21		-1.07	-1.25	-1.78[a]	-1.91	*tw*
$Ph_3CorCo(PPh_3)$ **9**	0.94	0.51	-0.73[a]		-1.62[a]		---	10
$(NO_2Ph)Ph_2CorCo(PPh_3)$ **10**	0.99	0.57	-0.65[a]	-1.10	-1.63[a]		-1.63[a]	10
$(NO_2Ph)_2PhCorCo(PPh_3)$ **11**	1.03	0.62	-0.63[a]	-1.09	-1.68[a]		-1.68[a]	10
$(NO_2Ph)_3CorCo(PPh_3)$ **12**	1.05	0.67	-0.56[a]	-1.06	-1.71[a]		-1.71[a]	10
$(MePh)_3CorFe(NO)$ **13**	0.82	0.82	-0.35		-1.74[a]		---	25
$(NO_2Ph)_3CorFe(NO)$ **14**	1.18[a]	0.97	-0.14	-1.08	-1.76[a]		-1.76[a]	25

[a]Irreversible peak potential at scan rate of 0.1 V/s. [b]Process overlapped with reduction of neutral $(NO_2)Ph$ group, [c]Process overlapped with irreversible reduction of nitrophenyl anion. [d]Three reductions are observed at E_p = -1.54, $E_{1/2}$ = -1.65 and $E_{1/2}$ = -1.81 V and may correspond to electron addition to the Zn porphyrin product. [e]Three reductions are observed at E_p = -1.60, $E_{1/2}$ = -1.65 and $E_{1/2}$ = -1.85 V and may correspond to electron addition to the Zn porphyrin product.

Each free-base or zinc nitrophenylporphyrin undergoes two oxidations and 2-5 reductions in CH_2Cl_2. Both oxidations and the first reduction are reversible when the potential scan is reversed at +1.60 V for oxidation and -1.20 V for reduction, respectively. The oxidations correspond to the stepwise formation of a porphyrin π cation radical and dication and are located at $E_{1/2}$ values which are shifted positively by 30-80 mV for each added NO_2Ph group on $(NO_2Ph)_xPh_{4-x}PorM$.

In contrast to the oxidations, the potentials for first reduction of $(NO_2Ph)_xPh_{4-x}PorZn$ and $(NO_2Ph)_xPh_{4-x}PorH_2$ are not significantly affected by the number of nitrophenyl groups on the porphyrin, with $E_{1/2}$ values being located at -1.07 (x =1) to -1.08 V (x = 2) for M = H_2 and -1.08 (x =1) or -1.12 V (x = 2) for M = Zn^{II}. These potentials are listed in Table 1 under the $[NO_2Ph]^{0/-1}$ process which also includes data from the earlier characterized cobalt and iron nitrophenylcorroles **10**-**12** and **14**.[10, 25]

The overall shapes of the current-voltage curves upon reduction of the free-base and zinc porphyrins are different from each other (see Figure 3-3) and they also differ from that of the Pd^{II} nitrophenylporphyrins whose cyclic voltammogram is shown in Figure 3-2. In the case of $(NO_2Ph)Ph_3PorPd$ **8**, four separate reductions are observed, the first two of which are separated by 180 mV and correspond to an electron addition involving the nitrophenyl group and the porphyrin π ring system, respectively. The first reduction of NO_2Ph group and the first reduction of porphyrin ring are overlapped for the free-base or zinc nitrophenylporphyrins and none of the reduction processes in Figure 3-3 beyond the first step were characterized in the present study. However, it should be noted that what seems to be a second reduction of the porphyrin ring can be detected at E_p = -1.50 V for $(NO_2Ph)Ph_3PorH_2$ **3** as compared to a reversible $E_{1/2}$ of -1.59 V for the second reduction of $(TPP)H_2$ **1** in CH_2Cl_2 (see Table 3-1).

It should also be noted that the last three reductions and reoxidations of $(NO_2Ph)_2Ph_2PorZn$ **5** in the cyclic voltammograms of Figure 3-3 are reversible to quasireversible and this redox behavior is clearly different from what is observed for the other

nitrophenylporphyrins and nitrophenylcorroles where only a single irreversible reduction of the singly reduced nitrophenyl group is observed. (see Figure 3-1, 3-2 and 3-3). As will be discussed below, the UV-vis spectra of the two singly reduced Zn nitrophenylporphyrins are quite different from the spectra of the singly reduced Pd^{II} and free-base nitrophenylporphyrins and I suggest the formation of linked porphyrin arrays which are electrogenerated in a chemical step which occurs after the initial one-electron reduction of the nitrophenyl group on $(NO_2Ph)_2Ph_2PorZn$ **5**. Evidence for this suggestion is given by the spectroelectrochemistry data described below.

3.2.3 Spectroelectrochemistry

Three distinctly different patterns of spectral changes are observed upon the first reduction of the investigated nitrophenylporphyrins. One pattern is for the Pd^{II} derivative **8**, another is for the free-base porphyrins **2** and **3** and the third is for the Zn^{II} nitrophenylporphyrins **4** and **5**. The time resolved UV-vis spectral changes observed for these five compounds during the first controlled potential reduction are shown in Figure 3-4.

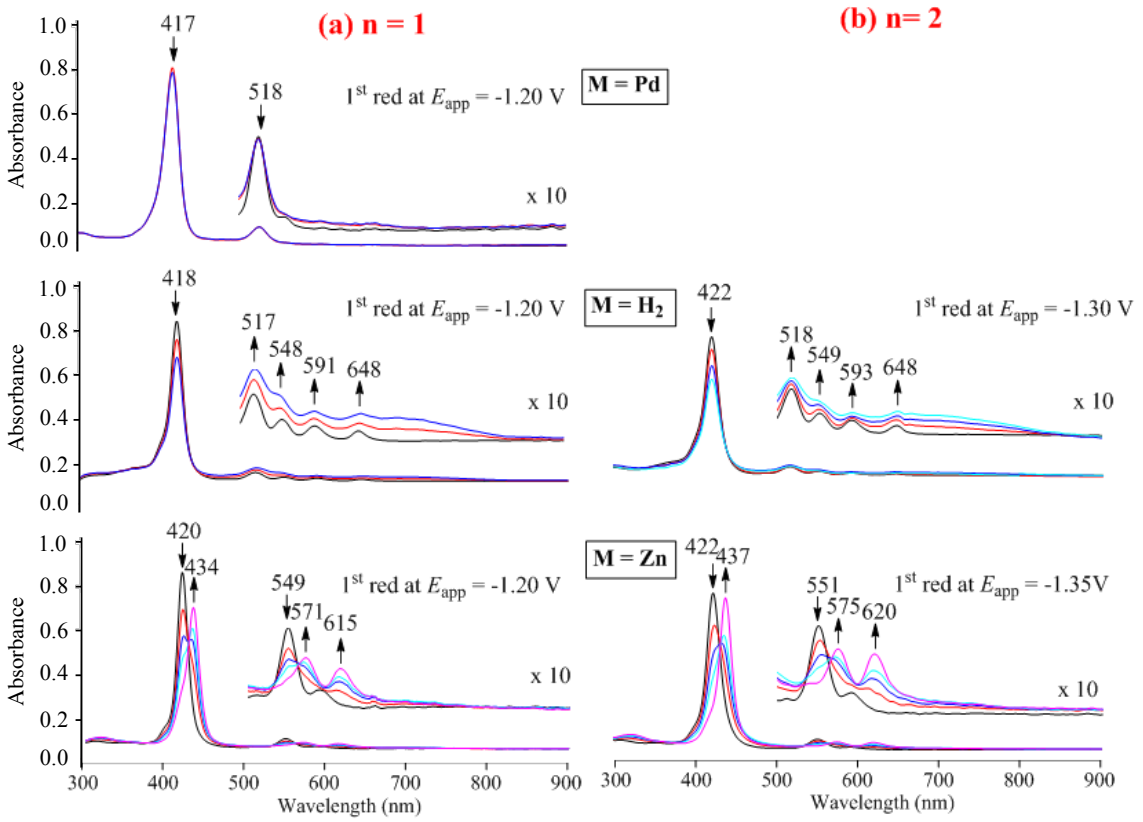

Figure 3-4. UV-vis spectral changes during first controlled potential reduction of $(NO_2Ph)_xPh_{4-x}PorM$ in CH_2Cl_2, 0.1 M TBAP, where M = Zn, Pd or 2H and (a) n = 1 or (b) n = 2.

The spectral changes upon controlled potential reduction of $(NO_2Ph)Ph_3PorPd$ **8**, $(NO_2Ph)Ph_3PorH_2$ **2** and $(NO_2Ph)_2Ph_2PorH_2$ **3** are consistent with the cyclic voltammetric data and are related to the potential separation between the first one-electron reduction at the nitrophenyl group and the first one electron reduction at the porphyrin π–ring system. In the case of **8**, both electron additions are well resolved, with $E_{1/2}$ values separated by 180 mV in CH_2Cl_2. The reversible reduction of the porphyrin π–ring system in $(NO_2Ph)Ph_3PorPd$ **8** occurs at $E_{1/2}$ = -1.25 V (see Figure 3-2) and thus only the nitrophenyl substituent is reduced in the thin-layer cell at an applied potential of -1.20 V. Under these conditions, almost no change is seen in the UV-vis spectrum of the singly reduced species which is dominated by bands associated with the unreduced porphyrin macrocycle.

This contrasts with what occurs for $(NO_2Ph)Ph_3PorH_2$ **2** and $(NO_2Ph)_2Ph_2PorH_2$ **3** where the porphyrin ring centered reduction is partially overlapped with reduction of the NO_2Ph group as seen in Figure 3-3. The UV-vis spectrum of the reduction product under these conditions exhibits features of a porphyrin π anion radical, namely a decrease of the Soret band intensity as compared to the neutral porphyrin and a broad absorption between 600 and 800 nm. However, the two electroreduced products also retain features of the unreduced porphyrin macrocycle, namely a well-defined Soret band and four Q bands in the visible region of the spectrum as seen in the figure.

The observed spectral changes during the first reduction of $(NO_2Ph)Ph_3PorZn$ **5** and $(NO_2Ph)_2Ph_2PorZn$ **6** are quite different than what is observed after reduction of the free-base or Pd^{II} nitrophenylporphyrins and can be interpreted in terms of a change from an initial four coordinate zinc nitrophenylporphyrin in the unreduced compounds to a five coordinate complex under the application of a controlled reducing potential. These spectral changes are illustrated in Figure 3-4, where the Soret band of the initial $(NO_2Ph)_xPh_{4-x}PorZn$ shifts from 420 to 434 nm for the mono-nitrophenyl compound (x = 1) and from 422 to 427 nm for the bis-substituted nitrophenylporphyrin (x = 2). There is also a change from a single Q band in the

spectra of the 4-coordinate Zn^{II} porphyrins to two Q bands in the spectra of the electrogenerated five coordinated complexes, these bands being located at 571 and 615 nm for x = 1 and 575 and 620 nm for x = 2. Both sets of spectral changes in Figure 3-4 show three well-defined isosbestic points with no evidence for formation of a porphyrin π anion radical, as is the case for the free-base nitrophenylporphyrins.

The above data suggest a linkage of two or more Zn(II) nitrophenylporphyrins after electroreduction, the linkage occurring axially through the metal center of one porphyrin and the reduced nitrobenzene substituent of another, perhaps to give species like those schematically shown in Scheme 3-1. The conversion of singly reduced $(NO_2Ph)Ph_3PorZn$ to the proposed linked Zn^{II} porphyrin reduction product is shown in Eq. 1 and is reversible as indicated by the spectroelectrochemical data in Figure 3-S8 where changing the applied potential from -1.20 to 0.0 V after controlled potential reduction leads to regeneration of the initial UV-vis spectrum with isosbestic points at 428, 531 and 561 nm. The same isosbestic points are seen upon reduction of $(NO_2Ph)Ph_3PorZn$, thus ruling out the possibility of multiple forms of the final reduction product.

$$\underset{420,\,549,\,590\ nm}{\mathbf{(NO_2Ph)Ph_3PorZn}} \underset{-1.20\ V}{\overset{+\,e}{\rightleftharpoons}} \mathbf{[(NO_2Ph)Ph_3PorZn]^-} \overset{Fast}{\rightleftharpoons} \underset{434,\,571,\,615\ nm}{\mathbf{Linked\ Zn\ porphyrin\ product}} \quad (1)$$

Scheme 3-1. Possible reduction products of $(NO_2Ph)Ph_3PorZn$ in CH_2Cl_2.

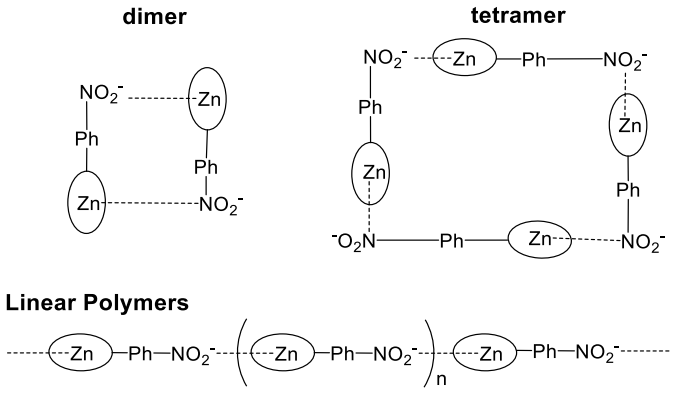

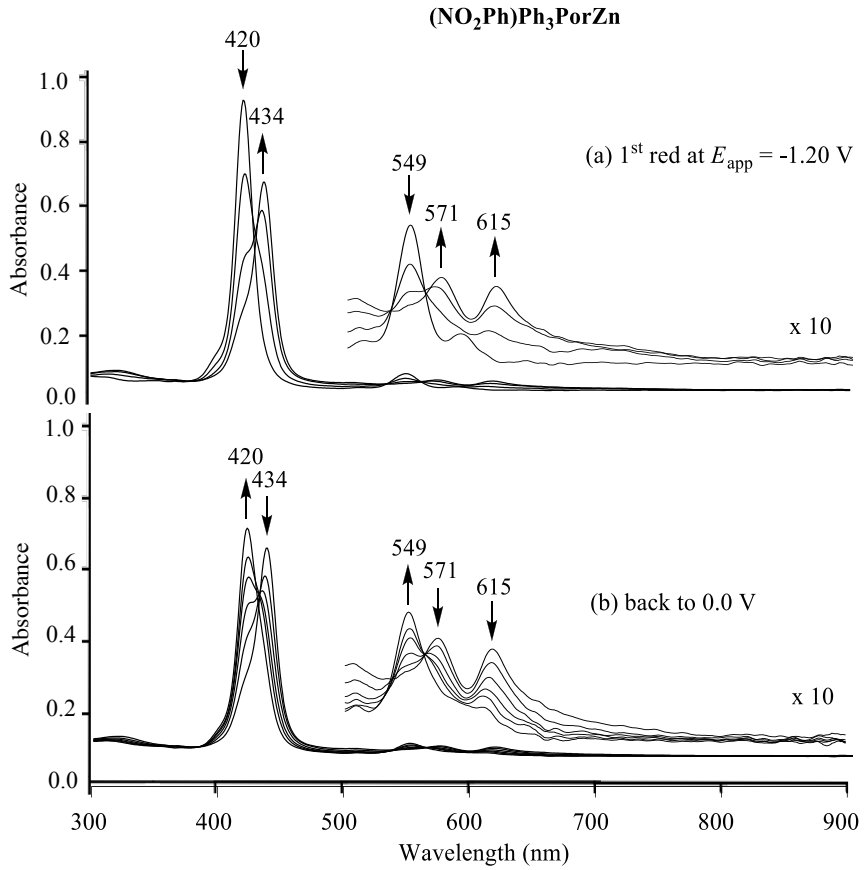

Figure 3-5. UV-vis spectral change of $(NO_2Ph)Ph_3PorZn$ **5** (a) first reduction at -1.20 V and (b) reoxidation at 0.0 V in CH_2Cl_2, 0.1 M TBAP.

Additional evidence for the binding of a reduced nitrobenzene substituent of one porphyrin to the Zn^{II} center of another is given by the data in Figure 3-6 where the same spectral pattern is seen when reducing free nitrobenzene in a solution of (TPP)Zn to give $(TPP)Zn(NO_2Ph)^-$ which is spectrally characterized by bands at λ_{max} = 434, 569 or 615 nm (Figure 3-6b) or when adding chloride ion to a solution of (TPP)Zn to give $[(TPP)ZnCl]^-$ which has λ_{max} = 434, 569 or 615 nm (Figure 3-6b). An identical UV-vis spectrum of the product is obtained in both experiments and these spectra are almost identical to the spectrum obtained by electrochemically reducing the nitro-substituted Zn porphyrin **5** in CH_2Cl_2, 0.1 M TBAP. The main difference between the UV-vis spectrum of singly reduced $(NO_2Ph)Ph_3PorZn$ **5** and the five coordinate $[(TPP)Zn(NO_2Ph)]^-$ and $(TPP)Zn(Cl)^-$ complexes in Figure 3-6 is a

broadened Soret band of the proposed linked Zn^{II} nitrophenylporphyrin product. This is consistent with the presence of multiple interacting macrocycles in solution. Finally, it should be noted that anion binding does not occur for Pd porphyrins and thus the electrosynthesis described above works only for the Zn^{II} derivatives.

In summary, the controlled potential reduction of $(NO_2Ph)Ph_3PorZn$ **5** and $(NO_2Ph)_2Ph_2PorZn$ **6** is proposed to generate dimers, tetramers or arrays of linked Zn porphyrins but not a polymer, as ascertained by the well-defined UV-vis spectra with three isosbestic points.

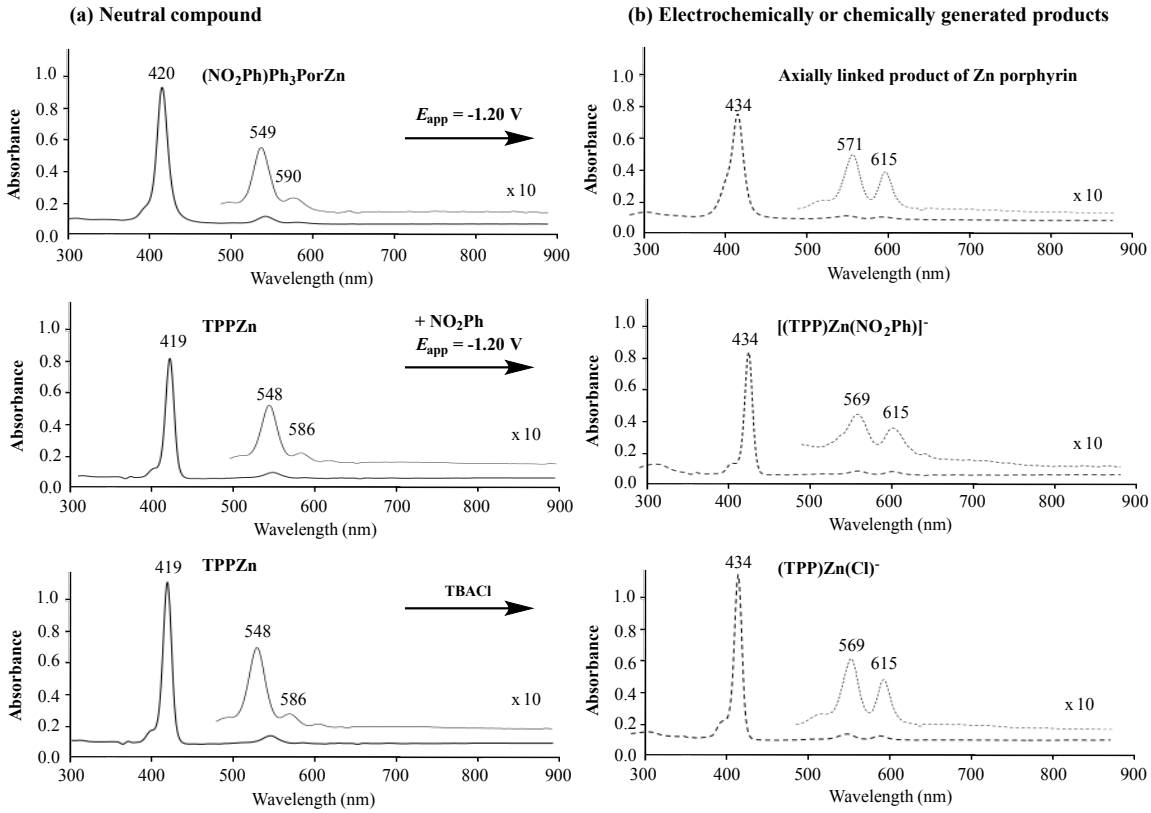

Figure 3-6. UV-vis spectrum of (a) neutral $(NO_2Ph)Ph_3PorZn$ and (TPP)Zn and (b) spectra of electrogenerated or chemically generated products under the indicated conditions.

3.3 References

(1) Bhyrappa, P.; Purushothaman, B. *J. Chem. Soc., Perkin Trans.* **2001**, *2*, 238-242.

(2) Wyrebeka, P.; Ostrowski, S. *J. Porphyrins Phthalocyanines* **2007**, *11*, 822-828.

(3) Horn, S.; Dahms, K.; Senge, M. O. *J. Porphyrins Phthalocyanines* **2008**, *12*, 1053-1077.

(4) Terekhov, S. N.; Sinyakova, G. N.; Lobkoa, E. E.; Pierrette, B.; Turpinc, P. Y.; Chirvony, V. S. *J. Porphyrins Phthalocyanines* **2007**, *11*, 682-690.

(5) Crossley, M. J.; King, L. G.; Pyke, S. M.; Tansey, C. W. *J. Porphyrins Phthalocyanines* **2002**, *6*, 685-694.

(6) Palacio, M.; Mansuy, M. V.; Loire, G.; Barch-Ozette K. L.; Leduc, P.; Barkigia, K. M.; Fajer, J.; Battioni, P.; Mansuy, D. *Chem. Commun*. **2000**, 1907-1908.

(7) Kadish, K. M.; Ou, Z. P.; Tan, X. Y.; Boschi, T.; Monti, D.; Fares, V.; Tagliatesta, P. *J.Chem. Soc., Dalton Trans*. **1999**, 1595-1601.

(8) Sibilia, S. A.; Czernuszewicz, R. S.; Crossley, M. J.; Spiro, T. G. *Inorg. Chem.* **1997**, *36*, 6450-6453.

(9) Ostrowski, S.; Grzyb, S. *Tetrahedron Lett.* **2012**, *53*, 6355-6357.

(10) Li, B. H.; Ou, Z. P.; Meng, D. Y.; Tang, J. J.; Fang, Y. Y.; Kadish, K. M. *J. Inorg. Biochem*. **2014**, *136*, 130-139.

(11) Crossley, M. J.; King, L. G. and Simpson, J. L. *J. Chem. Soc., Perkin Trans. 1: Org. Bio-Org. Chem.* **1997**, 3087-3096.

(12) Crossley, M. J.; King, L. G. *J. Chem. Soc., Perkin Trans. 1: Org. Bio-Org. Chem*. **1996**, 1251-1260.

(13) Crossley, M. J.; Gosper, J. J.; Wilson, M. G. *J. Chem. Soc., Chem.Comm.* **1985**, 1798-1799.

(14) Catalano, M. M.; Crossley, M. J.; King, L. G. *J. Chem. Soc., Chem. Comm.* **1984**, 1537-1538.

(15) Crossley, M. J.; Sheehan, C. S.; Khoury, T.; Reimers, J. R.; Sintic, P. J. *New J. Chem.* **2008**, *32*, 340-352.

(16) Ou, Z. P.; Kadish, K. M.; E, W.; Shao, J. G.; Sintic, P. J.; Ohkubo, K.; Fukuzumi, S.; Crossley, M. J. *Inorg. Chem.* **2004**, *43*, 2078-2086.

(17) Martelli, C.; Canning, J.; Khoury, T.; Skivesen, N.; Kristensen, M.; Huyang, G.; Jensen, P.; Neto, C.; Sum, T.J.; Hovgaard M. B.; Gibson B. C.; Crossley M. J. *J. Mat. Chem.* **2010**, *20*, 2310-2316.

(18) Sun, Z. C.; She, Y. B.; Zhou, Y.; Song, X. F.; Li, K. *Molecules* **2011**, *16*, 2960-2970.

(19) Kadish, K. M.; Lin, X. Q.; Ding, J. Q.; Wu, Y. T.; Araullo, C. *Inorg. Chem*. **1986**, *25*, 3236-3242.

(20) Sintic, P. J.; E, W.; Ou, Z. P.; Shao, J. G.; McDonald, J. A.; Cai, Z. L.; Kadish, K. M.; Crossley, M. J.; Reimers, J. R. *Phys. Chem. Chem. Phys*. **2008**, *10*, 515-527.

(21) Kadish, K. M.; E, W.; Sintic, P. J.; Ou, Z. P.; Shao, J. G.; Ohkubo, K.; Fukuzumi, S.; Govenlock, L. J.; McDonald, J. A.; Try, A. C.; Cai, Z. L.; Reimers, J. R.; Crossley, M. J. *J. Phys. Chem. B;* **2007**, *111*, 8762-8774.

(22) Yang, S.; Sun, B.; Ou, Z. P.; Meng, D. Y.; Lu, G. F.; Fang, Y. Y.; Kadish, K. M. *J. Porphyrins Phthalocyanines* **2013**, *17*, 857-869.

(23) Kadish, K. M., Van, Caemelbecke E.; Royal, G. *The Porphyrin Handbook*, Kadish, K. M.; Smith, K. M.; Guilard, R. Eds., Academic Press: New York, **2000**, *8*, Ch. 55, 1-144.

(24) Stefanelli, M.; Pomarico, G.; Tortora, L.; Nardis, S.; Fronczek, F. R.; McCandless, G. T.; Smith, K. M.; Manowong, M.; Fang, Y.; Chen, P.; Kadish, K. M.; Rosa, A.; Ricciardi, G.; Paolesse, R. *Inorg. Chem.* **2012**, *51*, 6828-6942.

(25) Nardis, S.; Stefanelli, M.; Mohite, P.; Pomarico, G.; Tortora, L.; Manowong, M.; Chen, P.; Kadish, K. M.; Fronczek, F. R.; McCandless, G. T.; Smith, K. M; Paolesse, R. *Inorg. Chem.* **2012**, *51*, 3910-3920.

(26) Adler, A. D.; Longo, F. R.; Finarelli, J. D.; Goldmacher, J.; Assour, J. and Korsakoff, L. *J. Org. Chem.* **1967**, *32*, 476

(27) Rochford, J. and Galoppini, E. *Langmuir* **2008**, *24*, 5366-5374.

(28) Lin, T,; Shang, X. S.; Adisoejoso, J.; Liu, P. N.; Lin, N. *J. Am. Chem. Soc.* **2013**, *135*, 3576-3582.

(29) El-Khouly, M. E. J. B.; Kay, K-Y.; Ito, O.; Fukuzumi, S. *J. Phys. Chem.* **2009**, *113*, 15444-15453.

(30) Ostrowski, S.; Mikus, A.; Shim, Y. K.; Lee, J-C.; Seo, E-Y.; Lee, K-I.; Olejnik, M. *Heterocycles* **2002**, *57*, 1615-1626.

(31) To, W-P.; Liu, Y.; Lau, T-C.; Che, C-M.; *Chem. Eur. J.* **2013**, *19*, 5654-5664.

(32) Gabrielsson, A.; Lindsay, Smith.; J, R.; Perutz, R. N. *Dalton Trans*. **2008**, 4259-4269.

CHAPTER FOUR

Electrochemical and Spectroelectrochemical Studies of Diphosphorylated Metalloporphyrins. Generation of A Phlorin Anion Product

4.1 Introduction

Phosphonate derivatives have been recognized as convenient molecular precursors for functional materials starting from the late 1970s.[1-10] Ongoing research has focused on the development of new scaffolds and design strategies for their assembly.[11,12] Porphyrins are versatile functional molecules which have been used in catalysis, light harvesting, molecular sensing, and have gained extensive attention in material chemistry. Indeed, structural, photophysical, magnetic, electronic, and catalytic properties of tetrapyrrolic macrocycles are widely used in natural and artificial processes. The assemblage or immobilization of these derivatives provides attractive and simple routes to obtain advanced functional materials, including catalysts and photo- or electro-active materials.[7,13-17] Early studies on the immobilization of phosphoryl-substituted porphyrin derivatives[18-24] have gained a renewed interest after the development of new synthetic approaches towards metalloporphyrins bearing peripheral phosphorous-containing groups at the *β*-pyrrole and/or the *meso*-positions of the porphyrin macrocycle.[25,26] Moreover, phosphonate diesters were recently recognized as important molecular building blocks to mimic the natural photosynthesis process and to construct coordination polymers.[27-43]

Along these lines, it is important to gain insight into the electrochemical behavior of these porphyrins due to the importance of electron-transfer processes for catalytic and photochemical studies of supramolecular architectures and hybrid functional materials.[27]

Despite the large interest in phosphorylated porphyrins, only a few studies have been dedicated to elucidating, in detail, the electrochemical and spectroelectrochemical properties of porphyrins containing $P(O)(OR)_2$ at a peripheral position of the macrocycle where R is an alkyl group.[28-31] An initial study on the electrochemistry of *meso*-diphosphoryl porphyrins showed the unexpected presence of three reductions[28,29] but only the first was characterized and no spectroscopic measurements were made on the electroreduction products which would be needed for a mechanistic characterization of the reactions which occurred in solution

following electron transfer. This is addressed in the current chapter which expands upon the number of examined compounds and reports the electrochemistry and spectroelectrochemistry of two series of *meso*-bis(diethoxyphosphoryl)porphyrins in three non-aqueous solvents (see structures in Chart 4-1). One aim of the work described in this chapter is to characterize electrochemistry of the *meso*-substituted phosphoryl porphyrins while another is to examine how the nature of the central metal ion, solvent and/or the site of electron transfer will influence the electronic properties and oxidation/reduction mechanisms of these compounds.

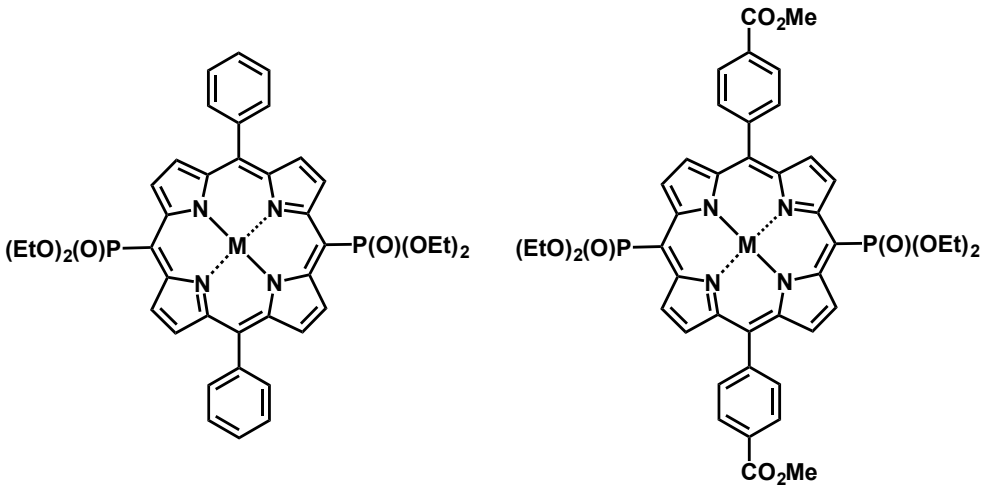

M = 2H, Ni(II), Cu(II), Pd(II), Zn(II), Cd(II), Co(II)

Chart 4-1. Structures of investigated porphyrins.

4.2 Results and Discussion

4.2.1 Synthesis

5,15-bis-(diethoxy-phosphoryl)-10,20-diphenylporphyrin (**$1H_2$**) and 5,15-bis-(diethoxy-phosphoryl)-10,20-di(*para*-carbomethoxyphenyl)porphyrin (**$2H_2$**) were obtained according to the Hirao reaction.[32] Metalation was performed using the traditional porphyrin coordination chemistry approach and consisted of reacting the free-base pophyrin with acetates of the target metal ion. The synthesis were done by our collaborator and detailed synthesis method are given in the literature.[66]

4.2.2 Electrochemistry

The electrochemical properties of each compound were examined in three non-aqueous solvents (PhCN, CH_2Cl_2 and pyridine) containing TBAP as supporting electrolyte. Half-wave potentials for oxidation and reduction in each solvent are given in Tables 4-1 (PhCN), 4-2 (Py) and 4-3 (CH_2Cl_2) and the electrochemical properties are discussed below, first for the porphyrins with redox inactive central metal ions and then for the Co(II) derivatives which undergo oxidation and reduction at the metal center to give Co(III) and Co(I) derivatives.

Table 4-1. Half-wave potentials (V vs SCE) for ring-centered redox reactions of investigated compounds in PhCN, containing 0.1 M TBAP (Data from this work are good to ±10 mV).

Compound	M	Oxidation		Reduction			H-L Gap	ref
		2nd	1st	1st	2nd	3rd		
$(Ph)_2(PO(OEt)_2)_2$PorM 1	2H	1.28	1.28	-0.77	-1.28	-1.70	2.05	28
	Ni	1.33	1.25	-0.83	-1.40	-1.76	2.08	*tw*
	Cu	1.36	1.22	-0.86	-1.43[a]	-1.73	2.08	28
	Pd	1.76[a]	1.32	-0.90	-1.49[a]	-1.81	2.22	*tw*
	Zn	1.32[a]	1.06	-0.97	-1.42[a]		2.13	28
	Cd	1.45[a]	1.05	-1.13	-1.43	-1.88[a]	2.18	*tw*
$(PhCOOMe)_2(PO(OEt)_2)_2$PorM 2	2H	1.36	1.36	-0.68	-1.20	-1.52	2.04	*tw*
	Ni	1.30	1.30	-0.81	-1.36	-1.64	2.11	*tw*
	Cu	1.36	1.22	-0.82	-1.34	-1.60[b]	2.04	*tw*
	Zn	1.24	1.10	-0.96	-1.40[a]	-1.80	2.06	*tw*
	Cd	1.14	1.14	-0.89	-1.32[a]	-1.79	2.03	*tw*
(TPP)M 3	2H	1.35	1.05	-1.19	-1.53		2.20	51
	Ni	1.13	1.02	-1.26	-1.75		2.28	52
	Cu	1.33	0.99	-1.28	-1.74		2.27	53
	Pd	1.55	1.14	-1.34	-1.80		2.48	54
	Zn	1.09	0.78	-1.32	-1.71		2.16	54
	Cd		0.72	-1.34			2.06	55

[a]Irreversible peak potential at scan rate = 0.1 V/s; [b]Additional peak observed at $E_{1/2}$ = -1.70 V; [c]Reduction of phlorin generated in solution after second electron addition.

Table 4-2. Half-wave potentials (V vs SCE) of investigated compounds with redox-inactive metal centers in Py containing 0.1 M TBAP (Data are good to ±10 mV).

Compound	M	Reduction		
		1st	2nd	3rd
$(Ph)_2(PO(OEt)_2)_2$Por 1	2H	-0.79	-1.33	
	Ni	-0.91	-1.48	-1.84
	Cu	-0.95	-1.47	-1.79
	Pd	-0.88	-1.45	-1.81
	Cd	-0.98	-1.55	-1.96
	Zn	-0.97	-1.53	-1.94
$(PhCOOMe)_2(PO(OEt)_2)_2$Por 2	2H	-0.74	-1.27	---
	Ni	-0.91	-1.44	-1.72
	Cu	-0.91	-1.41	-1.68
	Zn	-1.02	-1.59	-1.99
	Cd	-0.94	-1.48	-1.96[a]

[a]Additional peak observed at $E_{1/2}$ = -1.79 V

Table 4-3. Half-wave potential (V vs SCE) of investigated compounds in CH_2Cl_2, 0.1 M TBAP (Data are good to ±10 mV).

Macrocycle	M	Oxidation			Reduction			H-L
		3rd	2nd	1st	1st	2nd	3rd	Gap
$(Ph)_2(PO(OEt)_2)_2$PorM 1	2H		1.26	1.26	-0.79	-1.29	-1.75	2.05
	Co	1.40	1.30	0.68	-0.67	-1.60[a]	-1.76[a]	---
	Ni	1.79	1.34	1.21	-0.90	-1.39	-1.80	2.11
	Cu		1.36	1.23	-0.89	-1.39	-1.75	2.12
	Cd		1.46[a]	1.04	-1.12	-1.34[a]	-1.92	2.16
	Zn		1.47	1.02	-1.02	-1.40		2.04
	Pd		1.67	1.31	-0.90	-1.43[a]	-1.78	2.21
$(PhCOOMe)_2(PO(OEt)_2)_2$PorM 2	2H		1.33	1.33	-0.74	-1.21	-1.57	2.07
	Co	1.43	1.33	0.71	-0.64	-1.54[a]	-1.79[a]	---
	Ni	1.87	1.35	1.25	-0.86	-1.36	-1.68	2.11
	Cu		1.34	1.25	-0.88	-1.38	-1.66	2.13
	Cd		1.10	1.10	-1.08	-1.60[a]	-1.87	2.18

[a]Irreversible peak potential at scan rate = 0.1 V/s.

4.2.3 Porphyrins with Redox-inactive Metal Centers. Phlorin Generation

Similar redox behavior is observed for the 2H, Cu^{II}, Ni^{II}, Cd^{II}, Zn^{II} and Pd^{II} porphyrins (**1M** and **2M**) in PhCN and CH_2Cl_2. These porphyrins with electroinactive metal centers undergo four ring-centered processes to give π cation radicals and dications upon oxidation and π anion radicals and dianions upon reduction. However, the second one-electron reduction producing a porphyrin dianion is followed by a fast chemical reaction, providing a species which can be reoxidized to give back the starting porphyrin or which can be reversibly reduced by one electron at more negative potentials.

An illustration of the chemical reaction involving the doubly reduced porphyrins is given by the series of cyclic voltammograms in Figure 4-1 for **1Pd** in PhCN and pyridine. Three reductions are observed in PhCN between 0.00 and -2.00 V vs SCE. All three redox-processes have similar cathodic peak currents, indicating the same number of electrons transferred in each step. The first reduction, at $E_{1/2}$ = -0.90 V, is reversible when switching the direction of the potential sweep at -1.20 V (top CV in Figure 4-1a) and the third reduction at $E_{1/2}$ = -1.81 V is also reversible in PhCN when scanning to -2.00 V (third CV in Figure 4-1a). This contrasts with the reduction of **1Pd** at $E_{1/2}$ = -1.49 V which has a shape consistent with a reversible one electron addition (E_{pc} - $E_{p/2}$ = 60 mV) on the forward scan and the lack of a coupled anodic peak on the reverse sweep. This can be related with the chemical reaction to give a product which undergoes an irreversible oxidation at E_{pc} = -0.13 V and a reversible reduction at $E_{1/2}$ = -1.81 V in PhCN.

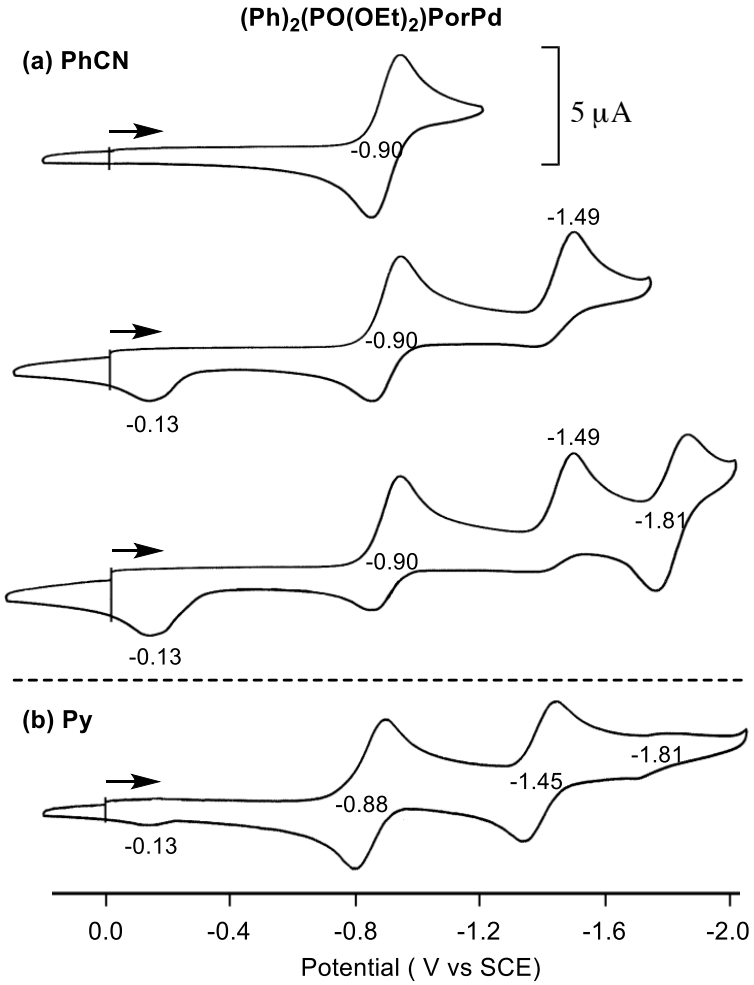

Figure 4-1. Cyclic voltammograms of $(Ph)_2(PO(OEt)_2)_2PorPd$ in (a) PhCN, (b) pyridine containing 0.1 M TBAP. Scan rate = 0.1 V/s.

I suspected that the product of the homogenous chemical reaction involved protonation of the doubly reduced porphyrins and the formation of a phlorin as earlier reported in the literature for (TPP)Zn and (TPP)H_2 which were chemically converted to a phlorin anion at the electrode surface after generation of the porphyrin dianion in dimethylformamide (DMF).[33,34] In order to prove this hypothesis, I switched to pyridine as a basic solvent. The cyclic voltammogram for **1Pd** under this solution conditions is shown in Figure 4-1b where the second reduction has become almost reversible while the currents for the processes at $E_{1/2}$ = -1.81 and E_p = -0.13 V are both significantly reduced in intensity, as compared to what is seen in PhCN (Figure 4-1a). A comparison of the electrochemistry for **1Pd** in PhCN and pyridine further suggests that the chemical reaction of the electrogenerated dianion involves protonation which would be minimized in the basic solvent, leading to a slower rate of the chemical reaction and reduced current for the third reduction.

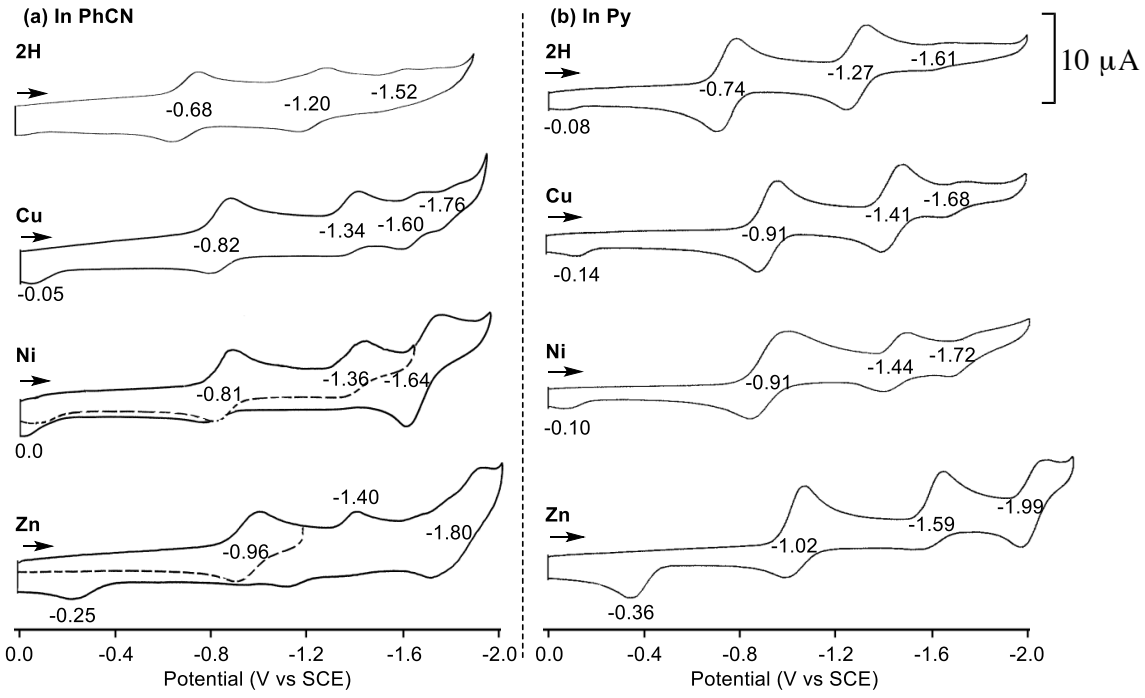

Figure 4-2. Cyclic voltammograms of investigated compounds $(PhCOOMe)_2(PO(OEt)_2)_2PorM$, where M = 2H, Cu, Ni and Zn in (a) PhCN and (b) Py, 0.1 M TBAP.

Similar solvent dependent redox behavior is seen for the 2H, Cu^{II} and Ni^{II} porphyrins as shown in Figure 4-2, where the currents for the third reduction at $E_{1/2}$ = -1.52 to -1.76 V in PhCN are significantly decreased in intensity when the measurement is carried out in the basic solvent pyridine. However, a different behavior is observed for the Zn^{II} porphyrin in pyridine where the third reduction remains well-defined, suggested that the chemical reaction following formation of the porphyrin dianion varies not only with the solvent but also with the nature of the central metal ion.

Cyclic voltammograms for reduction of the porphyrins with redox-inactive central metal ions in CH_2Cl_2, 0.1 M TBAP are similar to those in PhCN and an example of the voltammograms in CH_2Cl_2 are illustrated in Figure 4-3 for **1Zn** and **1Cd**. In this figure, the scan is first reversed at -1.20 V following the first reduction and then reversed at -2.00 V, a potential where all three reductions can be observed. The current-voltage curves are well-defined for both porphyrins and the measured half-wave or peak potentials are virtually identical to each other, as would be expected for these two transition metal porphyrins.

In summary, the cyclic voltammetric data in Figures 4-1, 4-2 and 4-3 are consistent with two one-electron reductions at the conjugated macrocycle followed by formation of an electroactive phlorin anion as shown in Scheme 4-1 which presents the proposed mechanism. The rationale for this mechanism is based on comparisons with earlier published literature data for the electroreduction of (TPP)Zn[34] and $(TPP)H_2$[33] in DMF as well as by the UV-vis spectroelectrochemistry data described below.

4.2.4 Spectroelectrochemical Monitoring of 1M Reduction Products, Where M = Cu(II), Ni(II) and Pd(II)

Examples of the UV-vis spectral changes obtained during the first two reductions of **1M** in PhCN are shown in Figure 4-3 for the porphyrins with M = Cu(II), Ni(II) and Pd(II). As presented in Scheme 4-1, the first one electron reduction leads to formation of a porphyrin π-anion radical and the spectral changes illustrated in Figure 4-3a are in each case consistent

with this assignment. The final spectrum of the singly reduced porphyrins exhibits a red-shifted and decreased intensity Soret band along with decreased intensity Q bands. This spectrum is characteristic of a porphyrin π anion radical bands in the near-IR region of the spectrum.

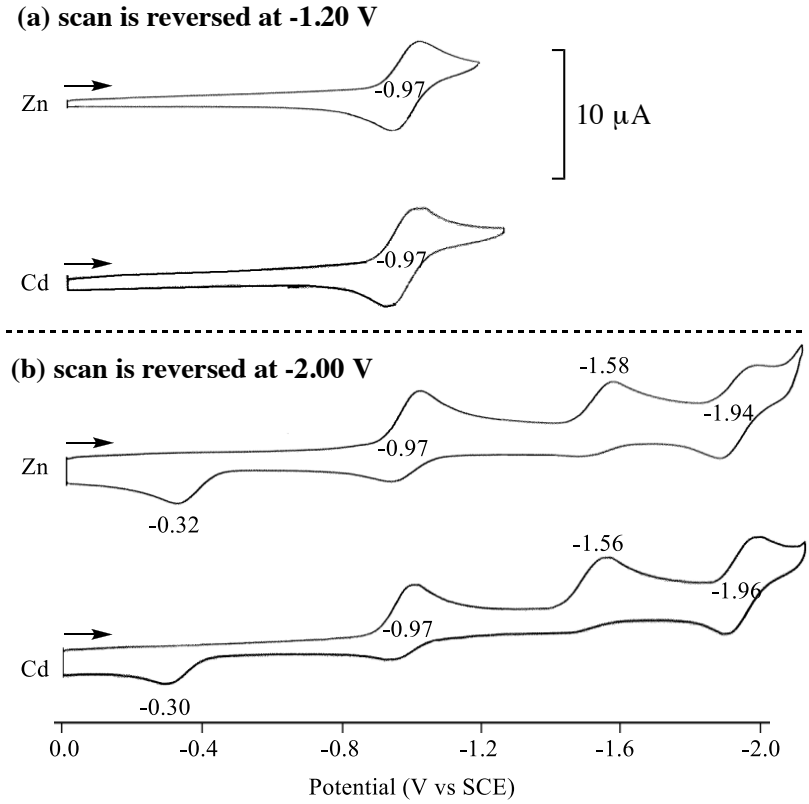

Figure 4-3. Cyclic voltammograms of $(Ph)_2(PO(OEt)_2)_2PorM$, M = Zn and Cd in CH_2Cl_2 containing 0.1 M TBAP, where (a) the scan is reversed at -1.20 V and (b) the scan is reversed at -2.00 V.

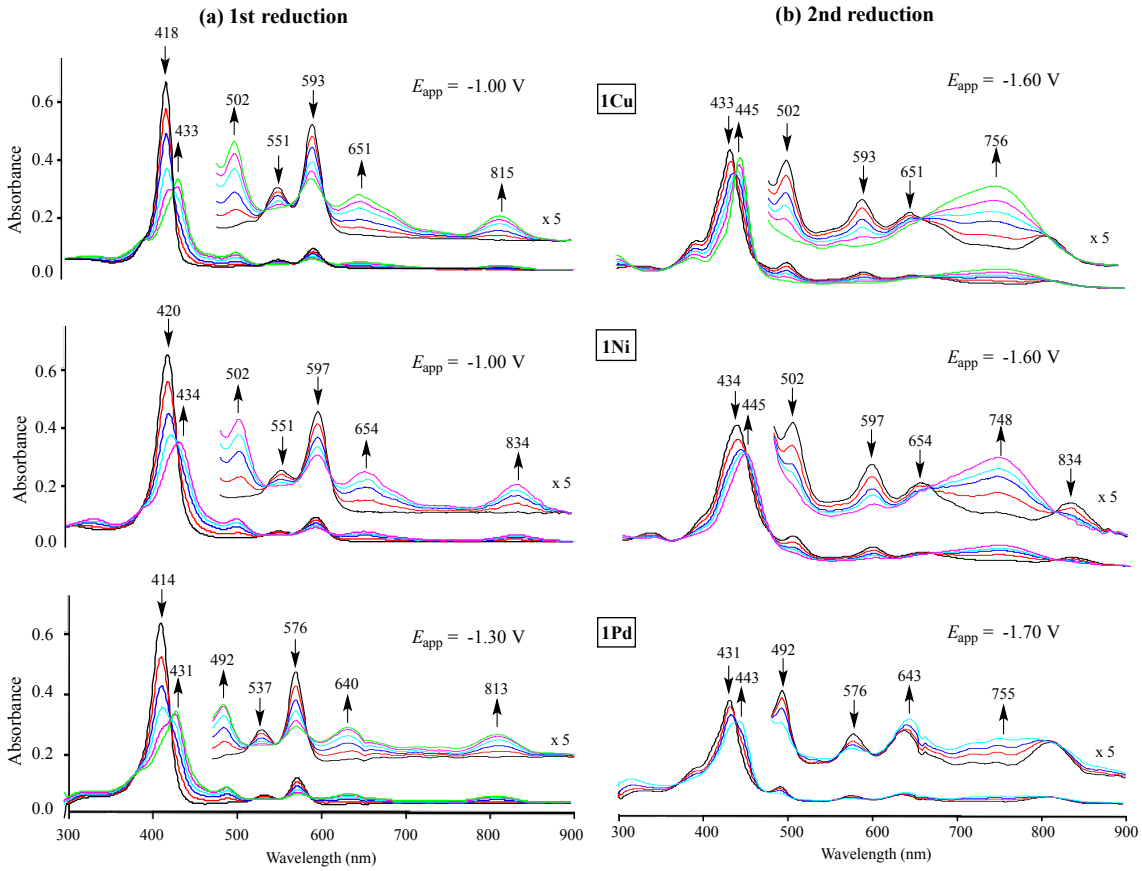

Figure 4-4. UV-vis spectral changes for solutions of $(Ph)_2(PO(OEt)_2)_2$PorM, M = Cu, Ni and Pd during (a) first reduction and (b) second reduction in PhCN, 0.1 M TBAP.

Scheme 4-1. Proposed mechanism for electron transfer of investigated compounds. The products in the scheme are those for the reduction of **$Ph_2(P(O)OEt)_2PorPd$** in PhCN.

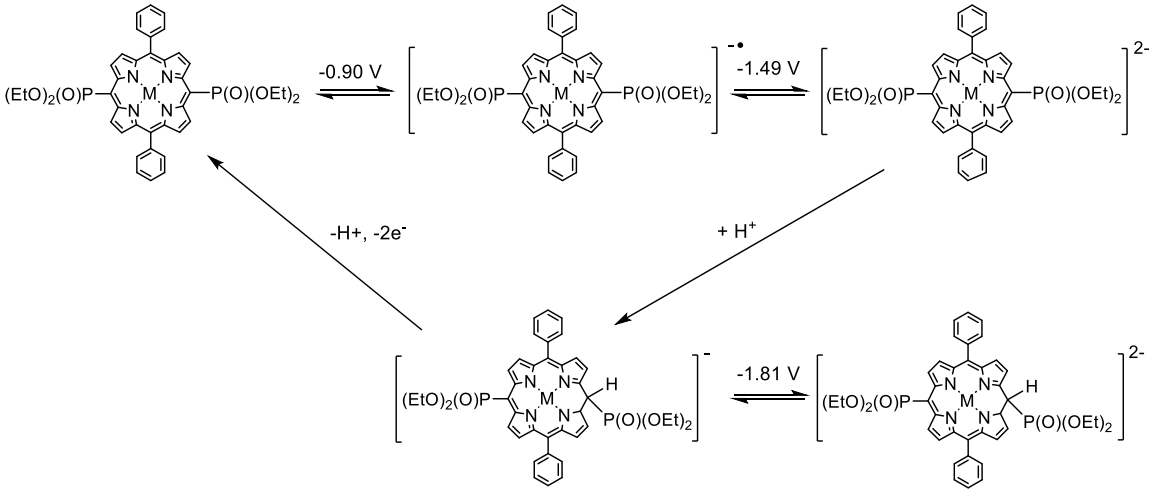

Several isosbestic points can be noted in the spectra during conversion of the neutral porphyrin to its radical monoanionic form and the final spectrum for all three porphyrins in Figure 4-4a (**1Cu**, **1Ni** and **1Pd**) are similar to each other. Each singly reduced porphyrin has a band at 431-433 nm in the Soret region of the spectrum and four bands in the visible and near-IR region, the three most intense of which are located at around 500 nm, 650 nm and 820 nm. By way of comparison, the porphyrin π anion radical of (TPP)Pd is characterized by bands at 438, 619 and 869 nm in CH_2Cl_2 while the π anion radical of (TPP)Zn in DMF has bands at 457, 725, 806 and 905 nm.

The second controlled potential reduction of the Cu(II), Ni(II) and Pd(II) porphyrins at -1.60 or -1.70 V gave the spectral changes illustrated in Figure 4-4b. Again, several isosbestic points are observed and the spectrum of the final reduction products are similar to each other, being characterized by a band in the Soret region at 443-445 nm and a broad band at 748-756 nm. These spectra are assigned as belonging to a phlorin anion and are similar to spectra reported for the electrogenerated phlorin dianions of (TPP)Zn and (TPP)H_2 in DMF.[33,34]

4.2.5 Electrooxidation

Cyclic voltammograms illustrating oxidation of the phosphoryl porphyrins with redox-inactive central ions are shown in Figure 4-5 and a summary of potentials for each oxidation are given in Table 4-1 (PhCN) and Table 4-3 (CH_2Cl_2). Two of the five porphyrins in **2M** (Cu^{II} and Zn^{II}) exhibit stepwise one-electron oxidations and three (2H, Ni^{II} and Cd^{II}) are characterized by two overlapping one-electron-transfer process at the same half-wave potential (see Figure 4-5). Only **$1H_2$** in the case of the **1M** derivatives shows overlapping processes upon conversion of the neutral porphyrin to its dicationic form.

An overlapping of the two porphyrin ring oxidations has often been observed for Ni porphyrins[35-39] and this has been explained as resulting from an enhanced axial binding of ClO_4^- from the supporting electrolyte to the doubly oxidized species. This may also be the case

for the H_2 and Cd(II) species in this study where a direct conversion of the neutral porphyrin to its dication radical form occurs in a single step at the same half-wave potential.

Also, as earlier described in the literature, the oxidation of phosphoryl porphyrins is harder than for oxidation of related TPP compounds,[29] with the magnitude of positive shifts in $E_{1/2}$ for the first one electron abstraction ranging from 230 mV in the case of the Cu(II) porphyrins (0.99 V for (TPP)Cu *vs.* 1.22 V for **1Cu**) to 420 mV in the case of the Cd(II) derivatives (0.72 V for (TPP)Cd *vs.* 1.14 V for **1Cd**). Finally, a third oxidation is observed for **1Ni** and **2Ni**; consistent with the well-known Ni(II)/Ni(III) reactions described in earlier publications.[36-38]

4.2.6 Electrochemistry of 1Co and 2Co

The investigated cobalt porphyrins differ from the other phosphoryl porphyrins with electro-inactive central metal ions in that the first one-electron addition and first one-electron abstraction are both metal-centered processes, Co(II)/Co(I) upon reduction and Co(II)/Co(III) upon oxidation. Three additional redox processes are also seen and these correspond to the formation of a Co(III) π cation radical and dication upon oxidation and a Co(I) π anion radical upon reduction (see $E_{1/2}$ values in Table 4-3).

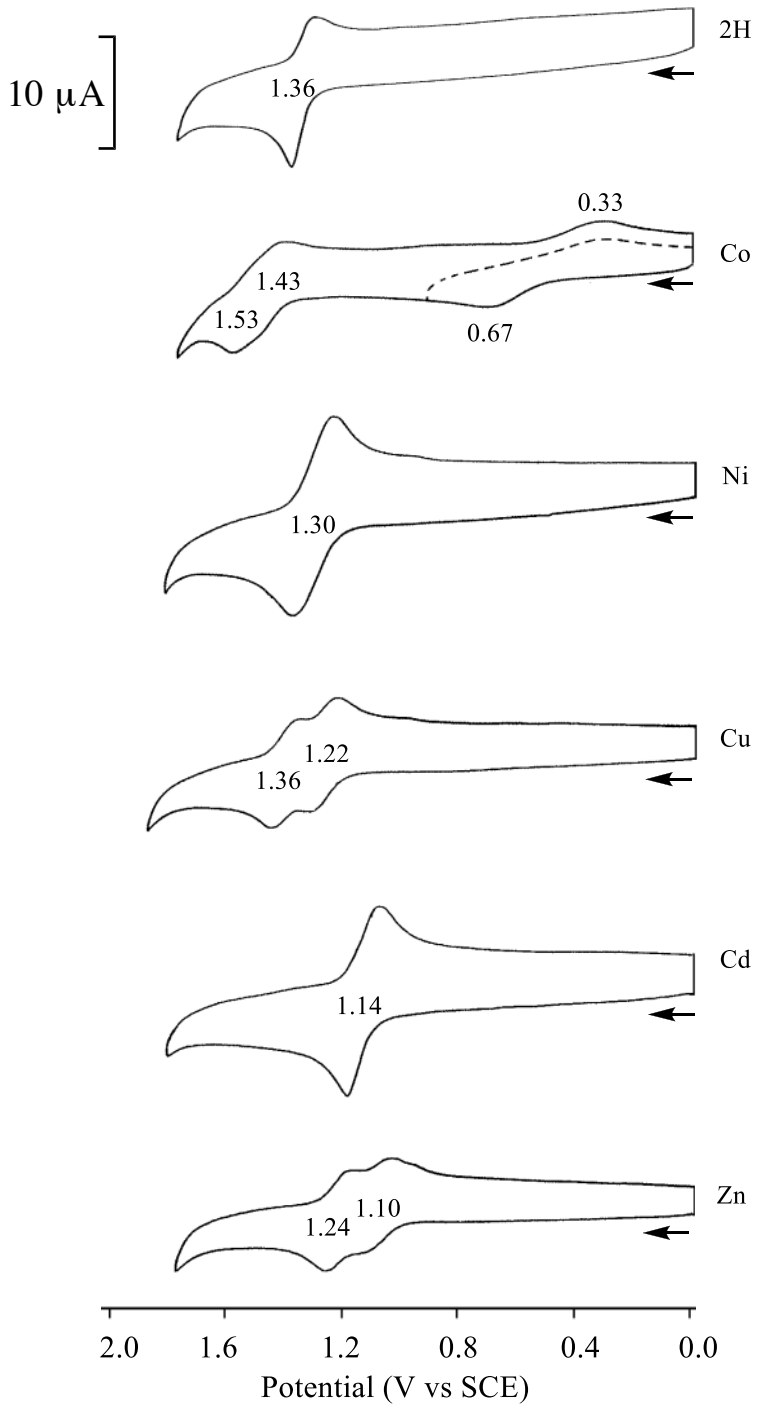

Figure 4-5. Cyclic voltammograms (illustration of oxidations) of $(PhCOOMe)_2(PO(OEt)_2)_2PorM$ in PhCN, 0.1 M TBAP.

Table 4-4. Half-wave potentials (V vs SCE) of Co(II) porphyrins in CH_2Cl_2, PhCN and Py, 0.1 M TBAP (Data from this work are good to ±10 mV).

Compound	Solvent	Oxidation				Reduction		Ref
		Ring		$Co^{II/III}$	$Co^{III/II}$	$Co^{II/I}$	Ring	
		3rd	2nd	*E*pa	*E*pc	1st	2nd	
$(Ph)_2(PO(OEt)_2)_2$Por 1	CH_2Cl_2	1.40	1.30	0.58	0.78	-0.67	-1.60[a]	*tw*
	PhCN	1.49	1.37	0.64	0.33	-0.68	-1.55	*tw*
	Py			-0.12	-0.34	-0.98	-1.61	*tw*
$(PhCOOMe)_2(PO(OEt)_2)_2$Por 2	CH_2Cl_2	1.43	1.33	0.61	0.81	-0.64	-1.54[a]	*tw*
	PhCN	1.53	1.43	0.67	0.34	-0.65	-1.51	*tw*
	Py			-0.04	-0.34	-0.95	-1.58	*tw*
TPP 3	CH_2Cl_2	1.16	0.97	0.78		-0.85	-2.05	56
	PhCN	1.39	1.20	0.62	0.38	-0.85	-1.97	57
	Py			-0.21[b]		-1.03		58

[a]Irreversible peak potential at scan rate = 0.1 V/s; [b]$E_{1/2}$ values for reversible Co^{II}/Co^{III} process.

Unlike the above discussed porphyrins with electro-inactive central metal ions, there is no evidence for formation of a phlorin anion after the second reduction. This is consistent with the different sites of electron transfer and the different oxidation states of doubly reduced compounds in the two series of porphyrins, *i.e.*. Co(I) porphyrin π anion radicals in one case and M(II) porphyrin dianions in the other. As seen in Figure 4-6, the electrogenerated Co(I) porphyrin and Co(I) porphyrin π anion radical are both stable in PhCN containing 0.1 M TBAP and there is no evidence for a coupled chemical reaction on the cyclic voltammetry timescale in this solvent.

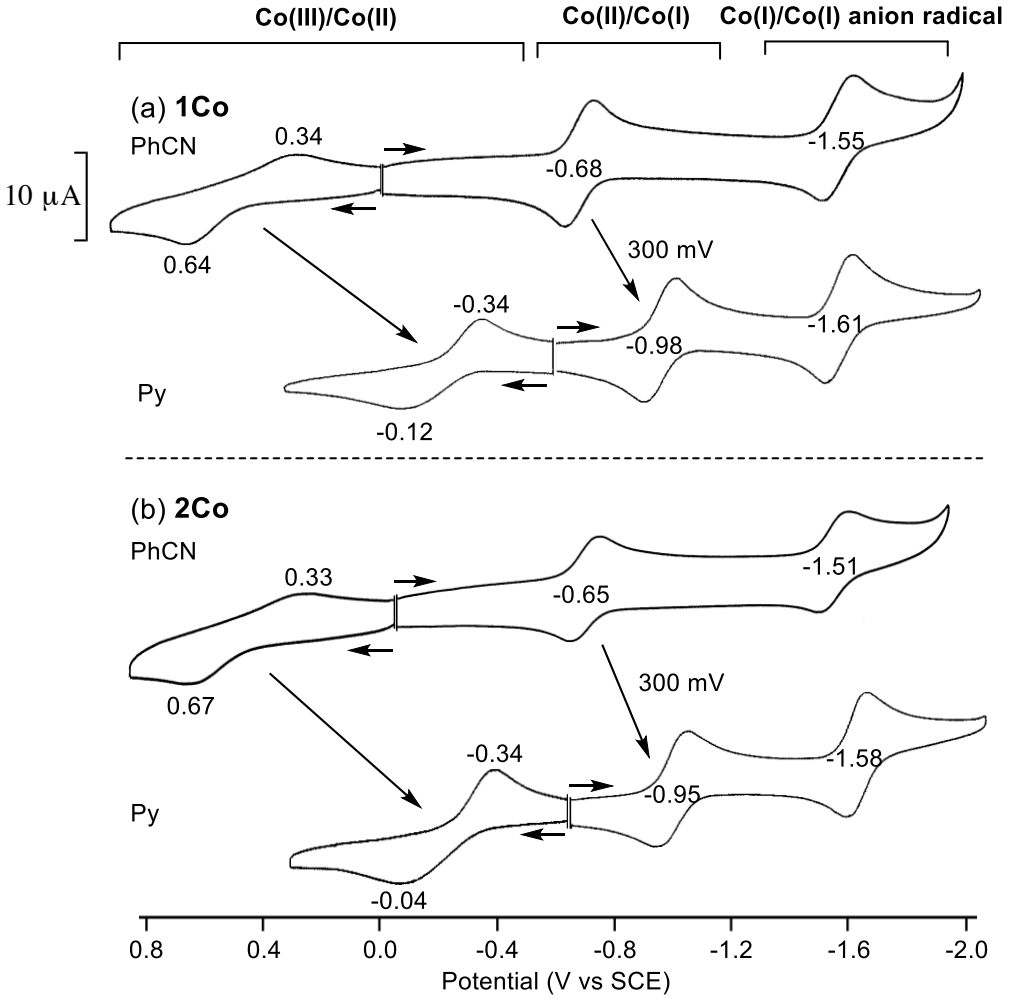

Figure 4-6. Cyclic voltammograms of (a) $(Ph)_2(PO(OEt)_2)_2PorCo$ and (b) $(PhCOOMe)_2(PO(OEt)_2)_2PorCo$ in PhCN and pyridine, 0.1 M TBAP.

Well-defined cyclic voltammograms are also obtained for the two diphosphorylated cobalt porphyrins in pyridine (Figure 4-6), with the Co(II)/Co(I) and Co(II)/Co(III) processes both having $E_{1/2}$ values which are shifting negatively from half-wave potentials for the same metal-centered reactions in PhCN. The large negative shift in potentials for these two reactions of **1Co** and **2Co** are consistent with the strong binding of two pyridine molecules to Co(III), one pyridine molecule to Co(II) and no pyridine binding to Co(I). This is consistent with results in the literature for related cobalt porphyrins[41-43] and was proven in the current study by an electrochemically monitored titration of **2Co** with pyridine in PhCN (Figure 4-7). All axial ligands are lost upon formation of Co(I) which is then reduced to give a stable Co(I) porphyrin π anion radical at $E_{1/2}$ = -1.55 (**1Co**) or -1.51 V (**2Co**) in PhCN. Because a porphyrin dianion is the reactive species which is converted to a phlorin in PhCN and CH_2Cl_2, this reaction does not occur for the two Co(II) phosphoryl porphyrins where the highest level of reduction within the negative potential limit of the solvent is the Co(I) π anion radical.

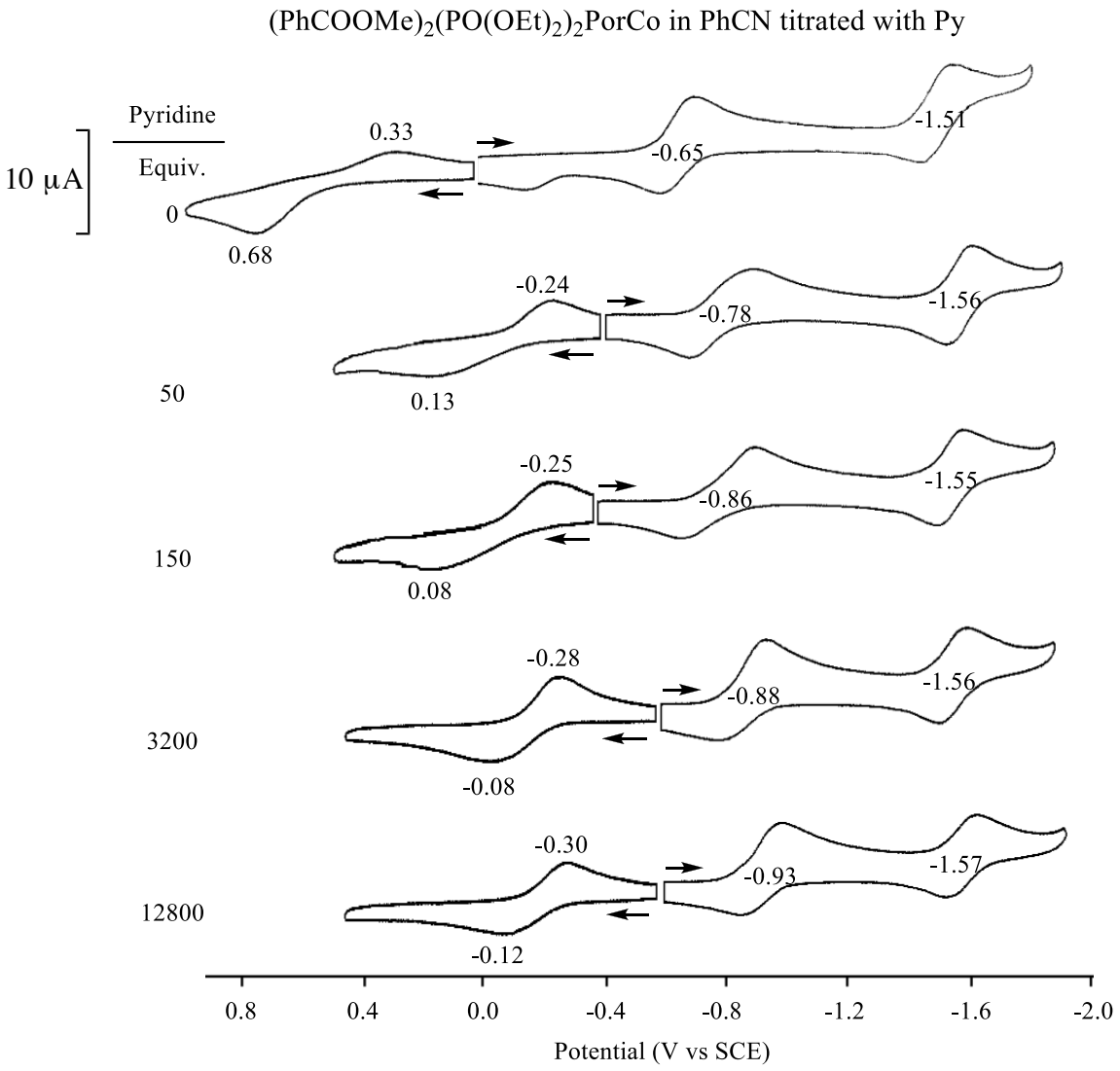

Figure 4-7. Cyclic voltammograms of $(PhCOOMe)_2(PO(OEt)_2)_2PorCo$ in PhCN containing 0.1 M TBAP with addition of 0-12800 equivalence of pyridine. Scan rate = 0.1 V/s.

UV-vis spectra of the Co(III), Co(II) and Co(I) forms of the two cobalt porphyrins are shown in Figure 4-8. During first reduction of **1Co**, the Co(II) porphyrins bands at 416 and 592 nm decrease in intensity as new bands assigned to the Co(I) porphyrin grow in at 351, 383, 432 and 572 nm. The Co(III) product of the first oxidation has bands at 441 and 605 nm and there are no absorptions between 700 to 900 nm, consisten with electrogeneration of a Co(III) porphyrin with unoxidized macrocycle. Two ring-centered oxidations of the Co(III) porphyrins are then observed at more positive potentials of 1.37 and 1.49 V (**1Co**) or 1.43 and 1.53 V (**2Co**).

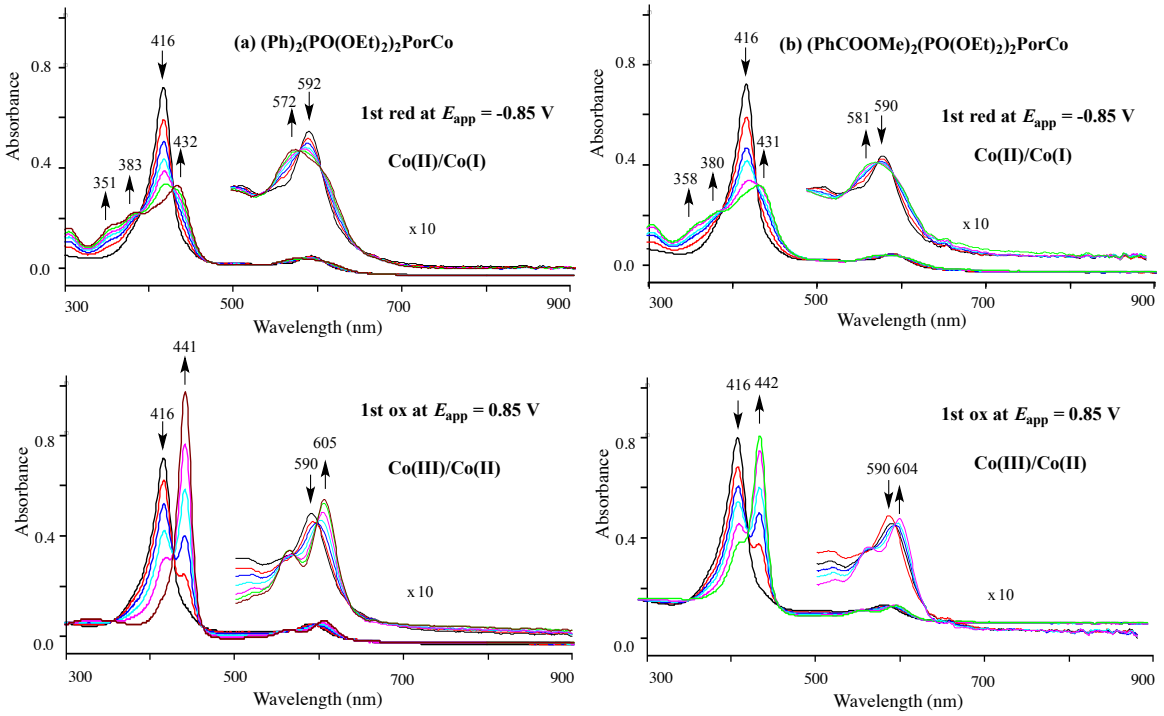

Figure 4-8. UV-vis spectral changes for solutions of (a) $(Ph)_2(PO(OEt)_2)_2PorCo$ and (b) $(PhCOOMe)_2(PO(OEt)_2)_2PorCo$ during the first reduction and the first oxidation in PhCN, 0.1 M TBAP.

4.2.7 Calculations of the Electronic Structure[66]

The theoretical calculations were done by our collaborators, and the result further confirms conclusions from the electrochemical and spectroelectrochemical study. Porphyrins studied herein have two different types of *meso*-substituents and therefore the formation of a phlorin from the porphyrin dianion can occur upon protonation at the 5,15-*meso*-carbon atoms having phosphoryl groups or at the 10, 20-*meso*-carbon atoms, with phenyl groups. To determine the most favorable protonation site, calculations for the electronic structure of the porphyrin dianions have been carried out in terms of analysis of the Fukui function[59-61] ($f^{-}(\mathbf{r})$) using **1Ni** as an example. This approach was previously applied to explain the reactivity of various metal porphyrinates,[62-64] including their aza-analogues.[65]

Since protonation can be considered as an electrophylic attack of H^+ on the dianion, the three-dimensional distribution of the $f^{-}(\mathbf{r})$ function were investigated by our collaborator[66] and the Fukui function $f^{-}(\mathbf{r})$ plotted for dianion **1Ni**$^{2-}$ is given in Figure 4-9. Analysis of the obtained map (Figure 4-9) provides evidence that the most reactive atoms of the dianion are located at the 5 and 15-*meso*-positions of the molecule.[66] These correspond to the phosphorylated carbon atoms, suggesting that they might be protonated, leading to phlorin anion formation. In contrast, protonation at the 10 and 20-*meso*-carbon atoms with phenyl groups was found to be less favorable. [66]

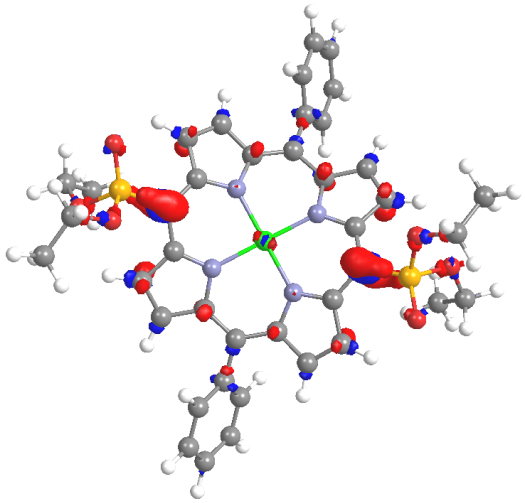

Figure 4-9. Fukui function $f^{-}(\mathbf{r})$ plotted for dianion **1Ni**$^{2-}$, isovalue – 3 x 10^{-3}, red and blue areas correspond to positive and negative values of $f^{-}(\mathbf{r})$. Figure is from Ref. 66.

The DFT optimized molecular structures of porphyrin **1Ni** and the phlorin anion, obtained by protonation of **1Ni**$^{2-}$ at the C5 atom were used for ZINDO/s calculations of their UV-vis spectra. Calculations were done by our collaborator[66] and the result revealed that formation of such a phlorin anion should result in a bathochromic shift of the Soret band and the appearance of a band shifted to the red with respect to the Q-band of the starting **1Ni** species (Figure 4-10). This calculated data is in agreement with the experimental data from spectroelectrochemistry (see Figure 4-4).

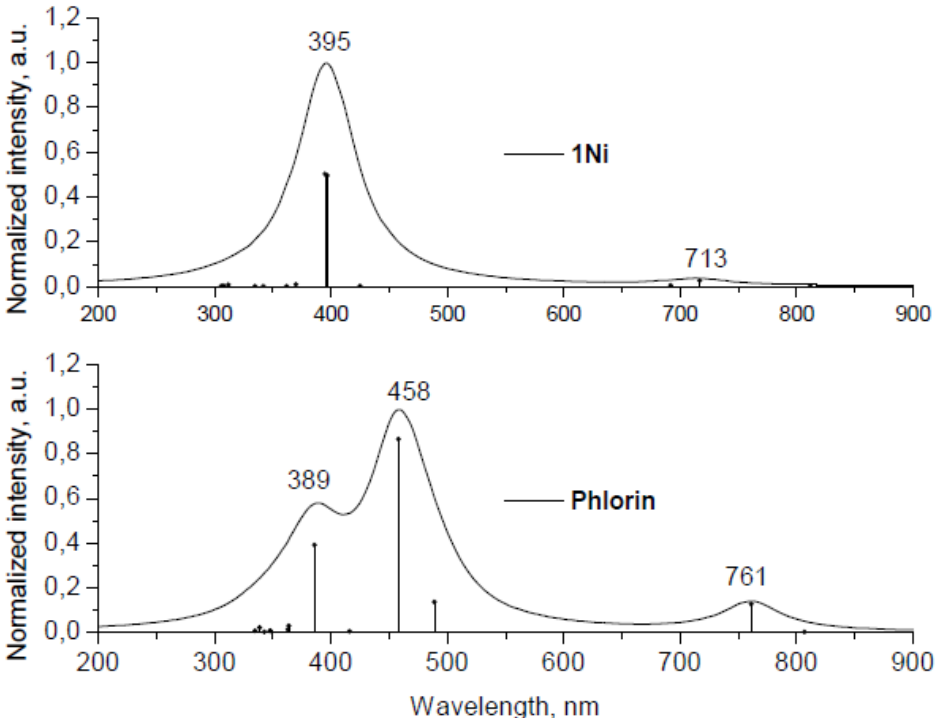

Figure 4-10. Calculated ZINDO/s spectra of **1Ni** and phlorin, formed by protonation of **1Ni**$^{2-}$ at C5 atom. Vertical lines correspond to calculated transitions, the curves correspond to Lorentzian lineshape with 30 nm linewidth. Figure is from Ref. 66.

4.2.8 Final Comments

I earlier demonstrated that the shift in reduction potential between (TPP)Zn and a related Zn porphyrins with one β-pyrrole phosphoryl group amounted to about 250 mV.[31] In the current study, I have examined phosphoryl porphyrins with two $P(O)(OEt)_2$ *meso*-substituents and negative shifts in reduction potentials of almost 500 mV are observed as compared to $E_{1/2}$ values for the same redox reactions of the related TPP derivatives.

The positive shift of oxidation potentials due to the electron-withdrawing $P(O)(OEt)_2$ substituents is less than that for reduction of the same compounds, and thus the phosphoryl-substituted porphyrins will have a smaller HOMO-LUMO gap than for the related TPP complexes or β-pyrrole mono-substituted phosphoryl porphyrins. The decrease in the HOMO-LUMO gap averages 120 mV upon going from (TPP)M to the diphosphoryl-substituted porphyrins with the same metal ion (see Table 4-1) and a slightly decreased HOMO-LUMO gap is then observed upon going from compounds in the **1M** series to those in **2M**. This results because the carbomethoxyl substituent on two *meso*-phenyl groups of **2M** is also electron-withdrawing and shows a larger substituent effect on the reduction potentials than on $E_{1/2}$ values for the oxidation.

4.3 References

(1) Alberti, G. *Acc. Chem. Res.* **1978**, *11*, 163-170.

(2) Cao, G.; Hong, H. G.; Mallouk, T. E. *Acc. Chem. Res.* **1992**, *25*, 420-427.

(3) Clearfield, A. *Prog. Inorg. Chem.* **1998**, *47*, 371-510.

(4) Clearfield, A.; Wang, Z. *J. Chem. Soc., Dalton Trans.* **2002**, 2937-2947.

(5) Thompson, M. E. *Chem. of Mater.* **1994**, *6*, 1168-1175.

(6) Vermeulen, L. A. **1997**, *44*, 143-166.

(7) Kalyanasundaram, K.; Grätzel, M. *Coord. Chem. Rev.* **1998**, *177*, 347-414.

(8) Maeda, K. *Microporous and Mesoporous Materials* **2004**, *73*, 47-55.

(9) Mutin, P. H.; Guerrero, G.; Vioux, A. *J. Mater. Chem.* **2005**, *15*, 3761-3768.

(10) Shimizu, G. K. H.; Vaidhyanathan, R.; Taylor, J. M. *Chem. Soc. Rev.* **2009**, *38*, 1430-1034.

(11) Gagnon, K. J.; Perry, H. P.; Clearfield, A. *Chem. Rev.* **2012**, *112*, 1034-1054.

(12) Queffelec, C.; Petit, M.; Janvier, P.; Knight, D. A.; Bujoli, B. *Chem. Rev.* **2012**, *112*, 3777-3807.

(13) Stern, C.; Bessmertnykh-Lemenue, A.; Gorbunova, Y.; Tsivadze, A.; Guilard, R. *Turkish J. Chem.* **2014**, *38*, 980-993.

(14) Lee, J.; Farha, O. K.; Roberts, J.; Scheidt, K. A.; Nguyen, S. T.; Hupp, J. T. *Chem. Soc. Rev.* **2009**, *38*, 1450-1459.

(15) Chou, J.-H.; Kosal, M. E.; Nalwa, H. S.; Rakow, N. A.; Suslick, K. S. In *The Porphyrin Handbook*; Kadish, K. M., Smith, K. M., Guilard, R., Eds.; Academic Press: San Diego, 2000; Vol. 6, 43-131.

(16) Suslick, K. S.; Bhyrappa, P.; Chou, J. H.; Kosal, M. E.; Nakagaki, S.; Smithenry, D. W.; Wilson, S. R. *Acct. of Chem. Res.* **2005**, *38*, 283-291.

(17) Zou, C.; Wu, C.-D. *Dalton Trans.* **2012**, *41*, 3879-3888.

(18) Ungashe, S. B.; Wilson, W. L.; Katz, H. E.; Scheller, G. R.; Putvinski, T. M. *JACS.* **1992**, *114*, 8717-8719.

(19) Deniaud, D.; Schollorn, B.; Mansuy, D.; Rouxel, J.; Battioni, P.; Bujoli, B. *Chem. Mater.* **1995**, *7*, 995-1000.

(20) Nixon, C. M.; Le Claire, K.; Odobel, F.; Bujoli, B.; Talham, D. R. *Chem. of Mater.* **1999**, *11*, 965-976.

(21) Deniaud, D.; Spyroulias, G. A.; Bartoli, J. F.; Battioni, P.; Mansuy, D.; Pinel, C.; Odobel, F.; Bujoli, B. *New J. Chem.* **1998**, *22*, 901- 905.

(22) Rao, P. D.; Littler, B. J.; Geier, G. R.; Lindsey, J. S. *J. Org. Chem.* **2000**, *65*, 1084

-1092.

(23) Li, Q. L.; Surthi, S.; Mathur, G.; Gowda, S.; Zhao, Q.; Sorenson, T. A.; Tenent, R. C.; Muthukumaran, K.; Lindsey, J. S.; Misra, V. *Appli. Phys. Lett.* **2004**, *85*, 1829 -1831.

(24) Loewe, R. S.; Ambroise, A.; Muthukumaran, K.; Padmaja, K.; Lysenko, A. B.; Mathur, G.; Li, Q. L.; Bocian, D. F.; Misra, V.; Lindsey, J. S. *J. Org. Chem.* **2004**, *69*, 1453-1460.

(25) Bessmertnykh-Lemeune, A. G.; Stern, C.; Gorbunova, Y. G.; Tsivadze, A. Y.Guilard, R. *Macroheterocycles* **2014**, *7*, 122-132.

(26) Atefi, F.; Arnold, D. P. *J. Porphyrins and Phthalocyanines* **2008**, *12*, 801-831.

(27) Harvey, P. D.; Stern, C.; Guilard, R. In *Handbook of Porphyrin Science* Kadish, K. M., Smith, K. M., Guilard, R., Eds.; World Scientific Publishing: Singapore, 2011; Vol. 11, 1-180.

(28) Sinelshchikova, A. A.; Nefedov, S. E.; Enakieva, Y. Y.; Gorbunova, Y. G.; Tsivadze, A. Y.; Kadish, K. M.; Chen, P.; Bessmertnykh-Lemeune, A.; Stern, C.; Guilard, R. *Inorg. Chem.* **2013**, *52*, 999-1008.

(29) Kadish, K. M.; Chen, P.; Enakieva, Y. Y.; Nefedov, S. E.; Gorbunova, Y. G.; Tsivadze, A. Y.; Bessmertnykh-Lemeune, A.; Stern, C.; Guilard, R. *J. Electroanal. Chem.* **2011**, *656*, 61-71.

(30) Matano, Y.; Matsumoto, K.; Terasaka, Y.; Hotta, H.; Araki, Y.; Ito, O.; Shiro, M.; Sasamori, T.; Tokitoh, N.; Imahori, H. *Chem. - Eur. J.* **2007**, *13*, 891-901.

(31) Fang, Y.; Kadish, K. M.; Chen, P.; Gorbunova, Y.; Enakieva, Y.; Tsivadze, A.; Bessmertnykh-Lemeune, A.; Guilard, R. *J. Porphyrins Phthalocyanines* **2013**, *17*, 1035-1045.

(32) Enakieva, Y. Y.; Bessmertnykh, A. G.; Gorbunova, Y. G.; Stern, C.; Rousselin, Y.; Tsivadze, A. Y.; Guilard, R. *Org. Lett.* **2009**, *11*, 3842-3845.

(33) Wilson, G. S.; Peychal-Heiling, G. *Anal. Chem.* **1971**, *43*, 545-550.

(34) Lanese, J. G.; Wilson, G. S. *J. Electrochem. Soc.* **1972**, *119*, 1039-1043.

(35) Fuhrhop, J.-H.; Kadish, K. M.; Davis, D. G. *JACS.* **1973**, *95*, 5140-5147.

(36) Kadish, K. M.; Van Caemelbecke, E.; Boulas, P.; D'Souza, F.; Vogel, E.; Kisters, M.; Medforth, C. J.; Smith, K. M. *Inorg. Chem.* **1993**, *32*, 4177-4178.

(37) Kadish, K. M.; Lin, M.; Van Caemelbecke, E.; De Stefano, G.; Medforth, C. J.; Nurco, D. J.; Nelson, N. Y.; Krattinger, B.; Muzzi, C. M.; Jaquinod, L.; Xu, Y.; Shyr, D. C.; Smith, K. M.; Shelnutt, J. A. *Inorg. Chem.* **2002**, *41*, 6673-6687.

(38) Fang, Y.; Senge, M. O.; Van Caemelbecke, E.; Smith, K. M.; Medforth, C. J.; Zhang,

M.; Kadish, K. M. *Inorg. Chem.* **2014**, *53*, 10772-10778.

(39) Kadish, K. M.; Van Caemelbecke, E.; Royal, G. In *The Porphyrin Handbook*; Kadish, K. M.; Smith, K. M.; Guilard, R. Eds.; Academic Press: New York, **2000**; *8*, 1-114.

(40) Zubatyuk, R. I.; Sinelshchikova, A. A.; Enakieva, Y. Y.; Gorbunova, Y. G.; Tsivadze, A. Y.; Nefedov, S. E.; Bessmertnykh-Lemeune, A.; Guilard, R.; Shishkin, O. V. *CrystEngComm*. **2014**, *16*, 10428-10438.

(41) Kadish, K. M.; Ou, Z.; Tan, X.; Boschi, T.; Monti, D.; Fares, V.; Tagliatesta, P. *J. Chem. Soc., Dalton Trans.* **1999**, 1595-1602.

(42) Fukuzumi, S.; Miyamoto, K.; Suenobu, T.; Van Caemelbecke, E.; Kadish, K. M. *JACS.* **1998**, *120*, 2880-2889.

(43) Kadish, K. M.; Han, B. C.; Endo, A. *Inorg. Chem.* **1991**, *30*, 4502-4506.

(44) Ditchfield, R.; Hehre, W. J.; Pople, J. A. *J. Chem. Phys.* **1971**, *54*, 724-728.

(45) Hehre, W. J.; Ditchfield, R.; Pople, J. A. *J. Chem. Phys.* **1972**, *56*, 2257-2261.

(46) Hariharan, P. C.; Pople, J. A. *Theor. Chim. Acta* **1973**, *28*, 213-222.

(47) Francl, M. M.; Pietro, W. J.; Hehre, W. J.; Binkley, J. S.; Gordon, M. S.; DeFrees, D. J.; Pople, J. A. *J. Chem. Phys.* **1982**, *77*, 3654-3665.

(48) Lee, C.; Yang, W.; Parr, R. G. *Phys. Rev. B: Condens. Matter* **1988**, *37*, 785-789.

(49) Becke, A. D. *J. Chem. Phys.* **1993**, *98*, 5648-5652.

(50) Neese, F. *Wiley Interdiscip. Rev.: Comput. Mol. Sci.* **2012**, *2*, 73-78.

(51) Fang, Y.; Bhyrappa, P.; Ou, Z.; Kadish, K. M. *Chem. - Eur. J.* **2014**, *20*, 524-532.

(52) Chang, D.; Malinski, T.; Ulman, A.; Kadish, K. M. *Inorg. Chem.* **1984**, *23*, 817-824.

(53) Wolberg, A.; Manassen, J. *JACS.* **1970**, *92*, 2982-2991.

(54) Fang, Y.; Jiang, X.; Ou, Z.; Michelin, C.; Desbois, N.; Gros, C. P.; Kadish, K. M. *J. Porphyrins Phthalocyanines* **2014**, *18*, 832-841.

(55) Kadish, K. M.; Shiue, L. R. *Inorg. Chem.* **1982**, *21*, 3623-3630.

(56) Kadish, K. M.; Mu, X. H.; Lin, X. Q. *Inorg. Chem.* **1988**, *27*, 1489-1492.

(57) D'Souza, F.; Villard, A .; Van Caemelbecke, E.; Franzen, M.; Boschi, T.; Tagliatesta, P.; Kadish, K. M. *Inorg. Chem.* **1993**, *32*, 4042-4048.

(58) Walker, F. A.; Beroiz, D.; Kadish, K. M. *JACS..* **1976**, *98*, 3484- 3489.

(59) Yang, W.; Mortier, W. J. *JACS..* **1986**, *108*, 5708-5711.

(60) Parr, R. G.; Yang, W. *JACS.* **1984**, *106*, 4049-4050.

(61) Yang, W.; Parr, R. G.; Pucci, R. *J. Chem. Phys.* **1984**, *81*, 2862-2863.

(62) Zhao, L.; Qi, D.; Zhang, L.; Bai, M.; Cai, X. *J. Porphyrins Phthalocyanines* **2012**, *16*, 927-934.

(63) Feng, X.-T.; Yu, J.-G.; Liu, R.-Z.; Lei, M.; Fang, W.-H.; De Proft, F.; Liu, S. *J. Phys. Chem. A* **2010**, *114*, 6342-6349.

(64) Feng, X.-T.; Yu, J.-G.; Lei, M.; Fang, W.-H.; Liu, S. *J. Phys. Chem.* **2009**, *113*, 13381 -13389.

(65) Cardenas-Jiron, G. I. *Int. J. Quantum Chem.* **2003**, *91*, 389-397.

(66) Maerkl, G.; Reiss, M.; Kreitmeier, P.; Noeth, H. *Angew. Chem., Int. Ed. Engl.* **1995**, *34*, 2230-2234.

CHAPTER FIVE

Unsymmetrically Functionalized Benzoporphyrins

5.1 Introduction

π-Extended porphyrins in which one or more aromatic rings are fused to the porphyrin periphery at the β, β'-positions have attracted considerable attention owing to their unique combination of photophysical, optoelectronic, and physicochemical properties, and their potential applications in various areas such as organic electronics, optic electronic and photomedicines.[1-18] Although known for decades, the investigation of π-extended porphyrins has been mainly restricted to symmetrical structures. Reports for unsymmetrical π-extended porphyrins are rare due to the limited synthetic methods available to accessing these compounds.[19-22] In particular, reports for π-extended porphyrins with unsymmetrically substituted functional groups remain elusive in the literature. Unsymmetrically substituted porphyrins are expected to display different electronic and photo-physical properties from their symmetrical counterparts due to a splitting of the frontier orbitals, and may hold promise for future broader applications. Herein, a series of unsymmetrically functionalized benzoporphyrins in which a push (electron-donating) group and a pull (electron-withdrawing) group are installed at the porphyrin β-positions are characterized by UV-vis spectroscopy and cyclic voltammetry to provide insights into their electronic and optical properties.

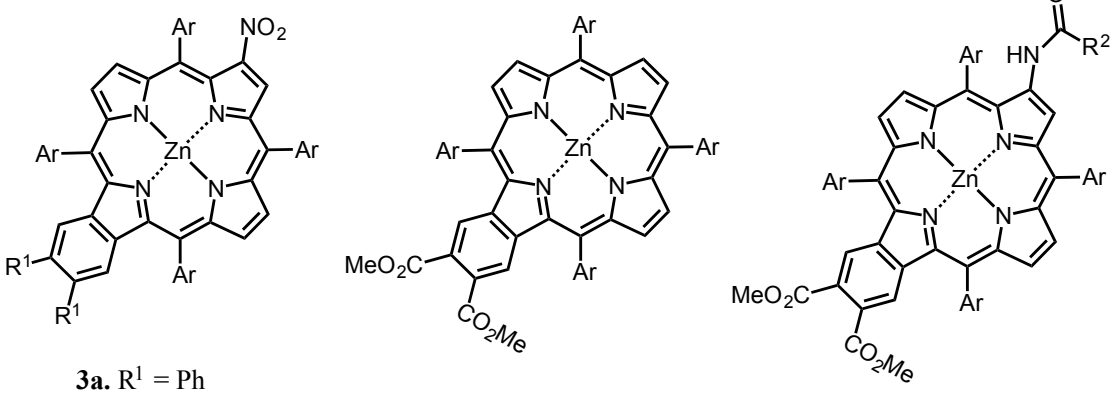

3a. R^1 = Ph
3b. R^1 = 4-Me-Ph
3c. R^1 = CO_2Me
Ar = 4-Me-Ph

6
Ar = 4-Me-Ph

4. R^2 = CH_3
5. R^2 = Ph
Ar = 4-Me-Ph

Chart 5-1. Structures of investigated mono-benzoporphyrins.

5.2 Results and Discussion

5.2.1 UV-vis spectroscopy

UV-vis spectra of these porphyrins are compiled in Figure 5-1. As compared with the symmetrical monobenzoporphyrin **6**, the unsymmetrical monobenzoporphyrins **3-5** all display broadened and red shifted Soret and enhanced Q bands corresponding to the symmetry breaking of the structure. The unsymmetrical *pull-pull* nitroporphyrin **3c** exhibits a Soret band at 446 nm. Upon switching from a moderately electron-withdrawing ester group to an electron-donating phenyl group (**3a**), the Soret band is red shifted to 449 nm, while the Q bands remain mostly unchanged; installing a strong electron-donating methoxy group at the 4-position of the phenyl ring (**3b**) pushes the Soret band slightly further to the red region (452 nm). These data demonstrate the expected "push-pull" effect. Interestingly, the push-pull benzoporhyrins **4** and **5** show blue shifted absorptions relative to those of *pull-pull* **3c**. The fluorescence spectra of these compounds were also measured by our collaborator and the obtained spectra also exhibit the "push-pull" effect.[23]

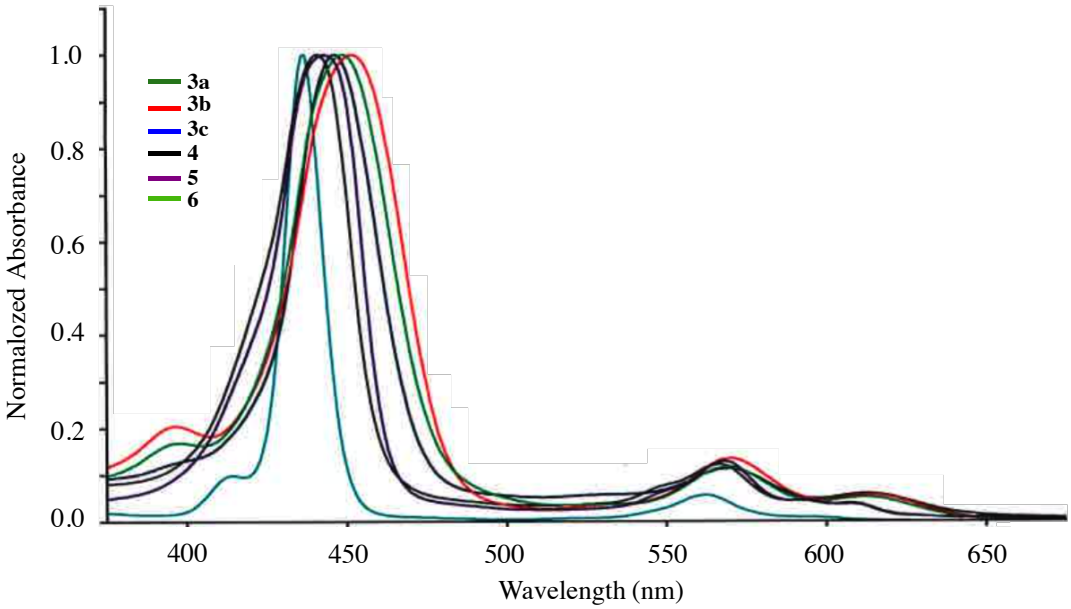

Figure 5-1. UV-vis spectra of **3a**-**3c** and **4**-**6** in CH_2Cl_2.

5.2.2 Cyclic Voltammetry

The electrochemical properties of these mono-benzoporphyrins were investigated using cyclic voltammetry (CV) (Figure 5-2). The reductions were measured in pyridine and the oxidations in CH_2Cl_2 in order to obtain thermodynamically reversible electrode reactions for all processes. For comparison purposes, the CV of (TPP)Zn was also measured under similar conditions. Several trends were observed in the electrochemical data. Porphyrin **6** displays two reversible oxidations and two reversible reductions, similar to (TPP)Zn. As compared with (TPP)Zn, both the first ($E_{1/2}$ = 0.75 V) and second oxidation ($E_{1/2}$ = 0.97 V) potentials of **6** are shifted negatively, while both the first reduction ($E_{1/2}$ = -1.34 V) and second reduction ($E_{1/2}$ = -1.78 V) move in a positive direction. These shifts in redox potentials are anticipated for porphyrin 6 due to its extended π-conjugation upon fusion of a benzene ring to the porphyrin periphery. The reduced HOMO-LUMO gap of **6** is also reflected by its red-shifted and broadened absorption bands relative to those of (TPP)Zn. Two reversible oxidations and two reversible reductions were also observed for porphyrin **3a-3c**. The introduction of a strong electron-withdrawing nitro group influenced the reduction potentials more significantly than the oxidation potentials. While the oxidation potentials of **3a-3b** only shifted positively by 30-90 mV relative to those of **6**, the reduction potentials shifted by 260-480 mV. The *push-pull* porphyrins **3a** and **3b** display exactly the same first oxidation and reduction potentials; the second oxidation and reduction potentials of **3a** and **3b** only deviate slightly from each other, are negatively shifted by 20 mV and 10 mV, respectively in **3b**. These data suggest that the presence of a strong electron-donating group (-OMe) at the *para*-position of the phenyl ring in **3b** does not significantly influence the electrochemical properties of the porphyrin. This is likely due to the hindered electronic communication between the electron-donating methoxy groups with the porphyrin ring. As shown in the calculated optimized geometry (Figure 5-3), the aryl groups on the fused benzene rings of **3a** and **3b** preferably adopt a perpendicular position to the porphyrin plane; as a result, the π-conjugation of the porphyrin does not effectively extend

to the attached aryl rings on the fused benzene unit. On the other hand, when the weakly electron-donating aryl groups in **3a** and **3b** are replaced with moderately electron-withdrawing ester groups of **3c**, oxidation and reduction potentials are positively shifted by 50 mV to 140 mV, showing a more pronounced substituent effect. Converting the strongly electron-withdrawing nitro group in **3c** into a moderately electron-donating carbonylamino group in porphyrins **4** and **5** significantly shifts the reduction potentials negatively by 320 to 460 mV. The oxidation potentials of **4** and **5** also shift moderately in a negative direction. It is notable that an extra reversible oxidation (third oxidation) was observed for **4** at $E_{1/2}$ = 1.38 V, which likely results from oxidation of the carbonylamino group.

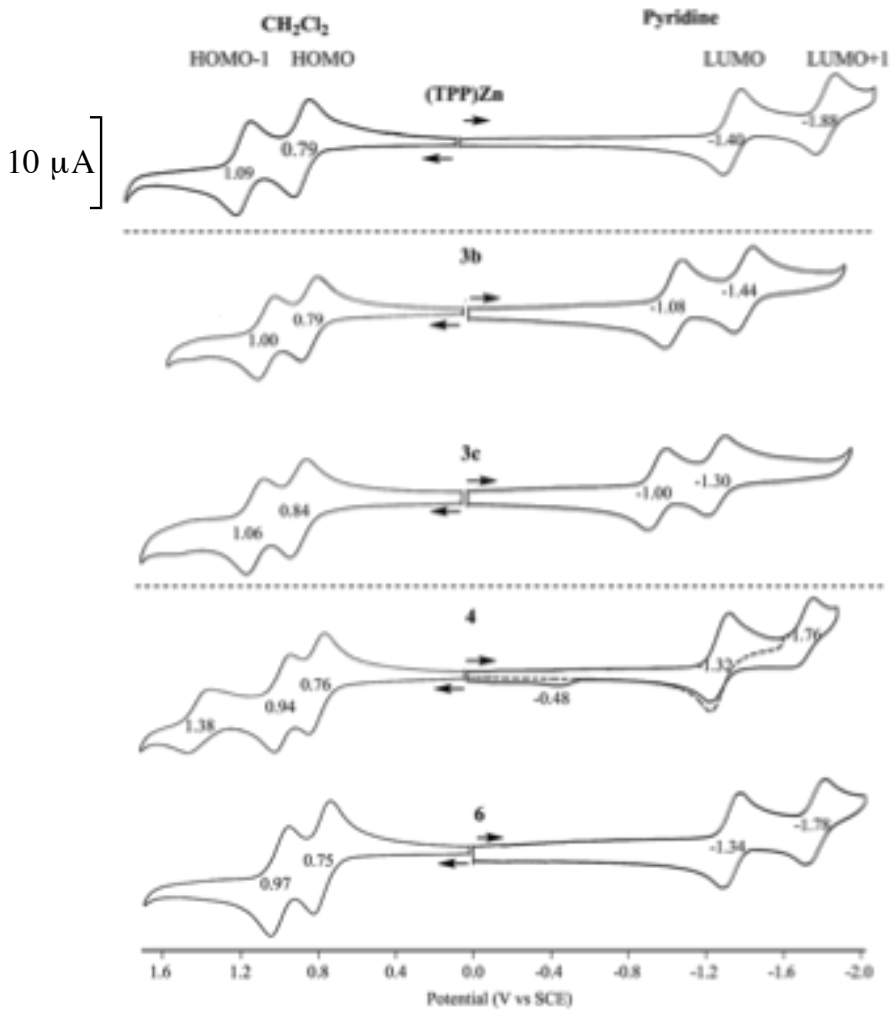

Figure 5-2. Cyclic voltammograms of investigated porphyrins in CH_2Cl_2 and pyridine containing 0.1 M TBAP at scan rate = 100 mV/s.

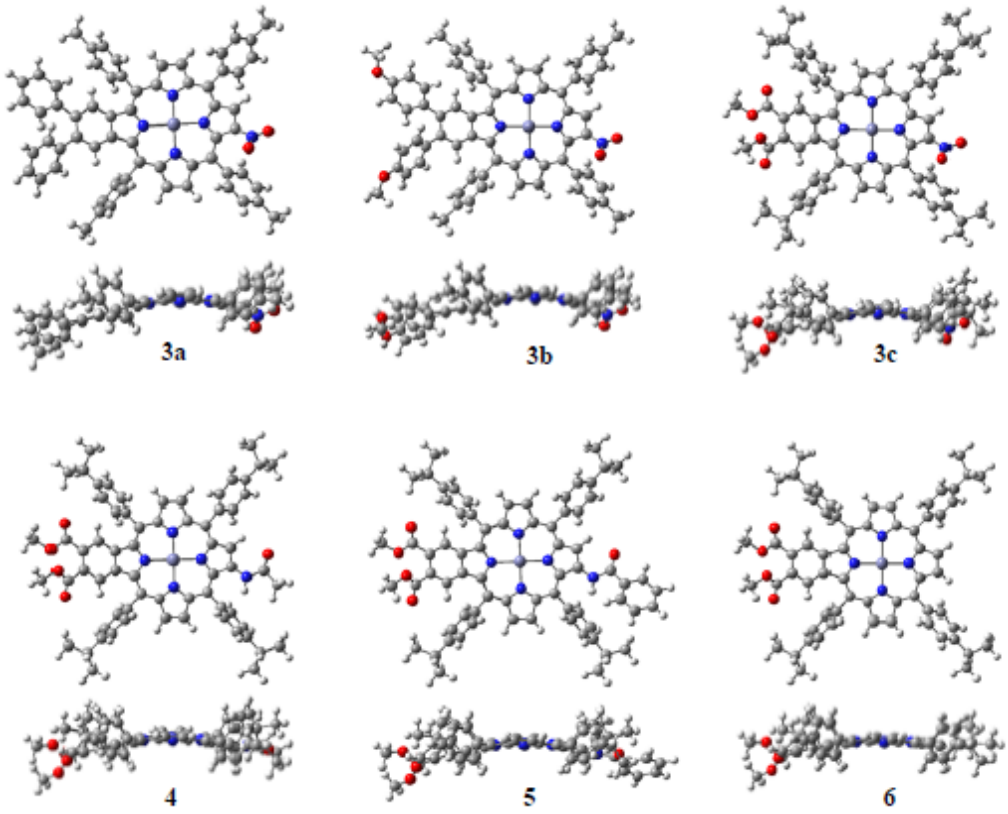

Figure 5-3. Molecular geometry of **3a**-**3c**, and **4**-**6** calculated at the B3LYP/6-31G(d) level of theory. Figure is from Ref. 23.

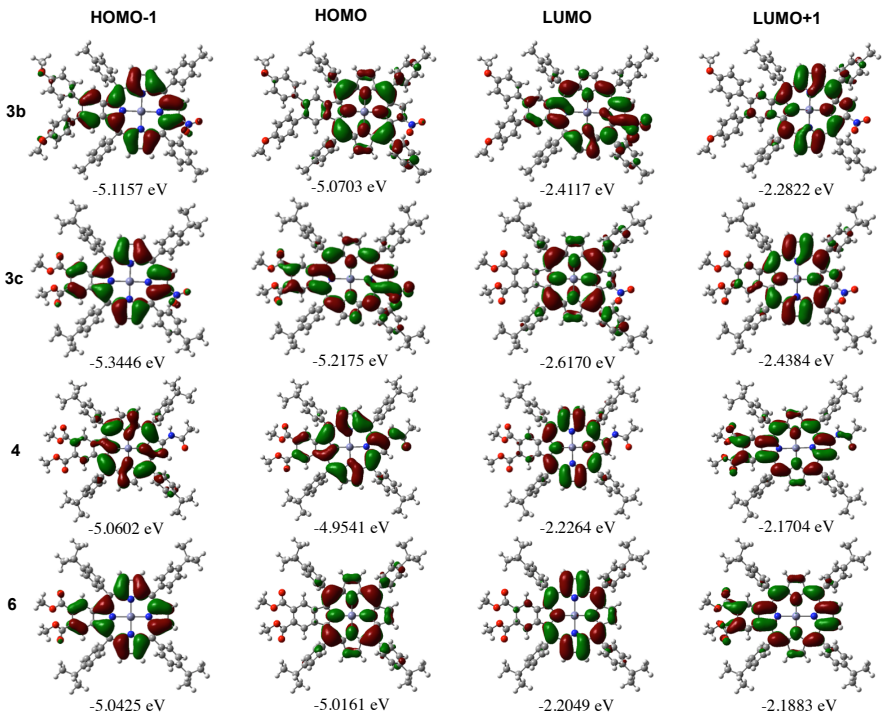

Figure 5-4. Calculated HOMOs and LUMOs and energy levels for **3b**, **3c**, **4** and **6 (**B3LYP/6-31G(d)). Figure is from Ref. 23.

5.2.3 DFT Calculations[23]

DFT calculations, done by our collaborators, were performed to provide some insights into the electronic and electrochemical properties of the porphyrins (Figure 5-3). The frontier orbitals of these porphyrins display different electron density patterns. While the HOMO and LUMO of symmetrical porphyrin **6** mainly involve the porphyrin core, the electron density in the HOMO of **4** and **5** is extended to the fused benzene ring and the carbonylamino group of the attached amide moiety. The HOMO orbitals of **4** and **5** are destabilized and the LUMOs of **4** and **5** are stabilized as a result of the introduction of the moderately electron-donating carbonylamino group to the porphyrin periphery, leading to a smaller HOMO-LUMO energy gap relative to that of **6**. The electron density of the HOMOs for *push-pull* porphyrins **3a** and **3b** is mainly located on the porphyrin core with partial extension to the fused benzene ring. The electron density on the HOMO of *pull-pull* **3c** is distributed from the fused benzene ring through the porphyrin core to the nitro group. On the other hand, the LUMO of **3a**, **3b** and **3c** shows a reversed trend in the electron density distribution. Both the HOMOs and LUMOs are stabilized relative to that of **6**. It is notable that the orbital splitting in the LUMOs of pull-pull **3a-3c** are more significant than that of **4** and **5**. The DFT calculations correlate well with the electronic and electrochemical properties demonstrated in this chapter.

5.3 Conclusion

In summary, unsymmetrically functionalized benzoporphyrins, in which an electron-withdrawing group and an electron-donating group are located at the porphyrin β-positions, were synthesized. Breaking the symmetry of the benzoporphyrin results in a significant broadening and red shifting of the absorption and emission bands. The introduction of different types of substituents to the porphyrin periphery makes a remarkable difference in the electrochemical and electronic properties of these porphyrins. The strongly electron-withdrawing nitro group appears to have a more pronounced impact on the properties of the benzoporphyrins than the electron-donating aminocarbonyl and aryl groups.

5.4 References

(1) Carvalho, C. M.; Brocksom, T. J.; de Oliveira, K. T. *Chem.Soc. Rev*. **2013**, *42*, 3302 -3317.

(2) Smith, K. M.; Lee, S. H.; Vicente M. G. H. *J. Porphyrins Phthalocyanines **2005**, 9,* 769-778.

(3) Lash, T. D.; *J. Porphyrins Phthalocyanines* **2001**, *5*, 267-288.

(4) Baluschev, S.; Yakutkin, V.; Miteva, T.; Avlasevich Y.; Chernov S.; Aleshchenkov, S.; Nelles, G.; Cheprakov, S.; Yasuda, A.; Mullen, K.; Wegner, G.; *Angew. Chem. Int. Ed.,* **2007**, *46*, 7693-7696.

(5) Borek, C.; Hanson, K.; Djurovich, P. I.; Thompson, M. E.; Aznavour, K.; Bau, R.; Sun, Y. R.; Forrest, S. R.; Brooks, J.; Michalski, L.; Brown, J.; *Angew. Chem. Int. Ed.,* **2007***, 46,* 1109-1112.

(6) Ongayi, O.; Gottumukkala, V.; Fronczek, F. R.; Vicente, M. G. H.; *Bioorg. Med. Chem. Lett.* **2005***, 15,* 1665-1668.

(7) Mack, J.; Bunya, M.; Shimizu, Y.; Uoyama, H.; Komobuchi, N.; Okujima, T.; Uno, H.; Ito, S.; Stillman, M. J.; Ono, N.; Kobayashi, N. *Chem. Eur. J.* **2008***, 14,* 5001-5020.

(8) Young, S. W.; Qing, F.; Harriman, A.; Sessler, J. L.; Dow, W. C.; Mody, T.D.; Hemmi, G. W.; Hao. Y. P.; Miller, R. A. *Proc. Natl. Acad. Sci.* **1996***, 93,* 6610-6615.

(9) Okujima, T.; Hashimoto, Y.; Jin, G.; Yamada, H.; Uno, H.; Ono, N.; *Tetrahedron,* **2008***, 64,* 2405-2411.

(10) Hayashi, H.; Touchy, A. S.; Kinjo, Y.; Kurotobi, K.; Toude, Y.; Ito, S.; Saarenpaa, H.; Tkachenko, N. V.; Lemmetyinen, H.; Imahori, H. *ChemSusChem,* **2013**, *6*, 508-517.

(11) Yan, J.; Feng, Y.; Peng, X.; Li, Y.; Zhang, N.; Li, X. and Zhang, B. *Tetrahedron Lett,* **2013**, *54*, 7198-7201.

(12) Mai, C. L.; Huang, W. K.; Lu, H. P.; Lee, C. W.; Chiu, C. L.; Liang, Y. R.; Diau, E. W. and Yeh, C. Y. *Chem. Commun.* **2010**, *46*, 809-811.

(13) Tanaka, M.; Hayashi, S.; Eu, S.; Umeyama, T.; Matano, Y. and Imahori, H. *Chem. Commun.* **2007**, 2069–2071.

(14) Imahori, H.; Iijima, H.; Hayashi, H.; Toude, Y.; Umeyama, T.; Matano, Y. and Ito, S. *ChemSusChem*, **2011**, *4*, 797-805.

(15) Kira, A.; Matsubara, Y.; Iijima, H.; Umeyama, T.; Matano, Y.; Ito, S.; Niemi, M.; Tkachenko, N. V.; Lemmetyinen, H. and Imahori, H. *J. Phys. Chem. C*, **2010**, *114*, 11293-11304.

(16) Hayashi, S.; Tanaka, M.; Hayashi, H.; Eu, S.; Umeyama, T.; Matano, Y.; Araki, Y. and Imahori, H. *J. Phys. Chem. C,* **2008**, *112*, 15576-15585.

(17) Jiao, C.; Zu, N.; Huang, K.-W.; Wang, P. and Wu, *J. Org. Lett.* **2011**, *13*, 3652-3655.

(18) Ball, J. M.; Davis, N. K. S.; Wilkinson, J. D.; Kirkpatrick, J.; Teuscher, J.; Gunning, R.; Anderson, H. L. and Snaith, H. J. *RSC Adv.* **2012**, *2*, 6846-6853.

(19) Carvalho, C. M.; Santos, S. M.; Neves, M. G.; Tome, A. C.; Silva, A. M.; Rocha, J. and Cavaleiro, J. A., *J. Org. Chem.*, **2013**, *78*, 6622-6631.

(20) Moura, N. M.; Faustino, M. A.; Neves, M. G.; Paz, F. A.; Silva, A. M.; Tome, A. C. and Cavaleiro, J. A. *Chem Commun.* **2012**, *48*, 6142-6144.

(21) Moura, N. M. M.; Nuñez, C.; Santos, S. M.; Faustino, M. A. F.; Cavaleiro, J. A. S.; Neves, M. G. P. M. S.; Capelo, J. L. and Lodeiro, C. *ChemPlusChem*, **2013**, *78*, 1230-1243.

(22) Khoroshutin, A. V.; Chumakov, D. E.; Anisimov, A. V. and Kobrakov, K. I. *Russ. J. Gen. Chem.* **2007**, *77*,1959-1964.

(23) Jinadasa, R. G. W.; Fang, Y.; Deng, Y.; Deshoande, R.; Jiang, X.; Kadish, K. M.; Wang, H. *RSC Adv.* **2015**, *5*, 51489-51492.

CHAPTER SIX

β-Functionalized Push-Pull *Opp*-Dibenzoporphyrins

6.1 Introduction

Push-pull porphyrins carrying both an electron-donating (push) and an electron-withdrawing group (pull) have been a topic of long-lasting research interest owing to their potential applications in organic electronics, *opto*-electronics and photonics.[1-5] Breakthroughs in the development of push-pull porphyrins were not made until 2011 when dye-sensitized solar-cells (DSSCs), which were based on a class of push-pull porphyrins bearing a diarylamine donor group and an ethynylbenzoic acid acceptor (linker) group at the porphyrin *meso*-positions (Figure 6-1), achieved a record-high solar-to-electric-power conversion efficiency (η = 12.3%).[6] This exciting achievement has drastically changed the traditional poor-performance profile of porphyrins in DSSC. Intense research efforts have been devoted to developing push-pull porphyrins since then,[7-9] and even more exciting results have been obtained,[10-18] demonstrating the huge potentials of push-pull porphyrins in this area.

Almost all of the reported push-pull porphyrins which are functionalized at the porphyrin *meso*-positions, and there are only three examples for β-functionalized push-pull porphyrins in the literature.[16, 19, 20] *Meso*- and β–functionalization at the porphyrin periphery are expected to have a different effect on their electronic and photophysical properties (Figure 6-1). Given the remarkable advances achieved with *meso*-functionalized push-pull porphyrins in recent years, β-functionalized push-pull porphyrins hold potential to make new breakthroughs. A key is to develop concise and versatile synthetic methods to access β–functionalized push-pull porphyrins. Recently our collaborator have developed a Pd^0 catalyzed cascade reaction for the synthesis of benzoporphyrins.[21] This cascade reaction allows the possibility to introduce a wide range of functional groups to the porphyrin β, β-positions. They wished to take advantage of the versatility of this reaction in conjunction with the bromination chemistry of porphyrins[22-26] and to develop a new synthetic route that can potentially lead to a large variety of β-functionalized push-pull porphyrins (Figure 6-1). Herein, I report the spectroscopic

and electrochemical characterization of a series of push-pull *opp*-dibenzoporphyrins where the push group features the *p*-methoxyphenyl group and the pull groups possess variable electron-withdrawing abilities.

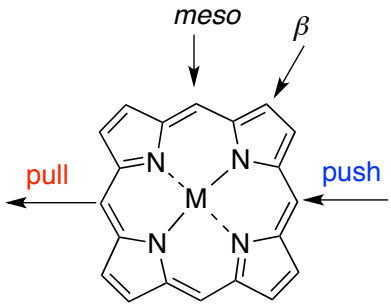

Linearly *meso*-functionalized push-pull porphyrin

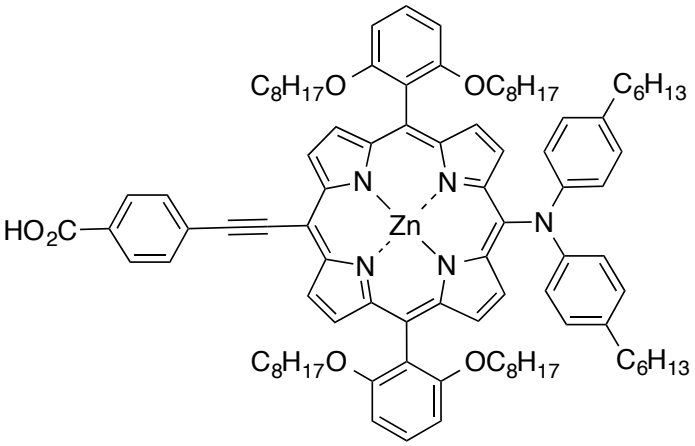

A representative example of *meso*-functionalized push-pull porphyrin (**YD2-o-C8**)[6]

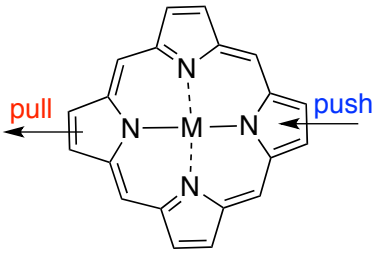

Linearly β-functionalized push-pull porphyrins

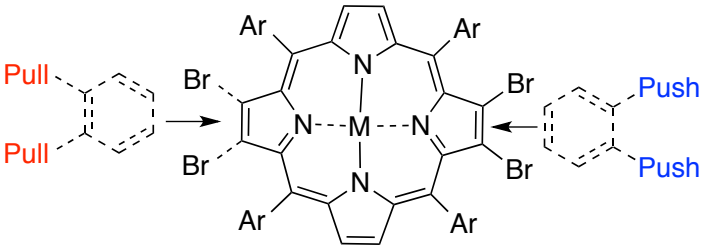

Our proposed synthetic plan for β-functionalized push-pull benzoporphyrins

Figure 6-1. Illustration of *meso*- and β-functionalized push-pull porphyrins.

6.2 Results and Discussion

6.2.1 Synthesis of the Materials

π-Extended porphyrins, in which one or more aromatic rings are fused to the porphyrin β, β'-positions, possess a unique set of electronic and photophysical properties, and thus constitute of an attractive research field.[27-30] In this chapter, push-pull *opp*-dibenzoporphyrins (**4a-4d** and **5a-5d**) were prepared by our collaborator through the cooperation of a Pd^0 catalyzed cascade reaction[21] using the bromination chemistry of porphyrins,[23,26] and the spectroscopic and electrochemical properties were then characterized and described in this work.

6.2.2 UV-vis Absorption Spectra

Push-pull *opp*-dibenzoporphyrins **5a-5d** and **4a-4d** bear the same 4-methoxyphenyl donating groups on one fused benzene ring of the porphyrin, and the groups with variable electron-withdrawing abilities are attached on the other fused benzene ring at the opposite β, β'-positions of the porphyrin. The UV-vis absorption spectra of **5a-5d** and **4a-4d** in DCM are compiled in Figure 6-2 and Figure 6-3, respectively. **4b**, which possesses moderate electron-withdrawing ester groups, displays a broad Soret band at 448 nm and four Q bands in the range of 500-750 nm.

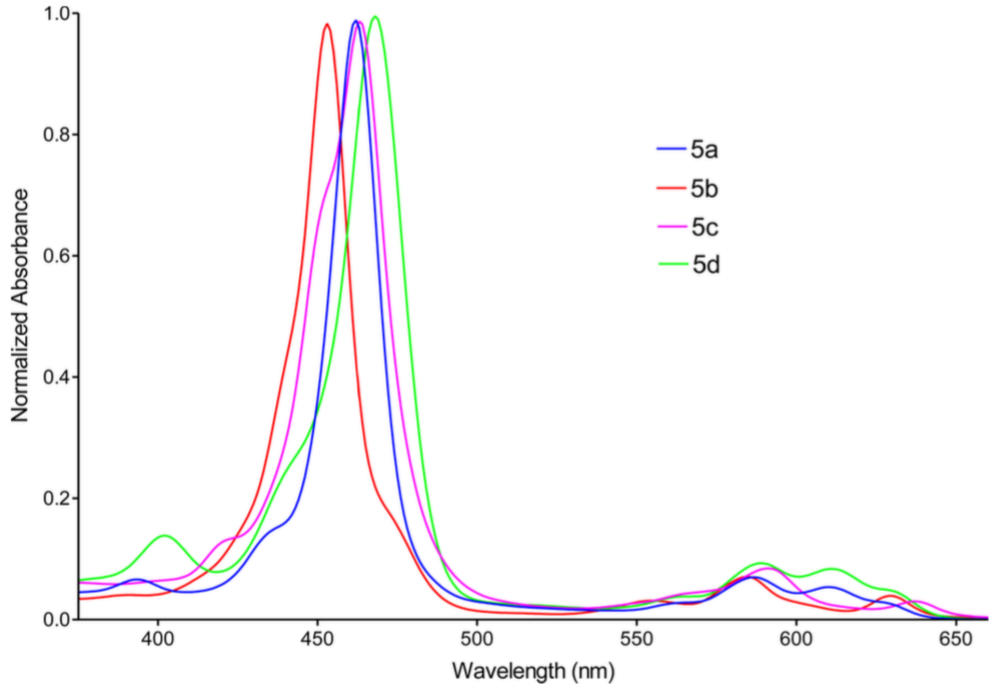

Figure 6-2. Normalized UV-vis spectra of **5a**-**5d** (see structures in Scheme 6-1) in CH_2Cl_2. (**5a:** 6.99 x 10^{-6} M, **5b:** 7.45 x 10^{-6} M, **5c:** 6.35 x 10^{-6} M, **5d:** 3.15 x 10^{-6} M).

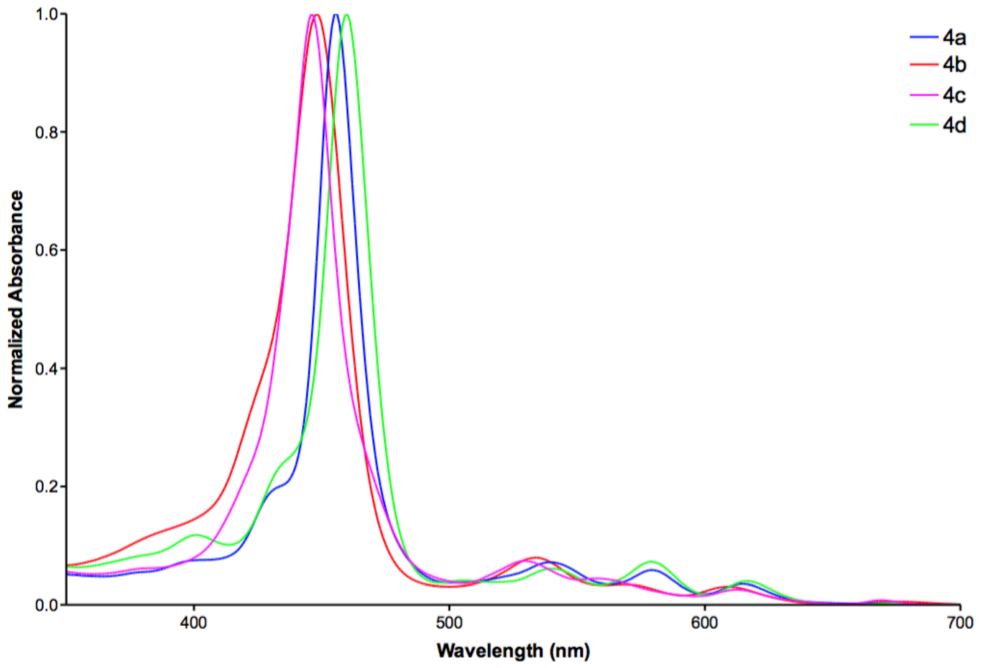

Figure 6-3. Normalized UV-vis spectra of **4a-4d** in CH_2Cl_2. (**4a:** 4.17 x 10^{-6} M, **4b:** 5.68 x 10^{-6} M, **4c:** 3.76 x 10^{-6} M, **4d:** 2.16 x 10^{-6} M).

Upon switching to much stronger electron-withdrawing cyano groups (**4a**), the Soret band is red-shifted by 8 nm to 456 nm; the Q bands of **4a** are also red-shifted relative to those of **4b**. These data demonstrate a stronger push-pull effect of **4a** than **4b**. Simply converting the vicinal ester groups of **4b** to a cyclic imide group in **4d** significantly red shifts the Soret band by 12 nm to 460 nm. The Q bands of **4d** are also red-shifted relative to those of **4b**. In terms of electron-withdrawing ability, the imide group and the ester group are similar. Such a remarkable push-pull effect displayed by **4d** is due to the fact that the planar cyclic imide group is more efficiently conjugated to the porphyrin π-system than the free-rotating ester groups. On the other hand, the pyridyl bearing **4c** shows blue-shifted Soret and Q bands relative to those of **4b, 4a** and **4d**. UV-vis absorption bands of **5a**, **5b** and **5d** are red-shifted relative to those of the corresponding free-base porphyrins **4a**, **4b** and **4d** by 5-8 nm, and exhibit a similar trend of spectral change as observed for **4a**, **4b** and **4d**. In sharp contrast, the pyridyl bearing **5c** shows bathochromic-shifted Soret and Q bands relative to those of **4a** and **4b**, displaying a reversed trend. It is remarkable that the Soret band of **5c** is red-shifted by 17 nm relative to that of its free base **4c**. Such a large shift of the Soret band upon metallation indicates that a different process has occurred during metallation. UV-vis spectra of **5a**-**5d** were then measured in pyridine (Figure 6-4). While **5a**, **5b** and **5d** all display large bathochromically shifted Soret bands (up to 14 nm) with significantly different absorption patterns at the Q band region (500-700 nm) in pyridine as compared with those in CH_2Cl_2, those of **5c** remain more or less similar with only a 2 nm red-shift of the Soret band. These data suggest that the pyridyl substituents of one **5c** molecule are able to coordinate to the central zinc of another **5c** molecule in CH_2Cl_2, and may possibly form a coordination framework (Figure 6-5).

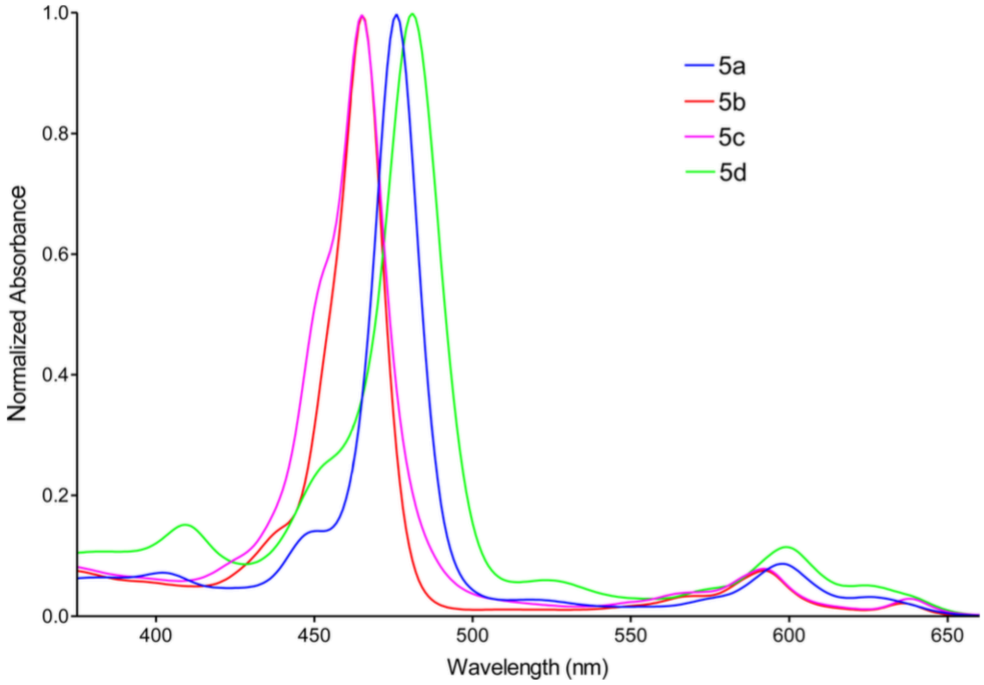

Figure 6-4. Normalized UV-vis spectra of **5a-5d** in pyridine.

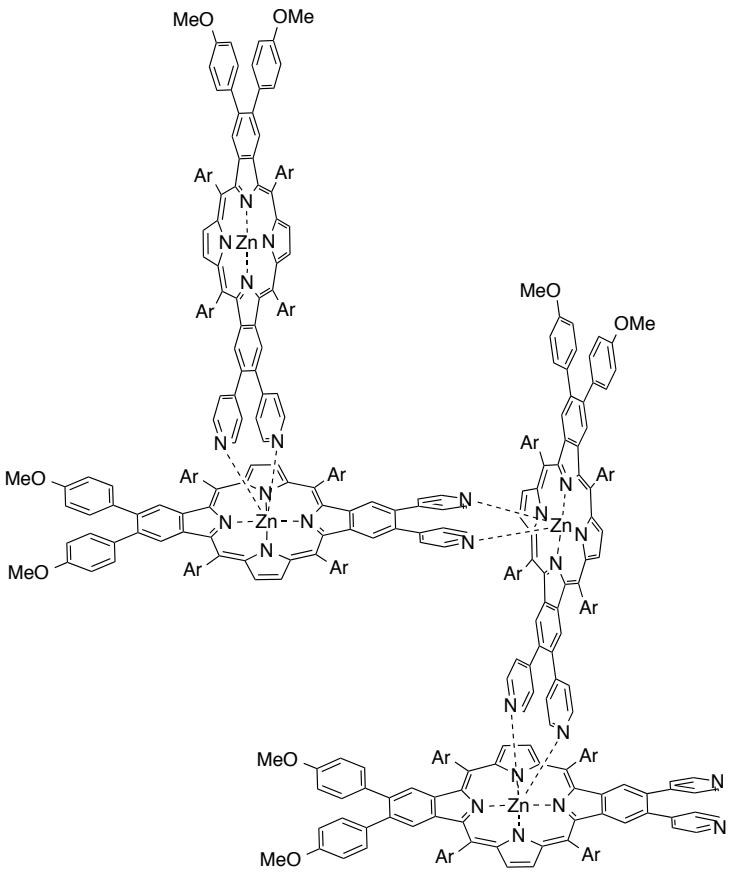

Figure 6-5. Proposed coordination framework of **5c** in CH_2Cl_2. Note, the framework is expected to exist as a mixture of oligomers.

Overall, the trend observed in the UV-vis spectra of **5a**-**5d** in pyridine is similar to that of **4a**-**4d** in CH_2Cl_2. The UV-vis absorption spectra of the synthesized push-pull *opp*-dibenzoporphyrins possess several unique features: 1) the Soret bands are shouldered; 2) an additional weaker absorption shows in the range of 380-405 nm; 3) extra Q bands are observed in the range of 500–650 nm, noting that four and two Q bands are expected for free base porphyrins and metallated porphyrins, respectively. These features become especially pronounced for the more strongly push-pull **4a**, **5a**, **4d** and **5d**. For example, zinc porphyrin **5d** shows four Q bands, both in CH_2Cl_2 and in pyridine. These features of the UV-vis spectra can be partially explained by breakage of the symmetry from D_{4h} to C_{2v}. However, we speculate that intramolecular charge transfers/electronic communication involving the push and pull groups, the porphyrin core and the central metal are likely to exist in these porphyrins.

6.2.2 Electrochemical Properties

Electrochemistry of the Zn(II) porphyrins **5a** to **5d** was investigated by cyclic voltammetry in CH_2Cl_2 and pyridine containing 0.1 M TBAP. Each compound exhibits two oxidations and two or three reductions in CH_2Cl_2 as shown in Figure 6-6. The two oxidations and the first reduction of each porphyrin are reversible. The second reduction of **5c** is also reversible but this process is irreversible for compounds **5a**, **5d** and **5b** in CH_2Cl_2. The first two electron additions are porphyrin ring centered and generate a porphyrin π anion radical and dianion but the dianion formed during the second reduction is not stable in the case of **5a**, **5b** or **5d** and is converted to a phlorin anion via a homogenous chemical reaction described in earlier publications for related compounds.[31-33] The chemically generated phlorin anion is electroactive and can be further reduced at more negative potentials to a phlorin dianion. It can also be re-oxidized to give back the neutral porphyrin at a peak potential of -0.38 to -0.40 V. Taking compound **5a** as an example, three reductions are observed in CH_2Cl_2 (Figure 6-6), the first at $E_{1/2}$ = -1.26 V, the second at E_{pc} = -1.65 V and the third at $E_{1/2}$ = -1.91 V. The reoxidation peak at E_{pa} = -0.38 V is coupled to the second reduction. A third reduction is not observed for porphyrins **5d** or **5b** due to the fact that this reaction occurs at $E_{1/2}$ values more negative than the solvent potential limit of CH_2Cl_2. A third reduction is also not seen for **5c,** which is more difficult to reduce than the other three porphyrins and lacks a re-oxidation peak at -0.38 V.

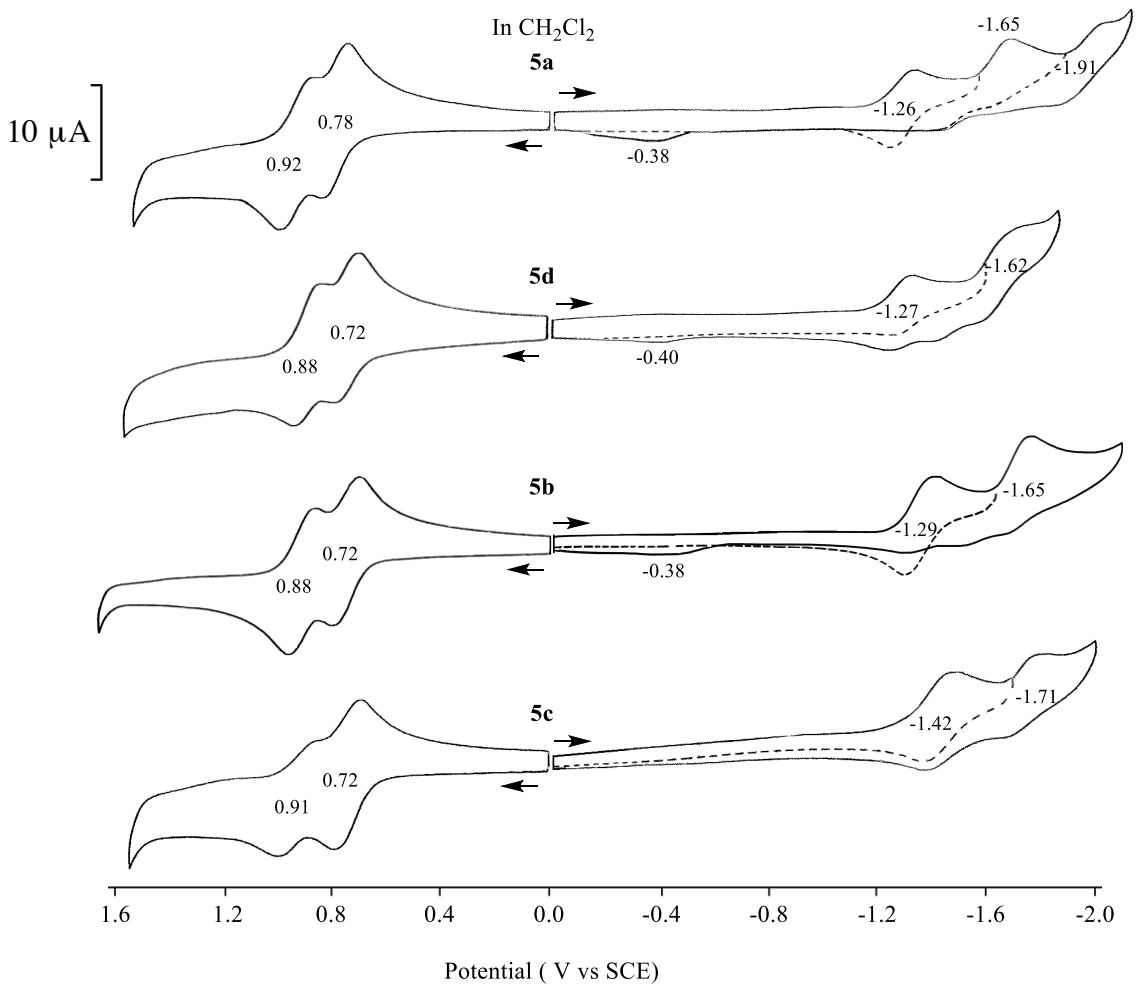

Figure 6-6. Cyclic voltammograms of investigated dibenzo zinc porphyrins in CH_2Cl_2 containing 0.1 M TBAP.

The first reduction of **5c**, which has the proposed coordination framework shown in Figure 6-5, is located at $E_{1/2}$ = -1.42 V which is 130-160 mV more negative than $E_{1/2}$ for reduction of **5a**, **5b** or **5d** ($E_{1/2}$ = -1.26 to -1.29 V) in the same solvent. This large negative shift in reduction potential for **5c** is consistent with a coordination between the Zn(II) center of one porphyrin molecule and the pyridyl group(s) from another as schematically shown in Figure 6-5. Changing from the non-binding solvent CH_2Cl_2 to the strongly binding solvent pyridine, results in a change from four coordinate Zn(II) to five coordinate Zn(Py) for compounds **5a**, **5d** and **5b** and the occurrence of two well-defined reversible reductions for all four porphyrins in pyridine (Figure 6-7). The $E_{1/2}$ for first reduction in pyridine ranges from -1.19 to -1.30 V and the second from -1.61 to -1.79 V. A chemical reaction following the second reduction of **5c**, **5b** and **5d** is not observed in pyridine (as is the case in CH_2Cl_2) due to the lower proton concentration in this solvent. In addition, the fact that **5b** and **5c** exhibit exactly the same reduction potentials in pyridine suggests the same five-coordinate Zn(Py) form of the porphyrin in this solvent.

The first oxidation of **5a** in CH_2Cl_2 occurs at $E_{1/2}$ = 0.78 V while $E_{1/2}$ = 0.72 V for **5b**, **5c** and **5d**. The second oxidation of **5a** and **5c** are identical within experimental error while the $E_{1/2}$ values for oxidation of **5b** and **5d** are exactly identical, as seen in Figure 6-6. Thus, conversion of the vicinal esters in **5b** to the cyclic imide in **5d** does not shift the oxidation potentials, but, replacing the moderately electron-withdrawing ester groups of **5b** with strongly electron-withdrawing cyano groups in **5a** positively shifts both the first and the second oxidations by 60 and 40 mV, respectively.

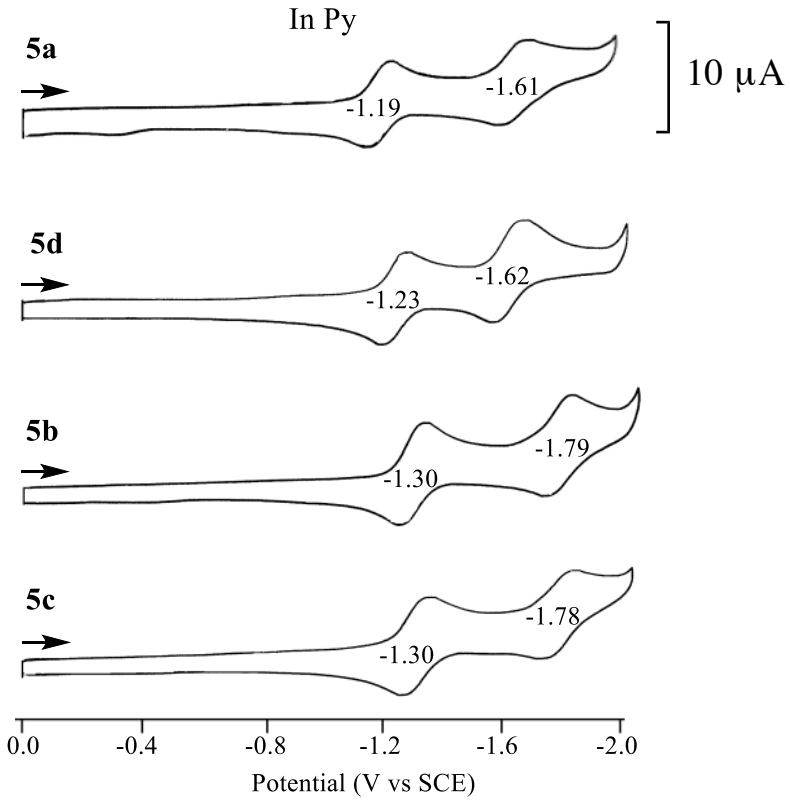

Figure 6-7. Cyclic voltammograms of investigated dibenzo zinc porphyrins in Py, 0.1 M TBAP.

While **5b** and **5c** exhibit almost the same reduction potentials, the first and the second reduction potentials of **5a** are shifted positively in this solvent by 110 mV and 180/170 mV, respectively, relative to those of **5b** and **5c** (Figure 6-7). The incorporation of two cyano groups in the push-pull *opp*-dibenzoporphyrin **5a** shifts both the oxidation and the reduction potentials positively as compared to the other porphyrins in CH_2Cl_2 (Figure 6-6). The electrochemical HOMO-LUMO energy gaps, calculated from reversible potentials for the first oxidation and first reduction in CH_2Cl_2 follows the order: **5d** (1.99 V) < **5b** (2.01 V) < **5a** (2.04 V) < **5c** (2.14 V). The CV data of **5a**-**5d** thus agree well with the UV-vis absorption spectra. Overall, a variation in the strength of the electron-withdrawing groups makes a bigger impact on the reduction potentials than the oxidation potentials for these β-functionalized push-pull *opp*-dibenzoporphyrins.

6.2.3 DFT Calculation[34]

DFT calculations for **5a**-**5d**, which were done by our collaborator,[34] to provide insights into the electronic and electrochemical properties of these compounds (Figure 6-8). The electronic density on the HOMO and the LUMO+1 of these porphyrins is significantly distributed over the porphyrin ring and the two fused benzene rings. The participation of the two pyrroles bearing no substituents in the LUMO+1 is much less than that of the two neighbouring pyrroles bearing substituents, suggesting some "locking effect" due to the fusion of the two benzene rings. The introduction of a strongly electron-withdrawing group (i.e., -CN) increases the participation of the electron-withdrawing group in the HOMO and the fused benzene ring bearing the electron-donating group in the HOMO-1. On the other hand, the LUMO and the HOMO-1 of these porphyrins principally involve the π-systems of the porphyrins. The introduction of a strongly electron-withdrawing group (i.e., -CN) enhances the participation of the benzene ring bearing the electron-donating groups in the HOMO–1, and the benzene ring carrying the electron-withdrawing groups in the LUMO. It is

notable that the electron-donating *p*-methoxyphenyl group is only minimally involved in the HOMO and HOMO–1 of these porphyrins due to their restricted rotation forcing the benzene rings to adopt a perpendicular position relative to the porphyrin plane.

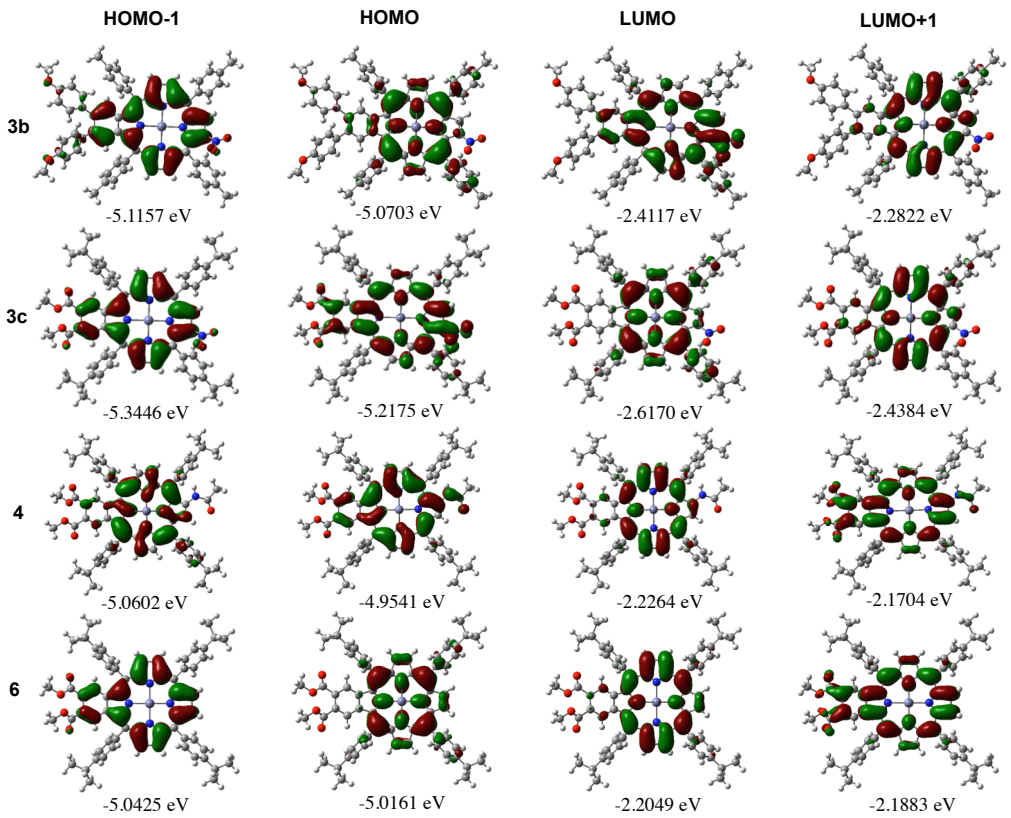

Figure 6-8 Calculated HOMOs and LUMOs and energy levels for **3b**, **3c**, **4** and **6 (**B3LYP/6-31G(d)).

6.3 Conclusions

In summary, the electronic and electrochemical properties of these push-pull *opp*-dibenzoporphyrins are susceptible to changes in substituents suggesting their easy tunability. For example, the conversions from the two vicinal ester groups (**5b**) both into two strongly electron-withdrawing cyano groups (**5a**) and into a cyclic imide group (**5d**) significantly red shifts the UV-vis absorption bands, reflecting their much smaller HOMO-LUMO energy gaps; however, the substituent effects on the energy levels of the frontier orbitals are different. While the energy levels for the HOMO and HOMO-1 of the imide carrying **5d** remain identical with those of the ester carrying **5b**, those of **5a** are both moderately lowered relative to those of **5b**.[34]

These push-pull *opp*-dibenzoporphyrins display interesting UV-vis absorption spectra and near-IR fluorescence,[34] which can be useful as sensors in a number of applications such as dye-sensitized solar cells and photodynamic therapy. They may also serve as model systems to study intra- and intermolecular electron transfer. The structure-property study has shown that the incorporation of a strong electron-withdrawing group has significant impact on the electronic and electrochemical properties of the porphyrins. On the other hand, the electron-donating group, i.e. *p*-methoxyphenyl group, shows a limited influence on the electronic and electrochemical properties of the porphyrins due to the restricted rotation arising from steric hindrance. Future direction for the development of β-functionalized push-pull benzoporphyrins will lie in the development of electron-donating groups that can conjugate to the porphyrin π–system more effectively in order to induce more efficient electronic communications that can actively engage the electron-donating group, the electron-withdrawing group and the porphyrin π-system.

6.4 References

(1) Verbiest, T.; Houbrechts, S.; Kauranen, M.; Clays, K. and Persoons, A. *J. Mater. Chem.* **1997**, *7*, 2175-2189.

(2) Senge, M. O.; Fazekas, M.; Notaras, E. G. A.; Blau, W. J.; Zawadzka, M.; Locos, O. B. and Mhuircheartaigh, E. M. Ni. *Adv. Mater.* **2007**, *19*, 2737-2774.

(3) Tanaka, T. and Osuka, A. *Chem. Soc. Rev.* **2015**, *44*, 943-969.

(4) Kato, S. and Diederich, F. *Chem. Commun.* **2010**, *46*, 1994-2006.

(5) Imahori, H.; Umeyama, T. and Ito, S. *Acc. Chem. Res.* **2009**, *42*, 1809-1818.

(6) Yella, A.; Lee, H.-W.; Tsao, H. N.; Yi, C.; Chandiran, A. K.; Nazeeruddin, M. K.; Diau, E. W.-G.; Yeh, C.-Y.; Zakeeruddin, S. M. and Grätzel, M. *Science*, **2011**, *334*, 629-634.

(7) Li, L. L. and Diau, E. W. *Chem. Soc. Rev.* **2013**, *42*, 291-304.

(8) Higashino, T. and Imahori, H. *Dalton Trans.* **2015**, *44*, 448-463.

(9) Urbani, M.; Gratzel, M.; Nazeeruddin, M. K. and Torres, T. *Chem. Rev.* **2014**, *114*, 12330-12396.

(10) Zhang, M.-D.; Zhang, Z.-Y.; Bao, Z.-Q.; Ju, Z.-M.; Wang, X.-Y.; Zheng, H.-G.; Ma, J. and Zhou, X.-F. *J. Mater. Chem. A* **2014**, *2*, 14883-14889.

(11) Yi, C.; Giordano, F.; Cevey-Ha, N. L.; Tsao, H. N.; Zakeeruddin, S. M. and Gratzel, M. *ChemSusChem*. **2014**, *7*, 1107-1113.

(12) Yella, A.; Mai, C. L.; Zakeeruddin, S. M.; Chang, S. N.; Hsieh, C. H.; Yeh, C. Y. and Gratzel, M. *Angew. Chem.* **2014**, *53*, 2973-2977.

(13) Mathew, S.; Yella, A.; Gao, P.; Humphry-Baker, R.; Curchod, B. F.; Ashari-Astani, N.; Tavernelli, I.; Rothlisberger, U.; Nazeeruddin, M. K. and Grätzel, M. *Nat. Chem.* **2014**, *6*, 242-247.

(14) Luo, J.; Xu, M.; Li, R.; Huang, K. W.; Jiang, C.; Qi, Q.; Zeng, W.; Zhang, J.; Chi, C.; Wang, P. and Wu, J. *JACS.* **2014**, *136*, 265-272.

(15) Lu, J.; Xu, X.; Cao, K.; Cui, J.; Zhang, Y.; Shen, Y.; Shi, X.; Liao, L.; Cheng, Y. and Wang, M. *J. Mater. Chem. A* **2013**, *1*, 10008-10015.

(16) Hayashi, H.; Touchy, A. S.; Kinjo, Y.; Kurotobi, K.; Toude, Y.; Ito, S.; Saarenpaa, H.; Tkachenko, N. V. and Lemmetyinen, H. *ChemSusChem*. **2013**, *6*, 508-517.

(17) Wang, C.-L.; Lan, C.-M.; Hong, S.-H.; Wang, Y.-F.; Pan, T.-Y.; Chang, C.-W.; Kuo, H.-H.; Kuo, M.-Y.; Diau, E. W.-G. and Lin, C.-Y. *Energy Environ. Sci.* **2012**, *5*, 6933-6840.

(18) Ripolles-Sanchis, T.; Guo, B. C.; Wu, H. P.; Pan, T. Y.; Lee, H. W.; Raga, S. R.; Fabregat-Santiago, F.; Bisquert, J.; Yeh, C. Y. and Diau, E. W. *Chem. Commun.* **2012**, *48*, 4368-4370.

(19) Chen, J.; Li, K.-L.; Guo, Y.; Liu, C.; Guo, C.-C. and Chen, Q.-Y. *RSC Adv.* **2013**, *3*, 8227-8231.

(20) Carlo, G. Di; Biroli, A. O.; Pizzotti, M.; Tessore, F.; Trifiletti, V.; Ruffo, R.; Abbotto, A.; Amat, A. and Angelis, F. *Chem. Eur. J.* **2013**, *19*, 10723-10740.

(21) Deshpande, R.; Jiang, L.; Schmidt, G.; Rakovan, J.; Wang, X.; Wheeler, K. and Wang, H. *Org. Lett.* **2009**, *11*, 4251-4253.

(22) Vicente, M. G. H.; Jaquinod, L.; Khoury, R. G.; Madrona, A. Y. and Smith, K. M.*Tetrahedron Lett.* **1999**, *40*, 8763-8766.

(23) Chen, Q.-Y.; Guo, C.-C. and Li, K.-L. *Synlett*. **2009**, *17*, 2867-2871.

(24) Chumakov, D. E.; Khoroshutin, A. V.; Anisimov, A. V. and Kobrakov, K. I. *Chem. Heterocycl. Compd.* **2009**, *45*, 259-283.

(25) Crossley, M. J.; Burn, P. L.; Chew, S. S.; Cuttance, F. B. and Newsom, I. A. *J. Chem. Soc., Chem. Commun*. **1991**, 1564-1566.

(26) Jaquinod, L.; Khoury, R. G.; Shea, K. M. and Smith, K. M. *Tetrahedron*, **1999**, *55*, 13151-13158.

(27) Ono, N.; Yamada, H. and Okujima, T. *Handbook of Porphyrin Science*, World Scientific, **2010**.

(28) Carvalho, C. M.; Brocksom, T. J. and Oliveira, K. T. *Chem. Soc. Rev.* **2013**, *42*, 3302-3317.

(29) Smith, K. M.; Lee, S. H. and Vicente, M. G. a. H. *J. Porphyrins Phthalocyanines* **2005**, *9*, 769-778.

(30) Lash, T. D. *J. Porphyrins Phthalocyanines* **2001**, *5*, 267-288.

(31) Peychal-Heiling, G. and Wilson, G. S. *Anal. Chem.* **1971**, *43*, 545-550.

(32) Lanese, J. G. and Wilson, G. S. *J. Electrochem. Soc.* **1972**, *119*, 1039-1043.

(33) Fang, Y.; Gorbunova, Y. G.; Chen, P.; Jiang, X.; Manowong, M.; Sinelshchikova, A. A.; Enakieva, Y. Y.; Martynov, A. G.; Tsivadze, A. Y.; Bessmertnykh-Lemeune, A.; Stern, C.; Guilard, R. and Kadish, K. M. *Inorg. Chem.*, **2015**, *54*, 3501-3512.

(34) Jinadasa, R. G. W.; Fang, Y.; Kumar, S.; Osinski, A. J.; Jiang, X.; Ziegler, C. J.; Kadish, K. M.; Wang, H. *J. Org. Chem.* **2015**, *80*, 12076-12087.

CHAPTER SEVEN

Triple-decker Complexes Containing Phthalocyanine and Nitrophenyl-corrole Macrocycles

7.1 Introduction

The study of new sandwich triple-decker tetrapyrrole derivatives represents an important area for researchers interested in exploring the potential use of these compounds in a variety of practical applications, from molecular magnets and nanomaterials to organic thin-film transistors and sensors.[1-11] The most often studied among the rare earth triple-decker tetrapyrrole derivatives are the homo- and heteroleptic complexes with porphyrin and/or phthalocyanine macrocyles.[1-11] These compounds can have different substituents at the peripheral positions of the molecular framework of each macrocycle and a judicious selection of the placement and properties of the substituents enables tuning of the optical, electrical and electrochemical properties.[12-17] Tuning the optical and electrochemical properties of triple-decker compounds with porphyrins, phthalocyanines and related molecules can also be accomplished by varying (i) the type of coordinated metal ions,[18-23] (ii) the arrangement of the tetrapyrrole macrocycles in the compound,[24-34] and/or (iii) the nature of the tetrapyrrole macrocycles themselves.[35-38]

With respect to the latter two points, it is demonstrated that a corrole macrocycle could be incorporated into triple-decker complexes.[36,39,40] The properties of corroles differ from both porphyrins and phthalocyanines in that these macrocycles are dianionic ligands while corroles are trianionic ligands having three inner core amine protons within a contracted tetrapyrrolic ring.[41] Corroles undergo a facile ligand-to-metal electron transfer, introducing so-called “non-innocent” behavior,[42-46] and can also stabilize the central metal ion of the complex in a formally higher oxidation state than for the related porphyrins or phthalocyanines.[47,48] These properties of corroles are particularly appealing for investigated applications of the compounds in the fields of catalysis, chemical sensors and/or dye- sensitized solar cells.[49-52]

In sharp contrast with large amount of research activities involving transition metal corroles,[49-54] very little is known about the corresponding rare earth complexes with this macrocyclic ligand. Studies of corroles with rare earth metal ions are limited to the

monometallic derivatives (Mes_2(*p*-OMePh)Cor)M (M = La·4.5DME; Tb·4DME or Gd·$TACNMe_3$)[55] and triple-decker complexes $M_2[Pc(OC_4H_9)_8]_2[Cor(ClPh)_3]$ (M = Pr-Tb and Y, except Pm) and $Eu_2[Pc(R)_8]_2[Cor(ClPh)_3]$ (R = H, OC_5H_{11} or OC_8H_{17}).[36,39,40]

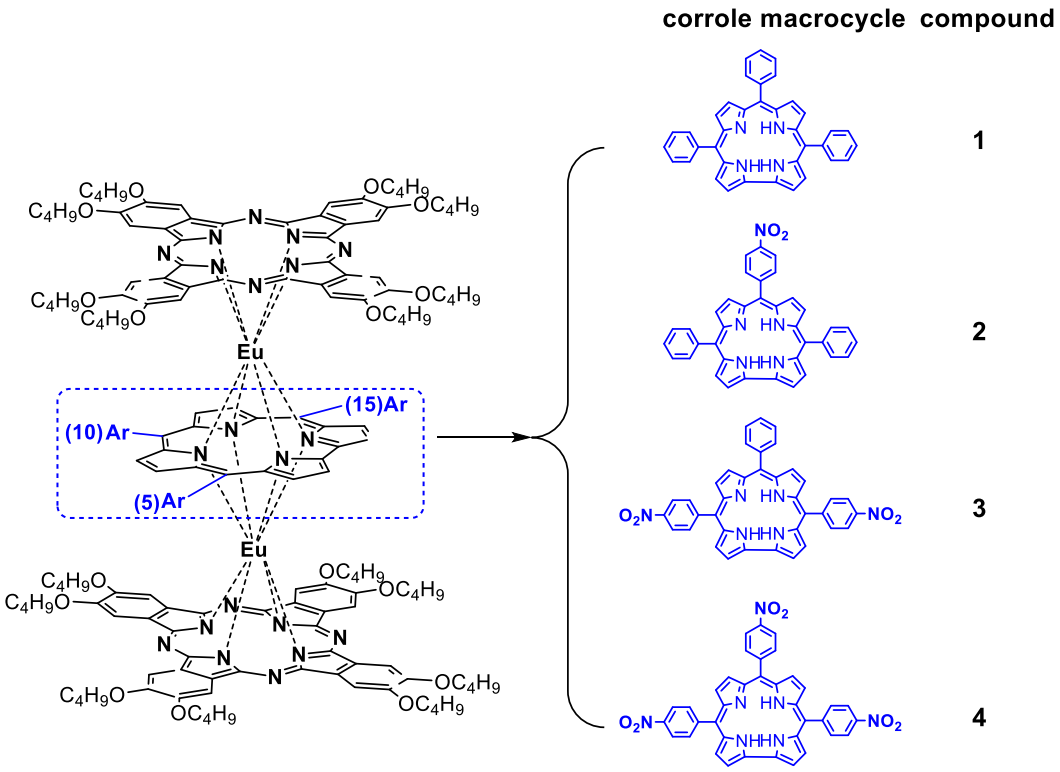

Chart 7-1. Molecular structures of investigated corrole-phthalocyanine europium triple-decker complexes.

This chapter reports the characterization of four heteroleptic corrole-phthalocyanine

europium triple-decker complexes containing nitrophenyl substituents on the *meso* positions of the corrole macrocycle. The investigated complexes are represented as $Eu_2[Pc(OC_4H_9)_8]_2$-$[Cor(Ph)_n(NO_2Ph)_{3-n}]$, where n varies from 0 to 3, $Pc(OC_4H_9)_8$ represents the phthalocyanine macrocycle and Cor the corrole ligand having NO_2Ph substituents at the 5-*meso*, 10,15-*meso* or 5,10,15-*meso* positions of the macrocycle (Chart 7-1).

It has been demonstrated that the presence of one or more nitro groups at the *meso*- or *β*-pyrrole positions of a corrole or porphyrin macrocycle will have a large effect on the $E_{1/2}$ for electroreduction of the mononuclear complex but it was not known what might be observed in the case of the triple-decker species where multiple redox reactions are observed.[42,56-59] Thus one aspect of the current study is to understand how nitro substituents introduced at the *para*-position of the three *meso*-phenyl rings of the corrole macrocycle in a triple-decker complex will influence the redox potentials in the sandwich corrole-phthalocyanine europium derivatives. This is examined in this chapter where the electrochemical and spectroscopic characterization of the synthesized triple-decker complexes and use the combined data to assign the probable site of electron transfer were reported.

7.2 Results and Discussion

7.2.1 Electronic Absorption Spectra

Electronic absorption spectra of the currently investigated triple-decker complexes were recorded in CH_2Cl_2, PhCN and Py and the data are summarized in Table 7-1.

As seen in the table, a characteristic phthalocyanine N band for compounds **1-4** is clearly observed at 294 nm in CH_2Cl_2. This band is assigned to electronic transitions associated with the deeply filled orbitals and the LUMO[60] and could not be detected in PhCN or Py due to the limited UV-visible spectral window of these solvents. Two sharp bands of **1-4** are located at 351-354 and 420-437 nm in CH_2Cl_2, PhCN or Py and these are attributed to the Soret bands of the complexes having a predominant phthalocyanine and corrole character, respectively. Two Q bands are also seen at 534-547 nm and 672-685 nm. These values are

similar to bands for the analogous complexes of $M_2[Pc(OC_4H_9)_8]_2[Cor(ClPh)_3]$ (M = Pr-Tb and Y, except Pm) and $Eu_2[Pc(R)_8]_2[Cor(ClPh)_3]$ (R = H, OC_5H_{11} or OC_8H_{17}.[36,39,40] An intense Q band at ~680 nm is also observed for double- or triple-decker phthalocyanine complexes[61,62] and, on this basis, the bands at 672-685 nm for the currently investigated compounds are also assigned to bands of the Pc macrocycles.

As shown in Table 7-1, three of the five UV-vis bands of the investigated complexes are sensitive to substituents on the corrole macrocycle, while two of the absorption bands are virtually independent of the corrole ring substituents. As will be demonstrated in the spectroelectrochemistry section of this chapter, the changes in intensity or position of the 420-439 nm (corrole) band and 672-684 nm (phthalocyanine) bands after oxidation or reduction can be used to provide indirect evidence for the site of electron transfer being predominantly corrole or phthalocyanine-centered in a specific redox process.

Table 7-1. Electronic absorption data for $Eu_2[Pc(OC_4H_9)_8]_2[Cor(Ph)_n(NO_2Ph)_{3-n}]$ in CH_2Cl_2, PhCN and pyridine.

Solvent	# of NO_2 groups n	λ_{max}/nm (logε)				
CH_2Cl_2	0	294 (5.17)	351 (5.27)	420 (4.90)	534 (4.57)[a]	682 (4.79)
	1	294 (5.28)	351 (5.36)	425 (4.97)	542 (4.66)[a]	674 (4.93)
	2	294 (5.19)	352 (5.27)	433 (4.90)	545 (4.58)[a]	685 (4.88)
	3	294 (5.17)	351 (5.24)	436 (4.87)	547 (4.56)[a]	680 (4.86)
PhCN	0	[b]	353 (5.06)	421 (4.71)	530 (4.33)[a]	680 (4.65)
	1	[b]	353 (5.18)	430 (4.80)	544 (4.47)[a]	675 (4.79)
	2	[b]	354 (5.24)	435 (4.86)	545 (4.53)[a]	683 (4.90)
	3	[b]	353 (5.07)	439 (4.70)	550 (4.39)[a]	680 (4.73)
Py	0	[b]	353 (5.25)	420 (4.92)	534 (4.52)[a]	680 (4.82)
	1	[b]	354 (5.23)	429 (4.84)	542 (4.47)[a]	672 (4.82)
	2	[b]	354 (5.27)	433 (4.92)	545 (4.55)[a]	684 (4.93)
	3	[b]	353 (5.28)	437 (4.90)	547 (4.55)[a]	680 (4.95)

[a] Broad and weak band. [b] This band could not be observed in PhCN or pyridine.

7.2.2 Electrochemistry

Corrole-phthalocyanine rare earth triple-decker complexes in CH_2Cl_2 containing 0.1 M TBAP were recently reported to undergo up to eight reversible or quasi-reversible one-electron oxidations and reductions, all of which are attributed to the successive removal or addition of electrons from the ligand-based orbitals of the compound.[36,39] The addition of 1-3 nitrophenyl groups at the *meso*-positions of the corrole macrocycle in compounds **2-4** should lead to additional reactions being observed at the redox active NO_2Ph substituents[56,57] as well as to a progressive shift of all redox potentials towards more positive values (easier reductions and harder oxidations) as compared to the parent triple-decker compound **1** with a central triphenylcorrole ligand. However, it was not clear what would be the magnitude of the potential shift for each added electron-withdrawing NO_2 group, since this would depend upon the specific site of each electron transfer. It was also not clear if the nitrobenzene substituents on compounds **3** and **4** would interact with each other and be reduced at different half-wave potentials as occurs for some mono-macrocyclic corroles with these substituents,[57] or if the redox active NO_2Ph substituents would be non-interacting and all be reduced at the same half-wave potential as has been reported to occur for other corroles with *meso*-NO_2Ph groups.[57,58]

In order to answer these questions, four $Eu_2[Pc(OC_4H_9)_8]_2[Cor(Ph)_n(NO_2Ph)_{3-n}]$ complexes containing different numbers of NO_2Ph groups were examined as to their electrochemistry in three nonoaqueous solvents (CH_2Cl_2, PhCN and Py) containing 0.1 M TBAP. A summary of the measured half-wave potentials in the different solvents is given in Table 7-2, which includes the proposed site of the initial electron transfer based on analysis of the electrochemical and spectroscopic data. Examples of cyclic voltammograms in the three solvents are shown in Figure 7-1 (PhCN), Figure 7-2 (CH_2Cl_2) and Figure 7-3 (Py).

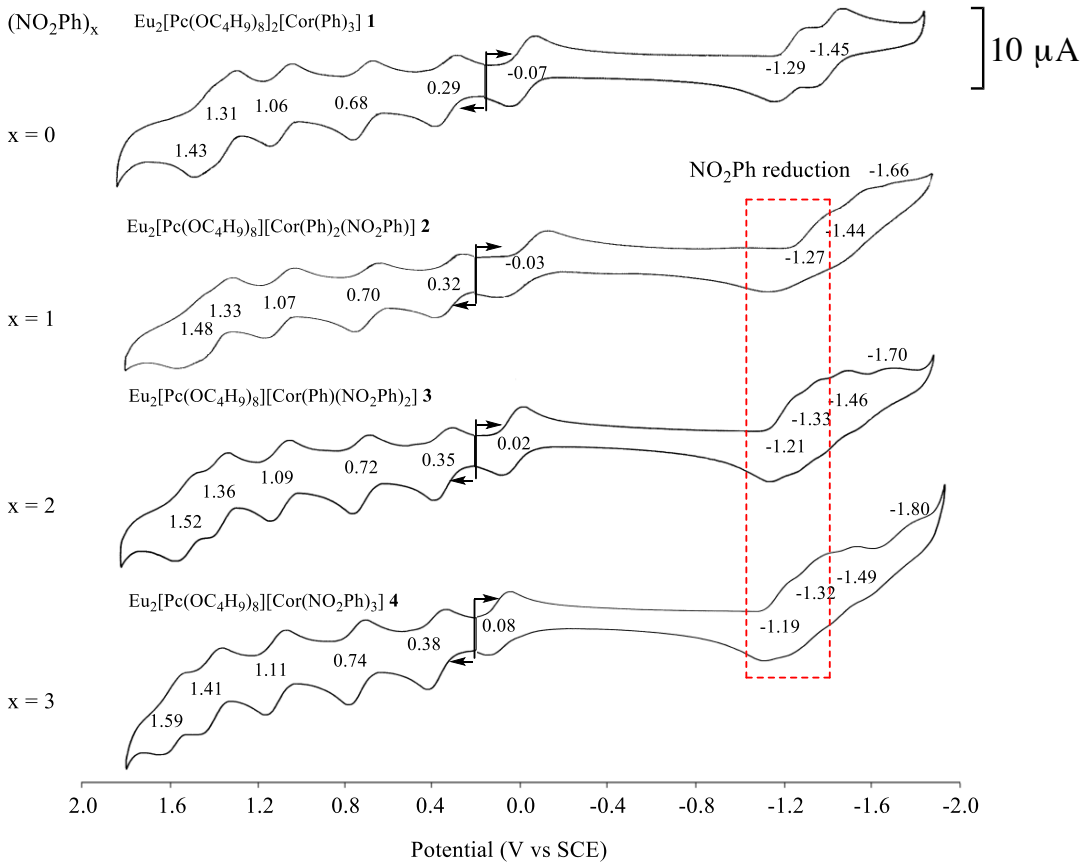

Figure 7-1. Cyclic voltammograms of compounds **1-4** in PhCN containing 0.1 M TBAP. Reductions of the *meso*-NO_2Ph substituents are indicated by processes within the box.

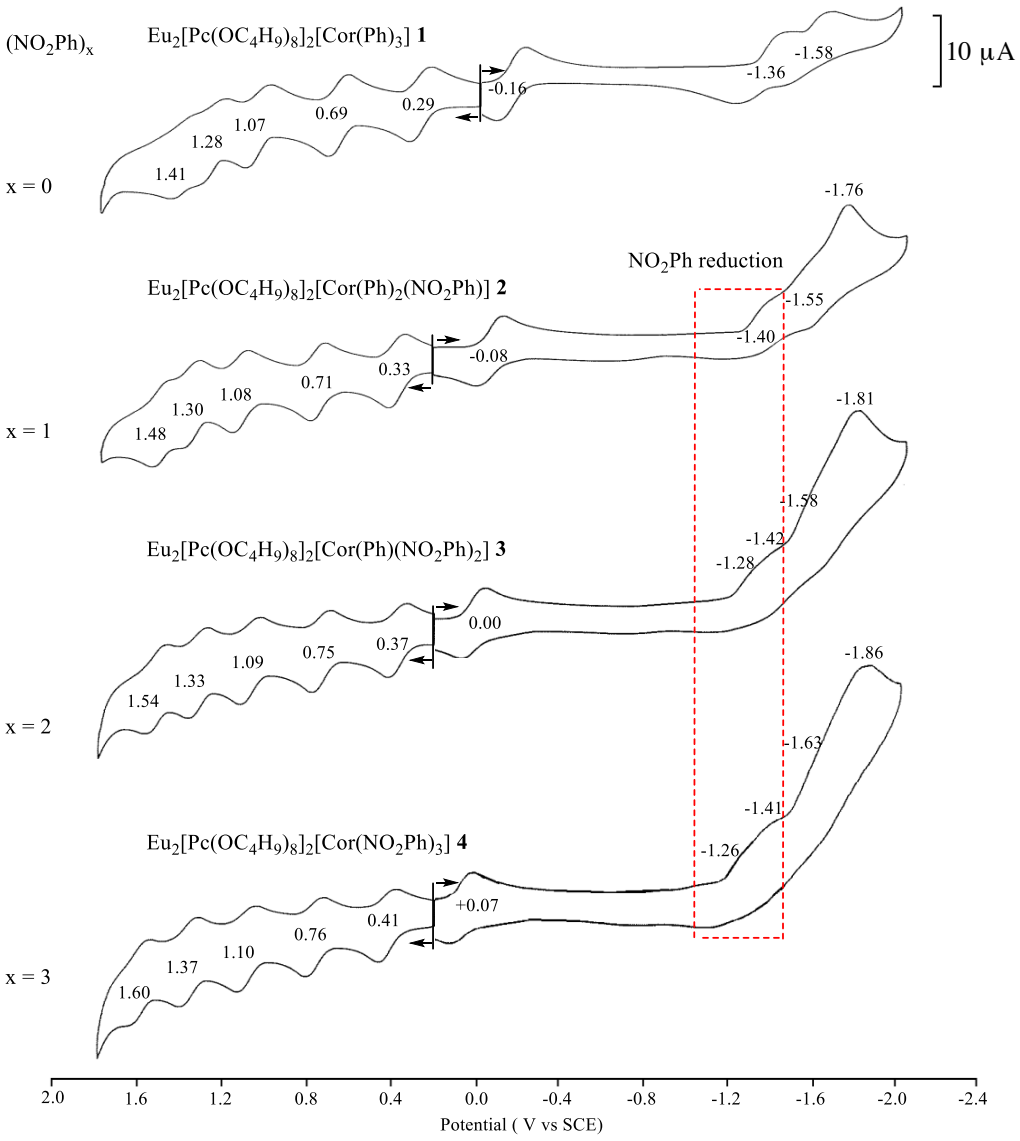

Figure 7-2. Cyclic voltammograms of compounds **1-4** in CH_2Cl_2 containing 0.1 M TBAP. The reductions of NO_2Ph are indicated by processes within the boxed area.

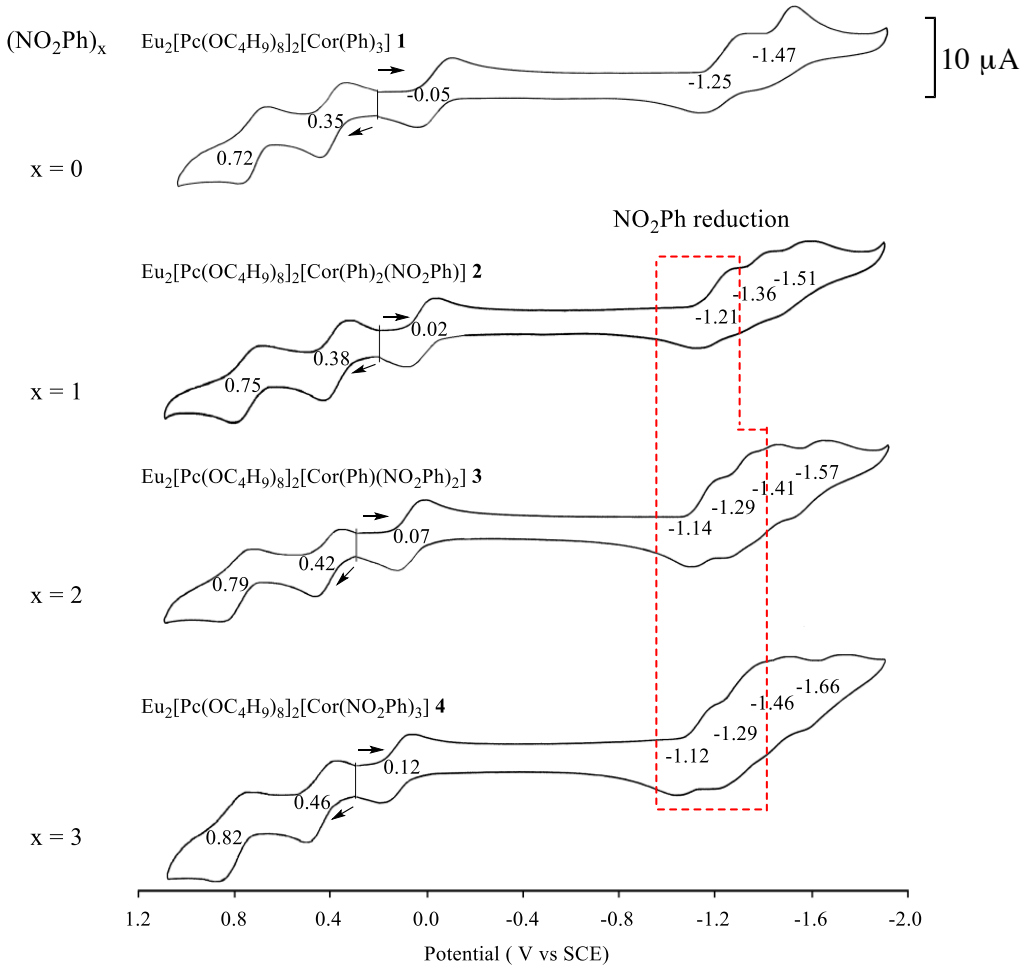

Figure 7-3. Cyclic voltammograms of compounds **1-4** in pyridine containing 0.1 M TBAP. The reductions of NO_2Ph are indicated by processes within the boxed area.

Table 7-2. Half-wave potentials ($E_{1/2}$, V *vs* SCE) and proposed sites of electron transfer (Cor or Pc) for the oxidations and reductions of $Eu_2[Pc(OC_4H_9)_8]_2[Cor(Ph)_n(NO_2Ph)_{3-n}]$ (**1-4**) and $Eu_2[Pc(OC_4H_9)_8]_2[Cor(PhCl)_3]$ (**5**) in PhCN, CH_2Cl_2 or Py containing 0.1 M TBAP. (Data are good to ±10 mV)

.

Solvent	# of NO_2 n	cpd	oxidation					reduction				
			fifth (Cor)	fourth	third (Pc)	second (Pc)	first (Cor)	first (Cor)	second (NO_2Ph)	third (NO_2Ph)	fourth	fifth
CH_2Cl_2	0	**1**	1.41	1.28	1.07	0.69	0.29	-0.16			-1.36	-1.58
	1	**2**	1.48	1.30	1.08	0.71	0.33	-0.08	-1.40[a]		-1.55[a]	-1.76[a]
	2	**3**	1.54	1.33	1.09	0.75	0.37	0.00	-1.28[a]	-1.42[a]	-1.58[a]	-1.81[a]
	3	**4**	1.60	1.37	1.10	0.76	0.41	0.07	-1.26[a]	-1.41[a]	-1.63[a]	-1.86[a]
		5[b]	1.46	1.30	1.09	0.72	0.33	-0.11			-1.36	-1.58
PhCN	0	**1**	1.43	1.31	1.06	0.68	0.29	-0.07			-1.29	-1.45
	1	**2**	1.48	1.33	1.07	0.70	0.32	-0.03	-1.27		-1.44	-1.66[a]
	2	**3**	1.52	1.36	1.09	0.71	0.35	0.02	-1.21	-1.33	-1.46	-1.70[a]
	3	**4**	1.59	1.41	1.11	0.74	0.38	0.08	-1.19	-1.32	-1.50	-1.80[a]
		5	1.43	1.31	1.08	0.71	0.33	-0.04			-1.25	-1.44
Pyridine	0	**1**				0.72	0.34	-0.05			-1.25	-1.47
	1	**2**				0.75	0.38	0.02	-1.21		-1.36	-1.51
	2	**3**				0.79	0.42	0.07	-1.14	-1.29	-1.41	-1.57
	3	**4**				0.82	0.46	0.12	-1.12	-1.29	-1.46	-1.66
		5				0.75	0.38	0.00			-1.24	-1.44

[a] Irreversible peak potential, E_p, at scan rate of 0.10 V/s. [b] Data for compound **5** is taken from Ref. 39. *tw* = this work.

Compound **1**, which has no nitro substituents on the corrole (see Chart 7-1), exhibits five oxidations and three reductions in PhCN (Figure 7-1) or CH_2Cl_2 (Figure 7-2), both containing 0.1 M TBAP. Each redox reaction involves a reversible one-electron transfer and each is attributed to a ligand-based redox process. Similar current-voltage curves are observed for reduction of compound **1** in Py (Figure 7-3), but only two oxidations can be detected in this solvent due to the limited positive potential window of about 1.0 V.

As expected, the electron-withdrawing nitrophenyl groups on the corrole macrocycles of **2**, **3** and **4** induce a positive shift of all oxidations as compared to the parent compound **1** which lacks NO_2 substituents. For example, as seen in Figure 7-1, the reversible $E_{1/2}$ value for the first oxidation of **1** (with no NO_2 groups) is located at 0.29 V, while $E_{1/2}$ for the same redox reaction shifts to 0.32 V for **2** (which contains one NO_2 group), 0.35 V for **3** (with two NO_2 groups) and 0.38 V for **4** (with three NO_2 groups). The difference in $E_{1/2}$ values between the reversible one-electron oxidations of **1** and **4** is 90 mV in PhCN (Figure 7-1), 120 mV in CH_2Cl_2 (Figure 7-2) and 170 mV in Py (Figure 7-3).

A significant positive shift in $E_{1/2}$ also occurs for the first ligand-based reduction of compounds **2-4** as compared to compound **1** under the same solution conditions. This is seen from the electrochemical data in Table 7-2 as well as from the cyclic voltammograms in Figure 7-1 (PhCN), Figure 7-2 (CH_2Cl_2) and Figure 7-3 (py). The $E_{1/2}$ values for the first one-electron reduction of compounds **1-4** in PhCN are located at -0.07, -0.03, 0.02 and 0.08 V, respectively, and the difference in $E_{1/2}$ between compounds **1** and **4** is 150 mV. This $\Delta E_{1/2}$ value increases to 170 mV in pyridine (Figure 7-3) and 230 mV in CH_2Cl_2 (Figure 7-2), indicating that the potentials for reduction are dependent not only upon the electron-withdrawing characteristics of the *meso*-nitrophenyl substituents but also upon the solvent.

Smaller positive shifts in potential with an increase in the number of NO_2 groups are seen for the second, third and fourth oxidations of **1-4** in PhCN and the same trend in $E_{1/2}$ with

the number of NO_2Ph groups on the compound occurs in CH_2Cl_2 and py as shown in Figures 7-1, 7-2 and 7-3, as well as in Table 7-2.

Compound **1** (which has no NO_2 groups) exhibits three reversible one-electron transfer steps in PhCN containing 0.1 M TBAP. The first reduction is at $E_{1/2}$ = -0.07 V, the second at $E_{1/2}$ = -1.29 V and the third at $E_{1/2}$ = -1.45 V (Figure 7-1). In contrast, four reductions can be seen in the cyclic voltammogram of **2** in PhCN (which has one NO_2 group). These reductions are located at $E_{1/2}$ = -0.03, -1.27, -1.44 V and E_{pc} = -1.66 V, respectively (Figure 7-1). The second reduction of **2** is assigned to the *meso*-NO_2Ph substituent and the $E_{1/2}$ of -1.27 V in PhCN and is shifted negatively by 80 mV as compared to the $E_{1/2}$ of -1.19 V for reduction of unlinked nitrobenzene under the same solution condition (Figure 7-4). The second reduction of compounds **3** and **4** is also assigned as a one-electron addition to a *meso*-NO_2Ph group on the macrocycle. This conversion of the linked NO_2Ph group to $[NO_2Ph]^-$ occurs at $E_{1/2}$ = -1.21 V and -1.19 V for **3** and **4**, respectively, the latter value being exactly the same as the half-wave potential for reduction of unlinked nitrobenzene in PhCN (see Figure 7-4).

The singly reduced $[NO_2Ph]^-$ product of the *meso*-nitrobenzene substituents on compounds **2**, **3** and **4** is unstable in CH_2Cl_2 containing trace water or protons and this leads to irreversible processes as seen in Figure 7-2. However, greater reversibility is obtained in PhCN and pyridine where reversible half-wave potentials for the stepwise reduction of each NO_2Ph group can be measured from cyclic voltammograms of the type shown in Figures 7-1, 7-3 and 7-5. For example, compound **3** exhibits five one-electron reduction processes in pyridine ($E_{1/2}$ = 0.07, -1.14, -1.29, -1.41 and -1.57 V), the second and third of which correspond to electron addition at the 5 and 15 *meso*-NO_2Ph groups on the compound (Figures 7-5). The fact that the two equivalent NO_2Ph groups in compound **3** are reduced at different half-wave potentials indicates an interaction between these redox active centers across the molecule. The $\Delta E_{1/2}$ of 150 mV between these two one-electron reductions of the

NO_2Ph groups in pyridine (and 120 mV in PhCN) indicates a moderately strong interaction. Moreover, reduction of the three *meso*-NO_2Ph substituents on compound **4** in pyridine occurs in two steps, the first of which involves a reversible one-electron addition at $E_{1/2}$ = -1.12 V and the second, two overlapping one-electron transfer steps at the same half-wave potential of -1.29 V (Figure 7-3). Again, the first one-electron reduction potential of the *meso*-NO_2Ph groups on compounds **3** and **4** are virtually identical to each other in pyridine (-1.12 and -1.14 V) and they are also almost identical to the $E_{1/2}$ for reduction of unlinked nitrobenzene under the same solution conditions ($E_{1/2}$ = -1.15 V, as illustrated in Figure 7-4).

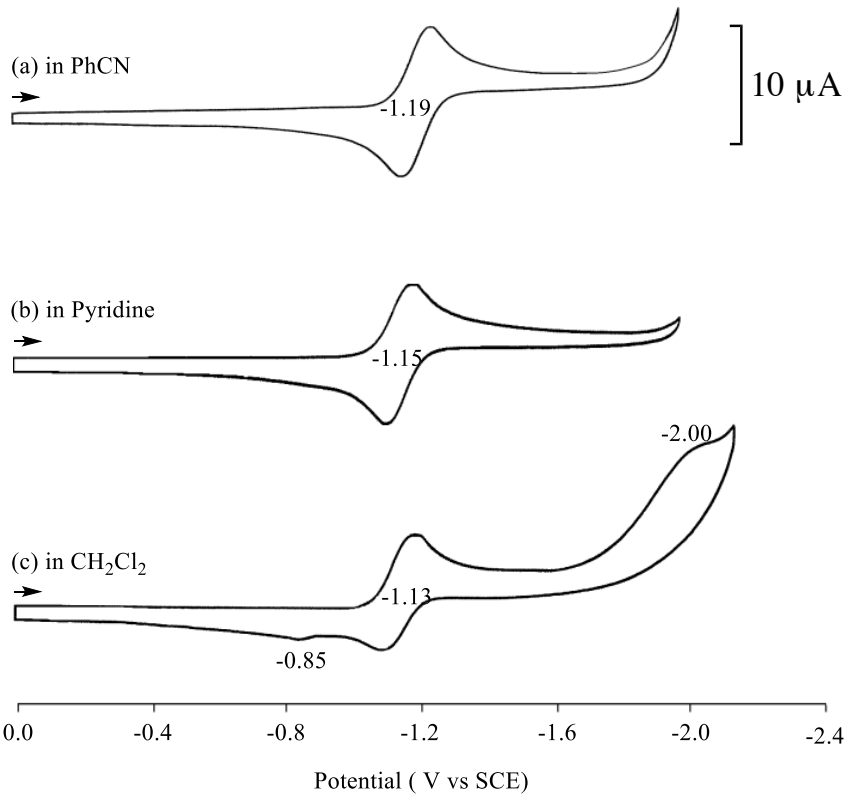

Figure 7-4. Cyclic voltammograms of NO_2Ph in (a) PhCN, (b) pyridine and (c) CH_2Cl_2 containing 0.1 M TBAP.

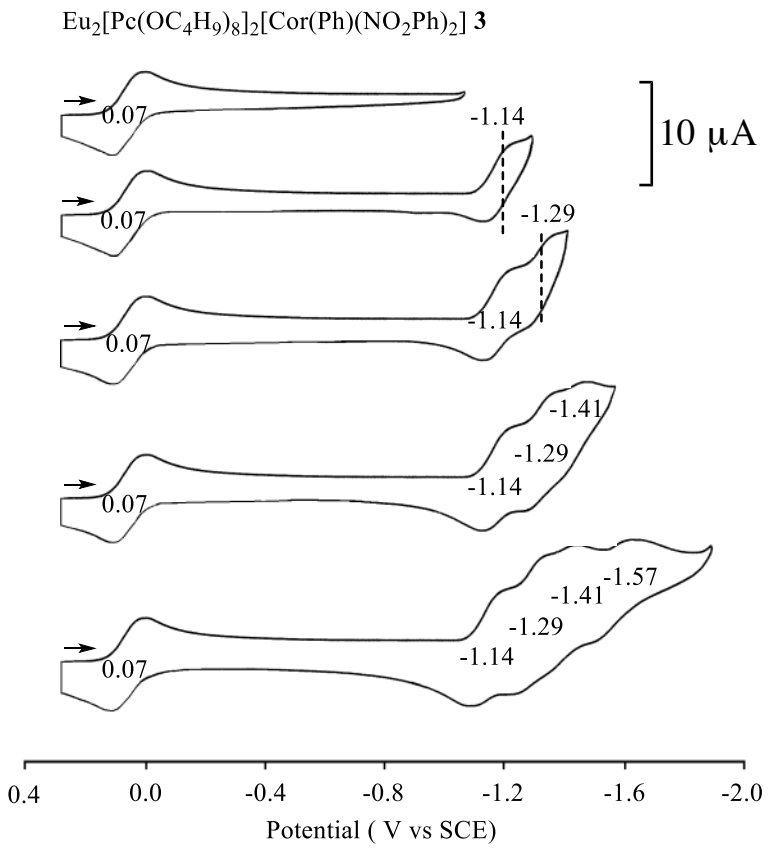

Figure 7-5. Cyclic voltammograms of $Eu_2[Pc(OC_4H_9)_8]_2[Cor(Ph)(NO_2Ph)_2]$ **3** in pyridine containing 0.1 M TBAP. The reversible processes at $E_{1/2}$ = -1.14 and -1.29 V are assigned to stepwise reductions of the *meso*-NO_2Ph substituents on the corrole.

In summary, compounds **2-4** exhibit one or two more reductions than compound **1** as shown in Figures 7-1, 7-2 and 7-3. These reductions are assigned to the electroactive NO_2Ph groups, each of which is reversibly converted to its $[NO_2Ph]^-$ form in a stepwise one-electron transfer. This result is quite different from what was reported for reduction of the *meso*-NO_2Ph groups on copper and cobalt corroles where all three nitrobenzene reductions occur at the same half-wave potential [58] and it is also different from free-base, palladium or zinc porphyrins having nitrophenyl substituents at the four *meso*-positions of the macrocycle, where a single multi-electron reduction is observed.[59]

Finally, it should be noted that the reduction of unlinked nitrobenzene in CH_2Cl_2 containing 0.1M TBAP proceeds in two steps, the second of which is irreversible and located at a peak potential of ~ -2.0 V (Figure 7-4c). Similar irreversible reductions are seen for the compounds **2-4** in CH_2Cl_2 (Figure 7-2) but the exact potential of these electron transfers could not be easily measured nor could the site of electron transfer be precisely determined.

As shown in the following section, the measured $E_{1/2}$ values for oxidation of **1-4** are linearly related to the number of NO_2Ph groups on the corrole, with the magnitude of the shift in potential for each redox reaction being related to the predominate macrocyclic site of electron transfer, either corrole or phthalocyanine.

7.2.3 Substituent Effects, Spectroelectrochemistry and Site of Electron Transfer

As described above, and shown in Figure 7-1, half-wave potentials for the five oxidations and first reduction of compounds **1-4** vary with the number of electron-withdrawing NO_2Ph groups on the compounds. Increasing the number of NO_2Ph groups on the corrole leads to a progressive positive shift in the reversible half-wave potentials for the first one-electron reduction and five one-electron oxidations of the compounds, with the magnitude of the shift being dependent upon both the solvent and the specific redox reaction as shown by the plots in Figure 7-6. A linear correlation exists between $E_{1/2}$ and the number of NO_2Ph groups on the corrole for the six examined redox reactions in PhCN or CH_2Cl_2 and the

trend in the substituent effect is the same in both solvents, namely a much larger effect of the NO_2Ph groups on $E_{1/2}$ for the first reduction and first oxidation, where the slopes of the plots in PhCN (Figure 7-6a) are 50 and 30 mV as compared to the second and third oxidations of the same compounds in PhCN where the slopes are 19 and 17 mV, respectively. The same relative trend in substituent effects is seen in CH_2Cl_2 (Figure 7-6b) where the largest slope is seen for the first reduction (77 mV) and the smallest for the third oxidation (10 mV), the latter of which displays an almost negligible effect of the electron-withdrawing NO_2Ph groups on the redox potentials.

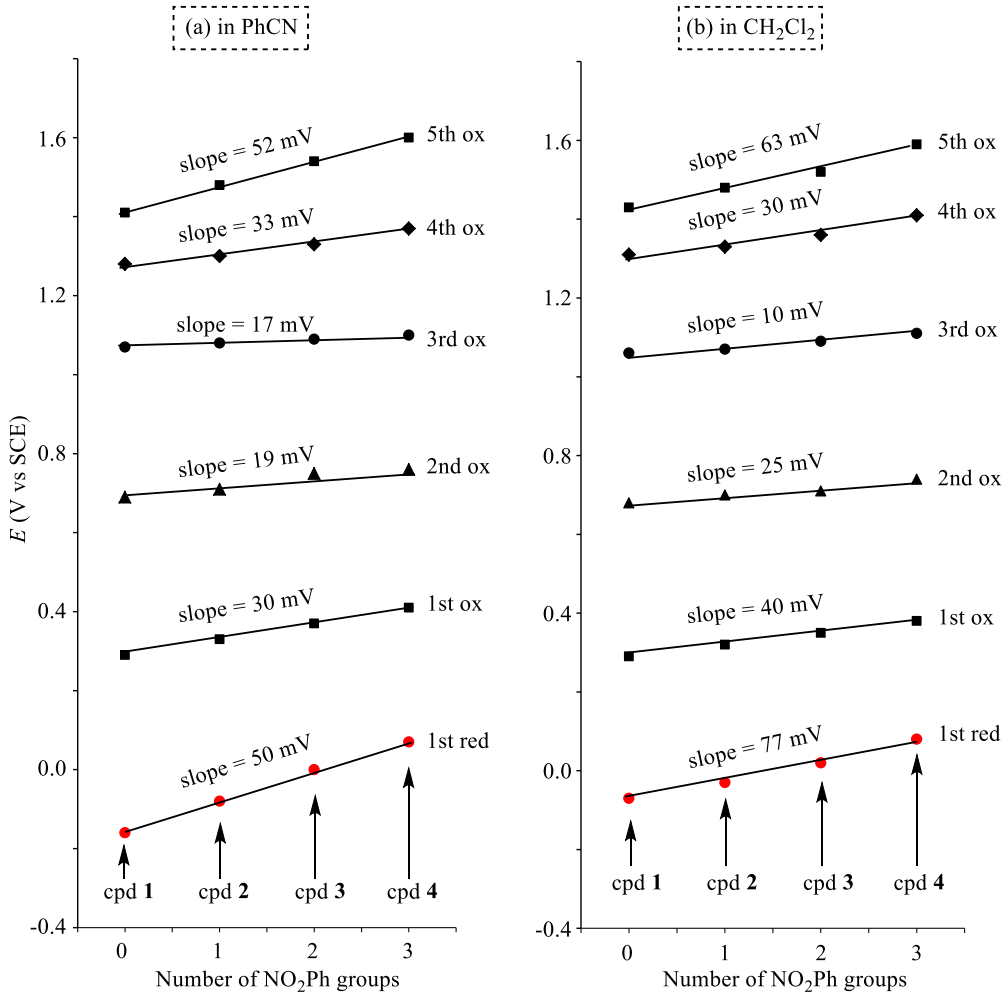

Figure 7-6. Plots of redox potentials *vs* the number of NO_2Ph groups on compounds **1-4** in (a) PhCN and (b) CH_2Cl_2 containing 0.1 M TBAP.

The relative magnitude of the substituent effect should be related to the probable site of electron transfer and the data in Figure 7-6 provides strong indirect evidence for the first reduction and first oxidation of **1-4** being located on the corrole macrocycle. This contrasts with the second and third oxidations of the compounds in the two solvents that "feel" only slightly the effect of the electron-withdrawing NO_2Ph groups, thus indicating an electron transfer site more localized on the two phthalocyanine macrocycles which are farther removed from the corrole *meso*-NO_2Ph substituents.

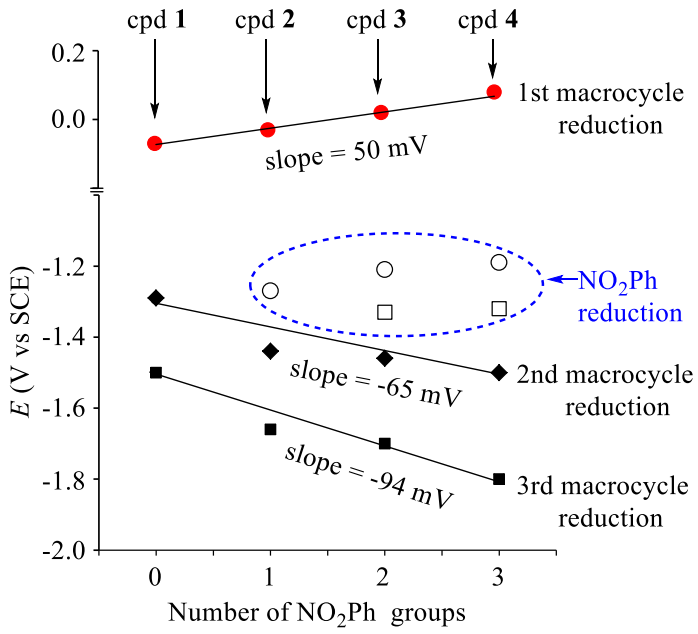

Figure 7-7. Plots of reduction potentials *vs* the number of NO_2Ph groups on compounds **1-4** in PhCN containing 0.1 M TBAP.

The effect of NO_2Ph groups on the second reduction potentials of **2-4** in PhCN (Figure 7-7), CH_2Cl_2 (Figure 7-8) and pyridine (Figure 7-9) also provides strong indirect evidence for this electron transfer process being totally localized on an NO_2Ph substituent of the compounds. This one-electron reduction occurs at $E_{1/2}$ = -1.19 to -1.27 V in PhCN (Figure 7-7), -1.12 to -1.21 V in pyridine (Figure 7-9), and E_{pc} = -1.26 to -1.40 V in CH_2Cl_2 (Figure 7-8), values which are almost identical to the measured half-wave potentials for the one-electron reduction of unlinked nitrobenzene under the same solution conditions (see Figure 7-4). The third reduction of compounds **3** and **4** also involves the NO_2Ph groups on the compounds. These processes occur at about -1.41 V in CH_2Cl_2, -1.33 V in PhCN and -1.29 V in pyridine (see Table 7-2).

The last two reductions of compounds **2**, **3** and **4** are assigned to electron additions at the corrole or phthalocyanine π ring system (as opposed to the redox active nitrobenzene substituents) and the negative shift of $E_{1/2}$ shown in Figure 7-7 with increasing number of NO_2Ph groups for these two processes can be accounted for by the increasing negative charge on the molecules with each conversion of a *meso*-NO_2Ph substituent to its $[NO_2Ph]^-$ form.

In summary, the data analysis in Figures 7-6 and 7-7 provides strong indirect evidence for assigning the probable the site of electron transfer in the first two one-electron reductions and first three one-electron oxidations of compounds **1-4**. Two additional pieces of evidence are given in support of these assignments. The first involves a correlation between the measured potentials for oxidation or reduction and the Hammett substituent constants associated with the nitro groups on the corrole (Figure 7-10). The second involves an analysis of UV-vis spectra for the electroreduced or electrooxidized species obtained by thin-layer UV-vis spectroelectrochemistry.

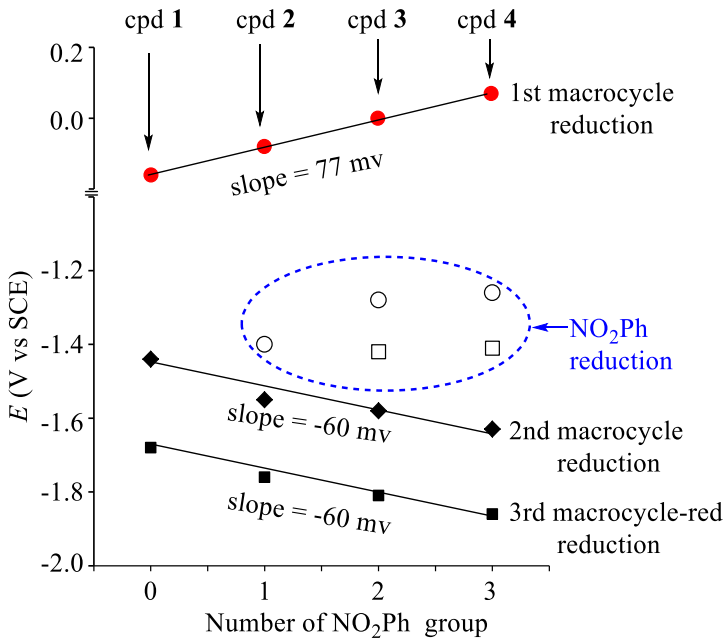

Figure 7-8. Plots of reduction potentials in CH_2Cl_2 containing 0.1 M TBAP vs. the number of NO_2Ph groups of compounds **1-4**.

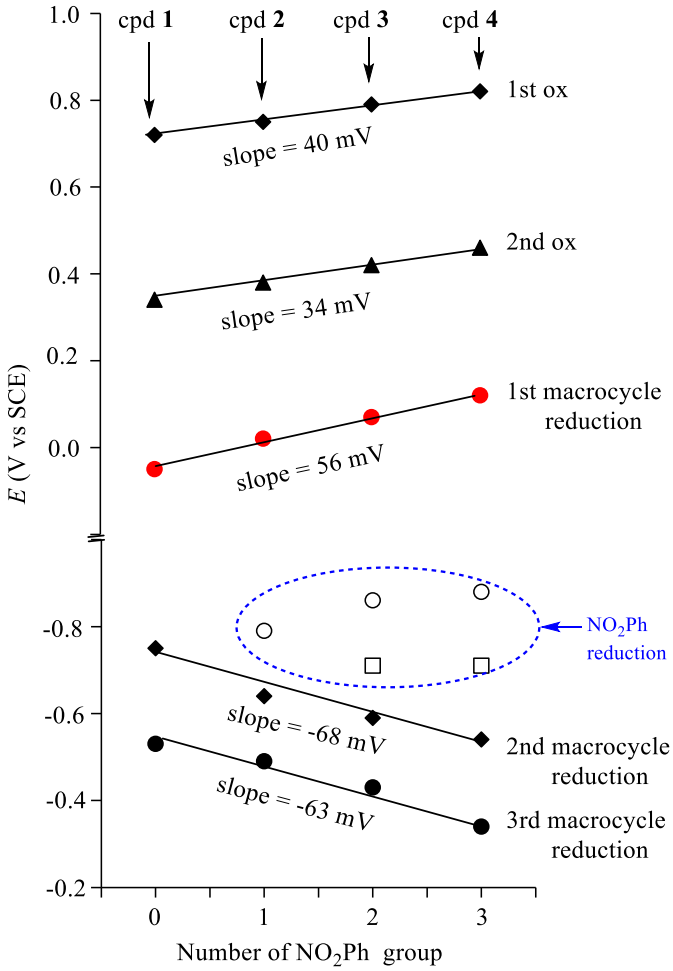

Figure 7-9. Plots of redox potentials in pyridine containing 0.1 M TBAP vs. the number of NO_2Ph groups on compounds **1-4**.

The effect of electron donating or electron withdrawing substituents on half-wave potentials for oxidation or reduction of compounds **1-4** can be quantified by the use of equation 1[63,64] where σ is the electron-donating or electron-withdrawing characteristic of the substituent[65] and ρ is the magnitude of the interaction between the substituent and the site of electron transfer. The larger the value of ρ, the larger the effect of the substituents on the reaction site. A plot $E_{1/2}$ vs Σσ can then be used to suggest the site of electron transfer in much the same way as the plots in Figures 7-6 and 7-7.

$$\Delta E_{1/2} = \Sigma\sigma\rho \qquad (1)$$

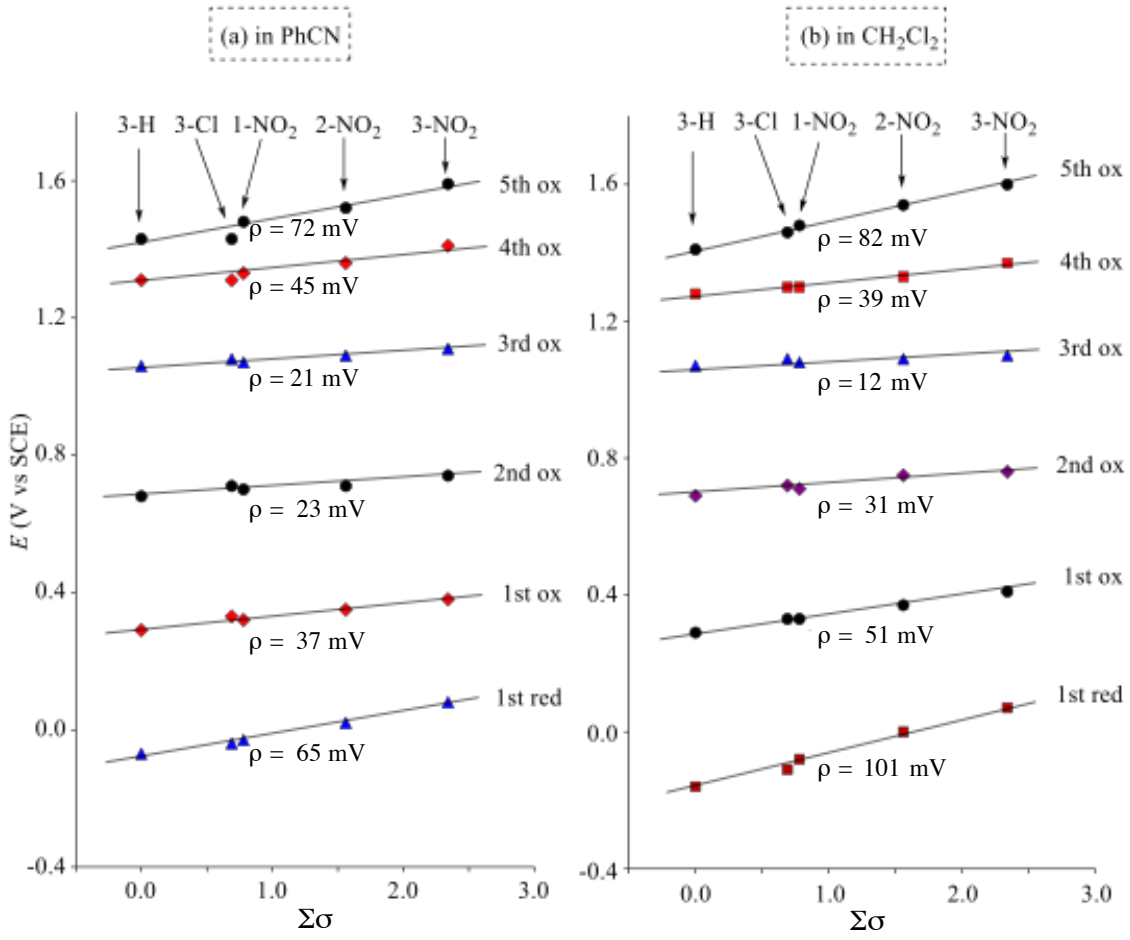

Figure 7-10. Plots of the redox potentials (a) PhCN and (b) CH_2Cl_2 containing 0.1 M TBAP *vs* the sum of the Hammett substituent constants (Σσ) for the triple-decker complexes containing Cl, H or NO_2 groups on the *para*-positions of the *meso*-phenyl rings of the corrole macrocycle in. The Hammett substituent constants are taken from Ref. 63.

A plot of the measured potentials for the first reduction and five oxidations of compounds **1-4** is given in Figure 7-10. Also included in this figure are potentials for the same six redox reactions of $Eu_2[Pc(OC_4H_9)_8]_2[Cor(PhCl)_3]$ **5** which possesses a ClPh substituent at the three *meso*-positions of the corrole macrocycle.

The values of ρ for ring-centered reductions or oxidations of porphyrins and corroles with phenyl substituted groups at the *meso*-positions of the macrocycle generally range from for 30-50 mV for monomeric compounds.[64] Much smaller values of ρ are sometimes observed when the reaction site is farther removed from the electron-donating or electron-withdrawing substituents, a good example being in the case of metal-centered redox reactions. With this in mind, one can use the linear free energy relationships in Figure 7-10 as a diagnostic criteria to propose the probable initial site of electron transfer in each redox reaction. A relatively large value of ρ suggests a redox reaction at the corrole macrocycle containing the substituents and relatively small value of ρ will suggest a reaction at the phthalocyanine macrocycles which are farther removed from the electron-withdrawing NO_2Ph substituents and separated from the corrole ligand by a europium ion.

The data in Figure 7-10 are consistent with the linear free energy relationships illustrated in Figures 7-6 and 7-8. The largest value of ρ (101 mV) is observed for the first reduction of the compounds in CH_2Cl_2 and this process is assigned as electron addition to the corrole macrocycle on the basis of the large ρ value. The smallest value of ρ is seen for the third oxidation of the compounds in CH_2Cl_2 (12 mV) and this process is assigned as involving electron abstraction from one or both of the Pc macrocycles. The ρ for the first oxidation of the five compounds in Figure 7-10 is 51 mV in CH_2Cl_2 compared to 31 mV for the second oxidation in this solvent. This is also consistent with assignment of electron abstraction from the corrole macrocycle in the first oxidation.

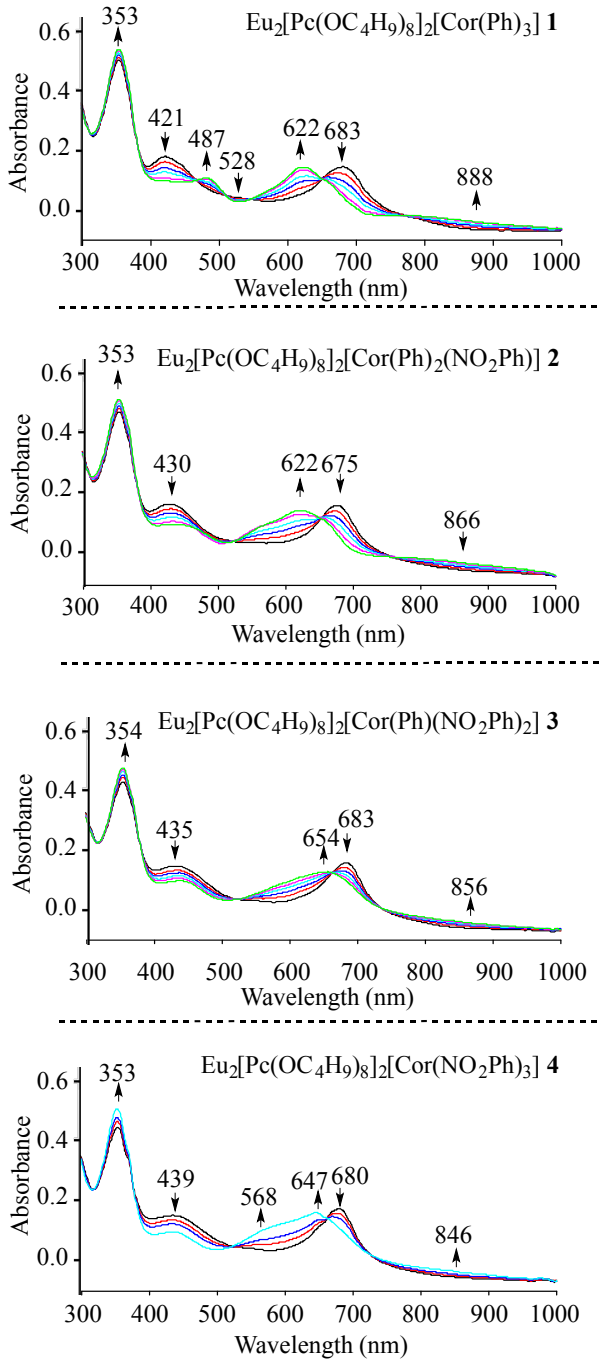

Figure 7-11. UV-vis spectral changes during the first controlled potential reduction of compounds **1**-**4** at -0.60 V in PhCN containing 0.1 M TBAP.

A similar comparison of ρ values can be made for the data in PhCN where the slopes are 37 mV and 23 mV for the first and second oxidations, repectively. This also suggests an oxidation at the corrole macrocycle but, as shown by the spectroelectrochemical data described below, this process also has some characteristics of a Pc-based electron abstraction.

The spectral changes which occur during the first controlled reduction of **1-4** in PhCN are illustrated in Figure 7-11 and are the most definitive in terms of assigning the probable site of electron addition. The band at 412-439 nm is attributed to the corrole Soret band. The fact that this band significantly decreases in intensity after the addition of one electron is consistent with electron addition to the π-ring system of the corrole and also fits with the very large ρ values in Figure 7-10. Also consistent with assignment of reaction at the corrole is the fact that the phthalocyanine Q band at 675-683 nm shifts to 622-647 nm but remains relatively unchanged in intensity. This later change indicates a reduction which is not located prominently on the π ring system of the phthalocyanine macrocycles although it should be noted that the singly reduced species has a broad band from 700-950 nm, which could indicate some radical character.

The Q band assigned to the phthalocyanine macrocycle at 676-683 nm remains well-defined after the first controlled potential oxidation of compounds **1-4** but deceases in intensity. This is illustrated in Figure 7-12 for the case of **1** and Figure 7-13 for **2** and **3**, where the controlled potential oxidation was carried out at +0.50 V (compounds **1** and **2**) or +0.60 V (compound **3**). The 353-356 nm band assigned to the Pc macrocycle also decreases slightly in intensity during the first oxidation of **1-4**, thus suggesting some degree of positive charge on the Pc macrocycles.

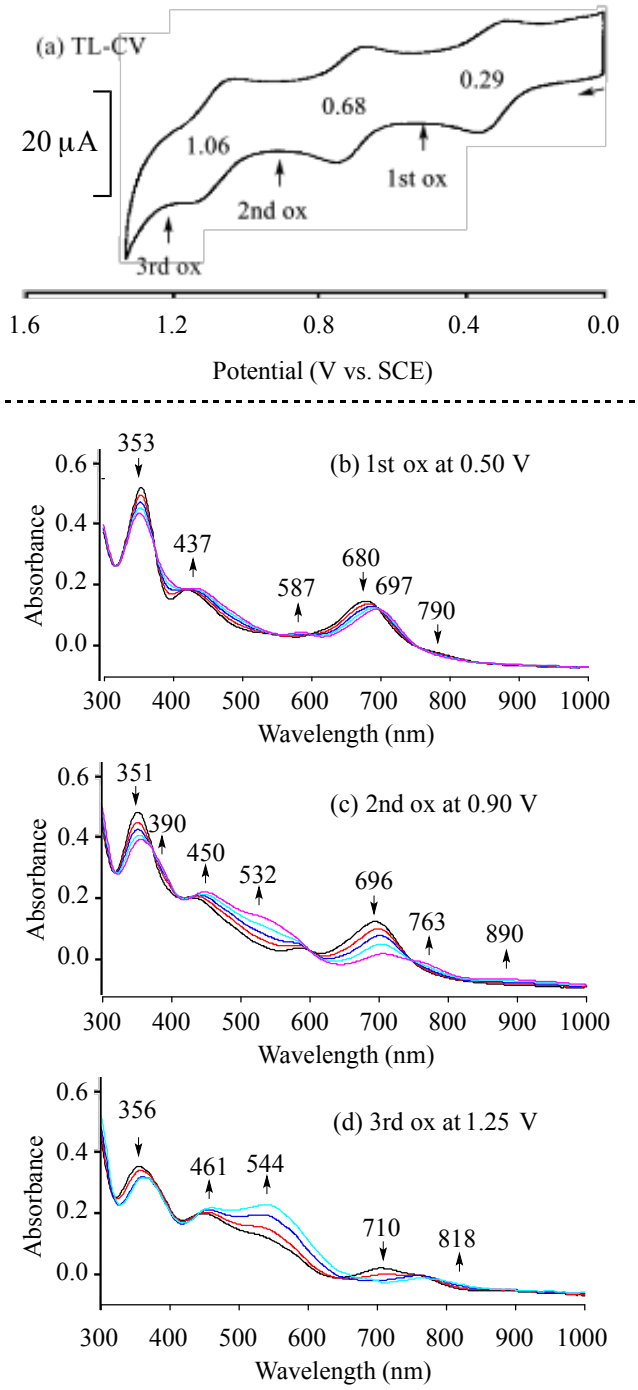

Figure 7-12. (a) Thin-layer cyclic voltammogram of $Eu_2[Pc(OC_4H_9)_8]_2[Cor(Ph)_3]$ **1** in PhCN containing 0.1 M TBAP and UV-vis spectral changes during the first three controlled potential one-electron oxidations at (b) 0.50 V, (c) 0.90 V and (d) 1.25 V.

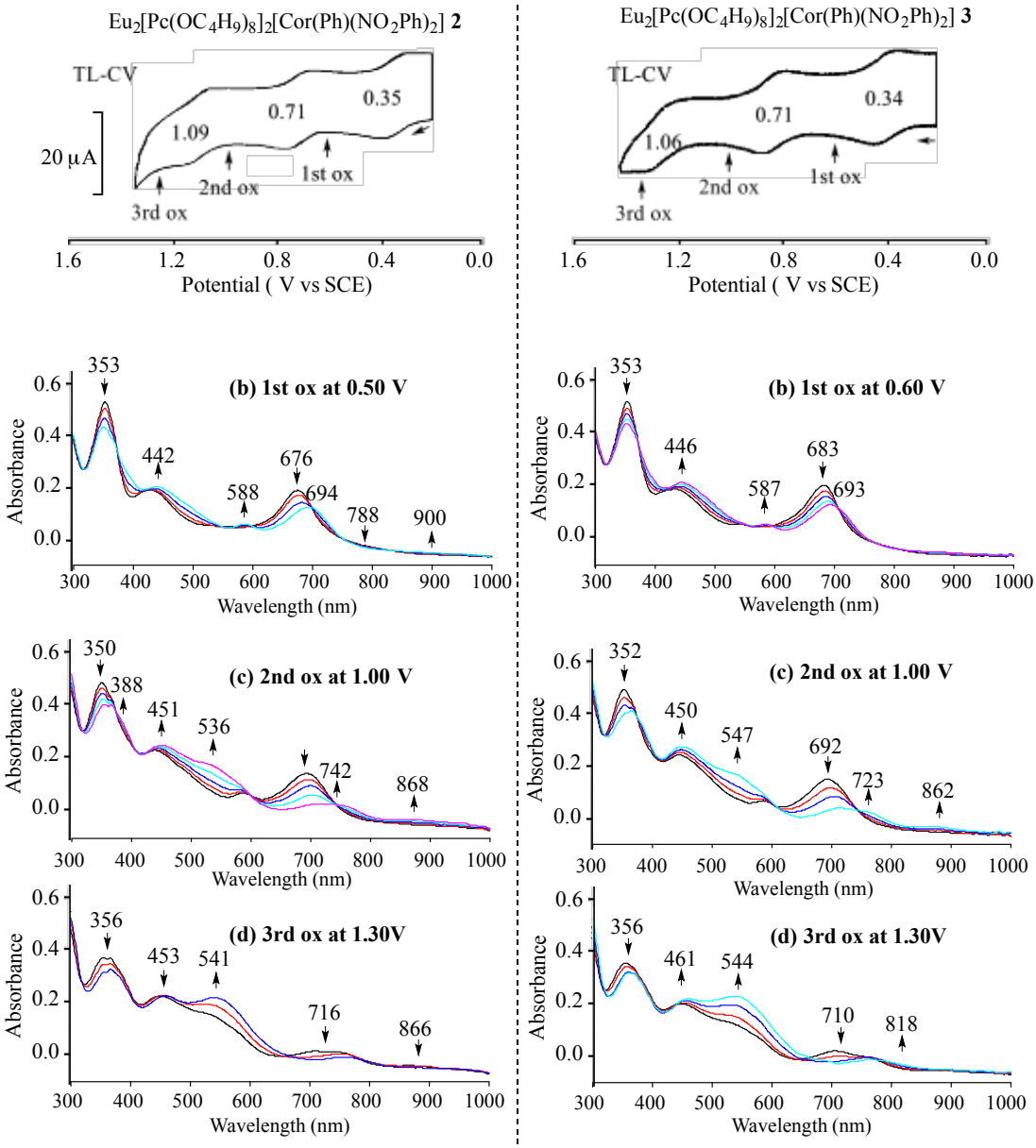

Figure 7-13. Thin-layer cyclic voltammograms of **2** (left) and **3** (right) in PhCN containing 0.1 M TBAP and UV-vis spectral changes during the first three one-electron controlled potential oxidations.

The second oxidation of **1-4** was assigned on the basis of the linear free-energy relationships in Figures 7-6 and 7-14 as occurring predominantly at the Pc ligands and the same conclusion can be reached by the significant loss in intensity of the Q band during the second oxidation of compound **1** (Figure 7-13), compound **2** (Figure 7-13a) and compound **3** (Figure 7-13b). The Q band of these triple-decker compounds as well as the band at ~350 nm are both further reduced in intensity after the third oxidation and this reaction can also be assigned as occurring at the Pc macrocycles of **1-4** on the basis of these changes.

In summary, a new series of europium triple-decker complexes containing two phthalocyanine and one nitrophenyl-substituted corrole macrocycle was synthesized and characterized by spectroscopic and electrochemical methods in three different nonaqueous solvents. One of the compounds was also structurally characterized. The investigated compounds can be reversibly oxidized in five one-electron transfer steps and they can also be reduced in 3-5 one-electron transfer steps, giving triple-decker complexes in up to eleven different oxidation states. The potentials for oxidation and reduction will depend upon the number and nature of substituents on both the corrole and phthalocyanine macrocycles. In this paper, we have only investigated substituent effects related to the corrole but new compounds with different phthalocyanine substituents are also possible and will be considered in future studies.

7.3 References

(1) Buchler, J. W.; Ng, D. K.P. In *The Porphyrin Handbook*, Kadish, K. M.; Smith, K. M.; Guilard, R., Eds.; Academic Press: San Diego, **2000**, *3*, 245-294.

(2) Weiss, R.; Fischer, J. In *The Porphyrin Handbook*; Kadish, K. M.;Smith, K. M.; Guilard, R., Eds.; Academic Press: San Diego, **2003**, *16*, 171-246.

(3) Jiang, J.; Ng, D. K. P. *Acc. Chem. Res.* **2009**, *42*, 79-88.

(4) Bian, Y.; Zhang, Y.; Ou, Z.; Jiang, J. In *Handbook of Porphyrin Science*; Kadish, K. M.;Smith, K. M.; Guilard, R., Eds.;World Scientific Publishing Co.: Singapore, **2011**, *14*, 249-460.

(5) Bouvet, M.; Gaudillat, P.; Suisse, J.-M. *J. Porphyrins Phthalocyanines* **2013**, *17*, 628-635.

(6) Pushkarev, V. E.; Tomilova, L. G.; Tomilov, Y. V. *Russ. Chem. Rev.* **2008**, *77*, 875 -907.

(7) Kan, J.; Chen, Y.; Qi, D.; Liu, Y.; Jiang, J. *Adv. Mater.* **2012**, *24*, 1755-1758.

(8) Sakaue, S.; Fuyuhiro, A.; Fukuda, T.; Ishikawa, N. *Chem. Commun.* **2012**, *48*, 5337-5339.

(9) Sheng, N.; Zhu, P.-H.; Ma, C.-Q.; Jiang, J.-Z. *Dyes Pigm.* **2009**, *81*, 91-96.

(10) Tanaka, H.; Ikeda, T.; Takeuchi, M.; Sada, K.; Shinkai, S.; Kawai, T. *ACS Nano.* **2011**, *5*, 9575-9582.

(11) Kong, X.; Zhang, X.; Gao, D.; Qi, D.; Chen, Y.; Jiang, J. *Chem. Sci.* **2015**, *6*, 1967-72.

(12) Gao, J.; Lu, G.; kan, J.; Chen, Y.; Bouvet, M. *Sens. Actuators, B* **2012**, *166-167*, 500-507.

(13) Lu, J.; Ma, P.; Zhang, X.; Jiang, J. *Dalton Trans.* **2011**, *40*, 12895-12900.

(14) Lu, G.; Chen, Y.; Zhang, Y.; Bao, M.; Bian, Y.; Li, X.; Jiang, J. *JACS.* **2008**, *130*, 11623-11630.

(15) Gross, T.; Chevalier, F.; Lindsey, J. S. *Inorg. Chem.* **2001**, *40*, 4762-4774.

(16) Gao, D.; Zhang, X.; Kong, X.; Chen, Y.; Jiang, J. *ACS Appl. Mater. Interfaces* **2015**, *7*, 2486-2493.

(17) Gao, D.; Zhang, X.; Luan, J.; Chen, Y. *Inorg. Chem. Commun.* **2015**, *54*, 50-53.

(18) Chen, Y.; Su, W.; Bai, M.; Jiang, J.; Li, X.; Liu, Y.; Wang, L.; Wang, S. *JACS.* **2005**, *127*, 15700-15701.

(19) Kan, J.; Wang, H.; Sun, W.; Cao, W.; Tao, J.; Jiang, J. *Inorg. Chem.* **2013**, *52*, 8505 -8510.

(20) Morita, T.; Katoh, K.; Breedlove, B. K.; Yamashita, M. *Inorg. Chem.* **2013**, *52*, 13555

-13561.

(21) Lysenko, A. B.; Malinovskii, V. L.; Padmaja, K.; Wei, L.; Diers, J. R.; Bocian, D. F.; Lindsey, J. S. *J. Porphyrins Phthalocyanines* **2005**, *9*, 491-508.

(22) Chabach, D.; De Cian, A.; Fischer, J.; Weiss, R.; Bibout, M. E. M. *Angew. Chem., Int. Ed. Engl.* **1996**, *35*, 898-899.

(23) Katoh, K.; Asano, R.; Miura, A.; Horii, Y.; Morita, T.; Breedlove, B. K.; Yamashita M. *Dalton Trans.* **2014**, *43*, 7716-7725.

(24) Huang, W.; Xiang, H.; Gong, Q.; Huang, Y.; Huang, C.; Jiang, J. *Chem. Phys. Lett.* **2003**, *374*, 639-644.

(25) Zhu, P.; Pan, N.; Ma, C.; Sun, X.; Arnold, D. P.; Jiang, J. *Eur. J. Inorg. Chem.* **2004**, 518-523.

(26) Sun, X.; Li, R.; Wang, D.; Dou, J.; Zhu, P.; Lu, F.; Ma, C.; Choi, C.-F.; Cheng, D. Y. Y.; Ng, D. K. P.; Kobayashi, N.; Jiang, J. *Eur. J. Inorg. Chem.* **2004**, 3806-3813.

(27) Sun, X.; Cui, X.; Arnold, D. P.; Choi, M. T. M.; Ng, D. K. P.; Jiang, J. *Eur. J. Inorg. Chem.* **2003**, 1555-1561.

(28) Gryko, D.; Li, J.; Diers, J. R.; Roth, K. M.; Bocian, D. F.; Kuhr, W. G.; Lindsey, J. S. *J. Mater. Chem.* **2001**, *11*, 1162-1180.

(29) Li, J.; Gryko, D.; Dabke, R. B.; Diers, J. R.; Bocian, D. F.; Kuhr, W. G.; Lindsey, J. S. *J. Org. Chem.* **2000**, *65*, 7379-7390.

(30) Padmaja, K.; Youngblood, W. J.; Wei, L.; Bocian, D. F.; Lindsey, J. S. *Inorg. Chem.* **2006**, *45*, 5479-5492.

(31) Schweikart, K.-H.; Malinovskii, V. L.; Yasseri, A. A.; Li, J.; Lysenko, A. B.; Bocian, D. F.; Lindsey, J. S. *Inorg. Chem.* **2003**, *42*, 7431-7446.

(32) Martynov, A. G.; Zubareva, O. V.; Gorbunova, Y. G.; Sakharov, S. G.; Nefedov, S. E.; Dolgushin, F. M.; Tsivadze, A. Y. *Eur. J. Inorg. Chem.* **2007**, 4800-4807.

(33) Birin, K. P.; Gorbunova, Y. G.; Tsivadze, A. Y. *Dalton Trans.* **2012**, *41*, 9672-9681.

(34) Lei, S.-B.; Deng, K.; Yang, Y.-L.; Zeng, Q.-D.; Wang, C.; Jiang, J.-Z. *Nano Lett.* **2008**, *8*, 1836-1843.

(35) Lu, J.; Deng, Y.; Zhang, X.; Kobayashi, N.; Jiang, J. *Inorg. Chem.* **2011**, *50*, 2562-2567.

(36) Lu, G.; Yan, S.; Shi, M.; Yu, W.; Li, J.; Zhu, W.; Ou, Z.; Kadish, K. M. *Chem. Commun.* **2015**, *51*, 2411-2413.

(37) Paolesse, R. In *The Porphyrin Handbook*; Kadish, K. M.; Smith, K. M.; Guilard, R., Eds.; Academic Press: San Diego, **2000**; *2*, pp201-232.

(38) Erben, C.; Will, S.; Kadish, K. M. In *The Porphyrin Handbook*; Kadish, K. M.; Smith, K. M.; Guilard, R., Eds.; Academic Press: San Diego, **2000**; *2*, 233−300.

(39) Lu, G.; Li, J.; Yan, S.; Zhu, W.; Ou, Z.; Kadish, K. M. *Inorg. Chem.* **2015**, *54*, 5795-5805.

(40) Lu, G.; Li, J.; Yan, S.; He, C.; Shi, M.; Zhu, W.; Ou, Z.; Kadish, K. M. *Dyes Pigm.* **2015**, *121*, 38-45.

(41) Gryko, D. T. *Eur. J. Org. Chem.* **2002**, 1735-1743.

(42) Stefanelli, M.; Nardis, S.; Tortora, L.; Fronczek, F. R.; Smith, K. M.; Licoccia, S.; Paolesse, R. *Chem. Commun.* **2011**, *47*, 4255-4257.

(43) Steene, E.; Wondimagegn, T.; Ghosh, A. *J. Phys. Chem. B* **2001**, *105*, 11406-13.

(44) Ghosh, A.; Steene, E. *J. Inorg. Biochem.* **2002**, *91*, 423-436.

(45) Pacholska, E.; Espinosa, E.; Guilard, R. *Dalton Trans.* **2004**, 3181-3183.

(46) Teo, R. D.; Gray, H. B.; Lim, P.; Termini, J.; Domeshek, E.; Gross, Z. *Chem. Commun.* **2014**, *50*, 13789-13792.

(47) Gross, Z. *JBIC, J. Biol. Inorg. Chem.* **2001**, *6*, 733-738.

(48) Nardis, S.; Cicero, D. O.; Licoccia, S.; Pomarico, G.; Berionni Berna, B.; Sette, M.; Ricciardi, G.; Rosa, A.; Fronczek, F. R.; Smith, K. M.; Paolesse, R. *Inorg. Chem.* **2014**, *53*, 4215-4227.

(49) Aviv-Harel, I.; Gross, Z. *Chem. - Eur. J.* **2009**, *15*, 8382-8394.

(50) Flamigni, L.; Gryko, D. T. *Chem. Soc. Rev.* **2009**, *38*, 1635-1646.

(51) Aviv-Harel, I.; Gross, Z. *Coord. Chem. Rev.* **2011**, *255*, 717-736.

(52) Liu, H.-Y.; Mahmood, M. H. R.; Qiu, S.-X.; Chang, C. K. *Coord. Chem. Rev.* **2013**, *257*, 1306-1333.

(53) Paolesse, R. *Synlett.* **2008**, 2215-2230.

(54) Thomas, K. E.; Alemayehu, A. B.; Conradie, J.; Beavers, C. M.; Ghosh, A. *Acc. Chem. Res.* **2012**, *45*, 1203-1214.

(55) Buckley, H. L.; Anstey, M. R.; Gryko, D. T.; Arnold, J. *Chem. Commun.* **2013**, *49*, 3104-3106.

(56) Stefanelli, M.; Mandoj, F.; Mastroianni, M.; Nardis, S.; Mohite, P.; Fronczek, F. R.; Smith, K. M.; Kadish, K. M.; Xiao, X.; Ou, Z.; Chen, P.; Paolesse, R. *Inorg. Chem.* **2011**, *50*, 8281-8292.

(57) Nardis, S.; Stefanelli, M.; Mohite, P.; Pomarico, G.; Tortora, L.; Manowong, M.; Chen, P.; Kadish, K. M.; Fronczek, F. R.; McCandless, G. T.; Smith, K. M.; Paolesse, R. *Inorg. Chem.* **2012**, *51*, 3910-3920.

(58) Li, B.; Ou, Z.; Meng, D.; Tang, J.; Fang, Y.; Liu, R.; Kadish, K. M. *J. Inorg. Biochem.* **2014**, *136*, 130-139.

(59) Fang, Y.; Jiang, X.; Ou, Z.; Michelin, C.; Desbois, N.; Gros, C. P.; Kadish, K. M. *J. Porphyrins Phthalocyanines* **2014**, *18*, 832-841.

(60) Lv, W.; Zhu, P.; Bian, Y.; Ma, C.; Zhang, X.; Jiang, J. *Inorg. Chem.* **2010**, *49*, 6628-6635.

(61) Lu, G.; Bai, M.; Li, R.; Zhang, X.; Ma, C.; Lo, P.-C.; Ng, D. K. P.; Jiang,J. *Eur. J. Inorg. Chem.* **2006**, 3703-3709.

(62) Zhang, Y.; Jiang, W.; Jiang, J.; Xue, Q. *J. Porphyrins Phthalocyanines* **2007**, *11*, 100-108.

(63) Zuman, P. *Substituent Effects in Organic Polarography*, **1967**.

(64) Kadish, K.M. Caemelbecke, E. Van, Royal G., in *The Porphyrin Handbook*; Kadish, K. M.; Smith, K. M.; Guilard, R., Eds.; Academic Press, San Diego, **2000**, *8*, 1- 114.

(65) Hansch, C.; Leo, A.; Taft, R. W. *Chem. Rev.* **1991**, *91*, 165-195.

CHAPTER EIGHT

Triple-decker Complexes Containing Phthalocyanine and Porphyrin Macrocycles

8.1 Introduction

As described in Chapter Seven of this dissertation, triple-decker complexes containing tetrapyrrolic phthalocyanine (Pc) and/or porphyrin (Por) macrocycles have been used in applications related to their characteristic properties, which are more than the sum of their compositional parts; examples of applications for these types of compounds include molecular-level information storage,[1-3] field effect transistors,[4-6] and single molecule magnets.[7-11]

Mixed porphyrin/phthalocyanine triple-decker compounds of the type (Pc)Ln(Pc)Ln(Por) are similar to other types of tetrapyrrole triple-decker complexes in that they exhibit a large number of redox states, reversible electrochemistry and relatively low oxidation potentials[12-14] (see also data in Chapter Seven). However, to the best of my knowledge, there have been no reports in the literature which have assigned the probable site of electron transfer for the initial oxidation or reduction of these complexes.

This point is addressed in the current chapter, which describes the electrochemical and spectroscopic properties for a series of newly synthesized triple-decker (Pc)Ln(Pc)Ln(Por) complexes with bulky substituents on the macrocycle, four of which are characterized as to their spectroscopic and electrochemical properties.

Structures of the investigated compounds (**TD-1** to **TD-4**) and corresponding monomers (**7a** and **7b**) and double-deckers (**6a**-**6c**) are shown in Chart 8-1 and were prepared by our collaborator, Dr. Silviu Balaban, from Aix Marseille University in France. By combining spectroscopic and electrochemical methods to characterize the final synthetic products, I am able to discern how the number of undecyl substituents introduced at the meso-positions of the porphyrin ring will influence the electronic absorption spectra, redox potentials, and perhaps also the initial site of electron transfer in the porphyrin-phthalocyanine heteroleptic complexes.

Monomer **7a**, **7b**

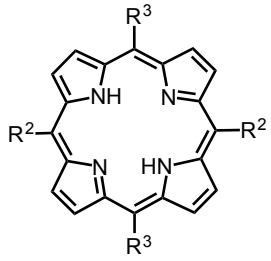

7a-b

7a: R^2 = $-(CH_2)_{10}CH_3$, R^3 = H
7b: $R^2 = R^3 = -(CH_2)_{10}CH_3$

Double-decker **6a-6c**

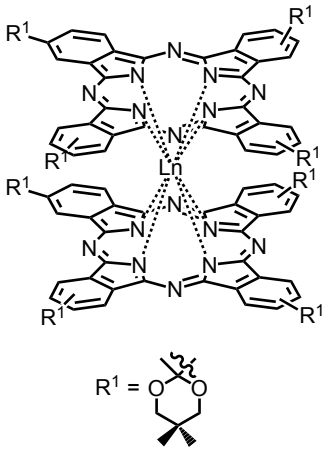

6a: Ln = Gd
6b: Ln = Tb
6c: Ln = Dy

Triple-decker **TD-1**-**TD-4**

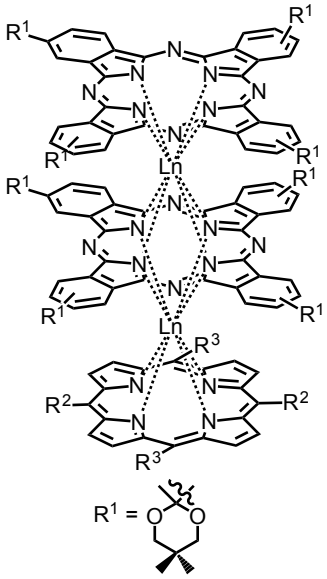

TD-1: Ln = Gd, R^2 = $-(CH_2)_{10}CH_3$, R^3 = H
TD-2: Ln = Gd, $R^2 = R^3 = -(CH_2)_{10}CH_3$
TD-3: Ln = Tb, $R^2 = R^3 = -(CH_2)_{10}CH_3$
TD-4: Ln = Dy, $R^2 = R^3 = -(CH_2)_{10}CH_3$

Chart 8-1. Structures of investigated triple-decker complexes and corresponding monomers and double-deckers.

8.2 Results and Discussion

8.2.1 Electronic Absorption Spectra

Electronic absorption spectra of these triple-decker complexes were recorded in $CHCl_3$ (Figure 8-1) and PhCN, and the salient spectral data are summarized in Table 8-1. The UV-vis absorption characteristics are similar to each other due to their similar molecular structures which are characterized by two phthalocyanines and one porphyrin connected by two lanthanide ions. The strong bands in the region of spectrum at 341-344 and 400-418 nm, are attributed mainly to the Soret bands of the phthalocyanine and the porphyrin macrocycle, respectively. The Q-bands of the compounds at 504-514, 579-585 and 621-636 nm are assigned as arising mainly from the two neighboring Pc ligands in the $[(Pc^{2-})Ln(Pc^{2-})]^-$ part of the molecule. The Q-band absorption at 728-752 nm, is mainly associated with the Pc ligand, together with some contributions from the Por ligand. These wavelengths are very similar to published wavelengths of analogous triple-decker sandwich complexes.[15,16]

Three of the six bands in Figure 8-1 and Table 8-1 vary with the number of *meso* substituents on the porphyrin macrocycle while three do not. The Soret and Q bands at 400-406, 621-631 and 728-752 nm are sensitive to the R^2 and R^3 substituents on the porphyrin ligand, while the three strong bands at 341-343, 506-507 and 579-580 nm are almost independent of these substituents. This can be seen by comparing the spectra shown in Figure 8-1 for **TD-1** and **TD-2**, which differ in the number of *meso*- substituted undecyl groups on the porphyrin macrocycle; **TD-1** has two *meso* undecyl groups while **TD-2** has four. The three bands of **TD-1** at 400, 621 and 728 nm in $CHCl_3$ are shifted to 406, 631 and 735 nm for **TD-2** under the same solution conditions. The same trends in electronic absorption spectra are observed for the triple-decker compounds in PhCN as in $CHCl_3$.

A 15 nm difference in the position of the Soret band is seen in Figure 8-2 between monomeric porphyrin **7a** (λ_{max} = 404 nm) and **7b** (λ_{max} = 419 nm) which are used to synthesize **TD-1** and **TD-2** to **TD-4**, respectively, confirming our assignment of the 400 and

406 nm bands in **TD-1** and **TD-2** as porphyrin-based. Furthermore, similar position of the peaks for **TD-2** and **TD-3** at 343, 406-407, 507-508 and 631 nm in $CHCl_3$ indicate a lack of sensitivity of these bands to the lanthanide metal ions of the compounds, in this case Gd and Dy.

From the above analysis, it is thus possible to assign the 400-418 nm band in $CHCl_3$ as porphyrin-based and all the other bands at 341-344, 506-511 and 579-585, 621-634 and 728-749 nm as phthalocyanine-based. The same assignments can be made for absorption bands of the other investigated compounds in PhCN and, when combined with the data from electrochemistry and spectroelectrochemistry, will provide indirect evidence for the site of oxidation or reduction being predominantly porphyrin or phthalocyanine-centered in a specific redox process.

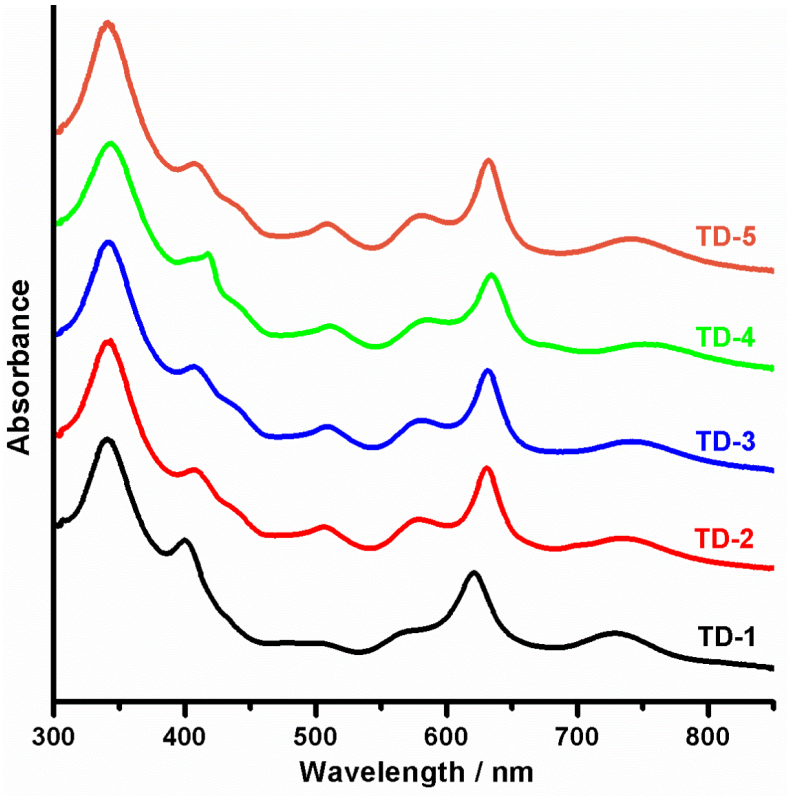

Figure 8-1. Normalized UV-vis absorption spectra of **TD-1**-**TD-5** in CH_3Cl (C = 8.5 x10^{-6}).

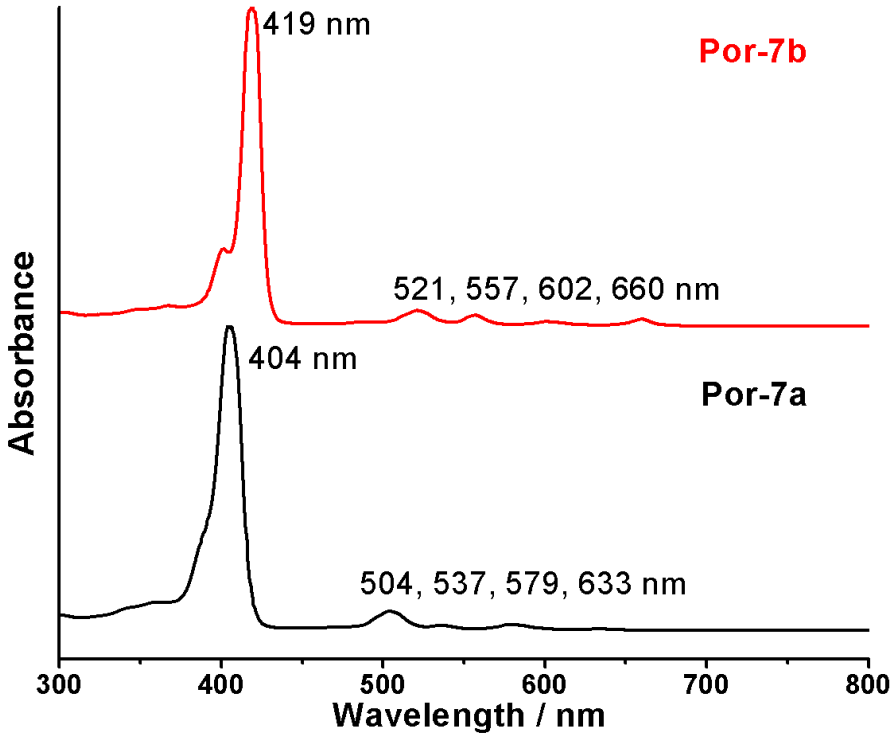

Figure 8-2. Normalized UV-vis absorption spectra of Por-**7a** and Por-**7b** in CH3Cl.

Table 8-1. UV-vis spectra data in $CHCl_3$ and PhCN with assignment of bands to specific macrocycles.

solvent	triple-decker	Ln	λ_{max} / nm (log ε)					
			Pc	**Por**	**Pc**	**Pc**	**Pc**	**Pc**
$CHCl_3$	**TD-1**	**Gd**	341 (5.16)	400 (4.92)	506 (4.33)	580 (4.44)[a]	621 (4.80)	728 (4.43)[a]
	TD-2	**Gd**	343 (5.20)	406 (4.86)	507 (4.55)	579 (4.60)	631 (4.87)	735 (4.43)[a]
	TD-3	**Tb**	343 (5.18)	407 (4.86)	508 (4.45)	581 (4.59)	631 (4.85)	742 (4.39)[a]
	TD-4	**Dy**	344 (5.21)	418 (4.93)	511 (4.58)	584 (4.63)	634 (4.86)	749 (4.41)[a]
	TD-5	**Tb**	341 (5.23)	407 (4.87)	509 (4.59)	581 (4.64)	632 (4.90)	741 (4.45)[a]
PhCN	**TD-1**	**Gd**	343 (5.02)	402 (4.79)	504 (4.18)	581 (4.27)[a]	622 (4.64)	734 (4.22)[a]
	TD-2	**Gd**	343 (5.08)	410 (4.95)	513 (4.47)	582 (4.49)	633 (4.75)	744 (4.27)[a]
	TD-3	**Tb**	342 (5.11)	409 (4.81)	514 (4.48)	584 (4.47)	633 (4.74)	745 (4.45)[a]
	TD-4	**Dy**	344 (5.09)	416 (4.77)	514 (4.47)	585 (4.45)	636 (4.71)	752 (4.22)[a]
	TD-5	**Tb**	344 (5.15)	410 (4.85)	511 (4.56)	583 (4.59)	634 (4.80)	745 (4.41)[a]

[a]Broad band

8.2.3 Electrochemistry

The electrochemical behavior of **TD-1-TD-4** was studied by cyclic voltammetry (CV) in PhCN containing 0.1 M TBAP (Figure 8-3). Under these conditions, each compound exhibits four one-electron oxidations and three one-electron reductions. Each redox reaction is reversible and attributed to a ligand-based process. The measured half-wave potentials are listed in Table 8-2 along with $E_{1/2}$ values taken from the literature for reduction and oxidation of three types of triple-decker complexes, one having the macrocyclic arrangement of (a) Pc-M-Pc-M-Por,[17] another (b) Pc-M-Pc-M-Pc (or $M_2(Pc)_3$)[18] and the third (c) Por-M-Por-M-Por (or $M_2(Por)_3$ where Por = OEP).[19] A schematic illustration for structures of these compounds is given in Figure 8-4.

It was expected that the earlier published data on the Pc-M-Pc-Por compounds[17] would be similar to that of the related heteroleptic Pc-M-Pc-Por complexes investigated in the present study, while quite different behavior was expected to occur for the triple-decker homoleptic compounds having only Pc or Por macrocycles, as shown by the structures in Figure 8-4. This is indeed the case, as seen from the table of redox potentials in Table 8-2.

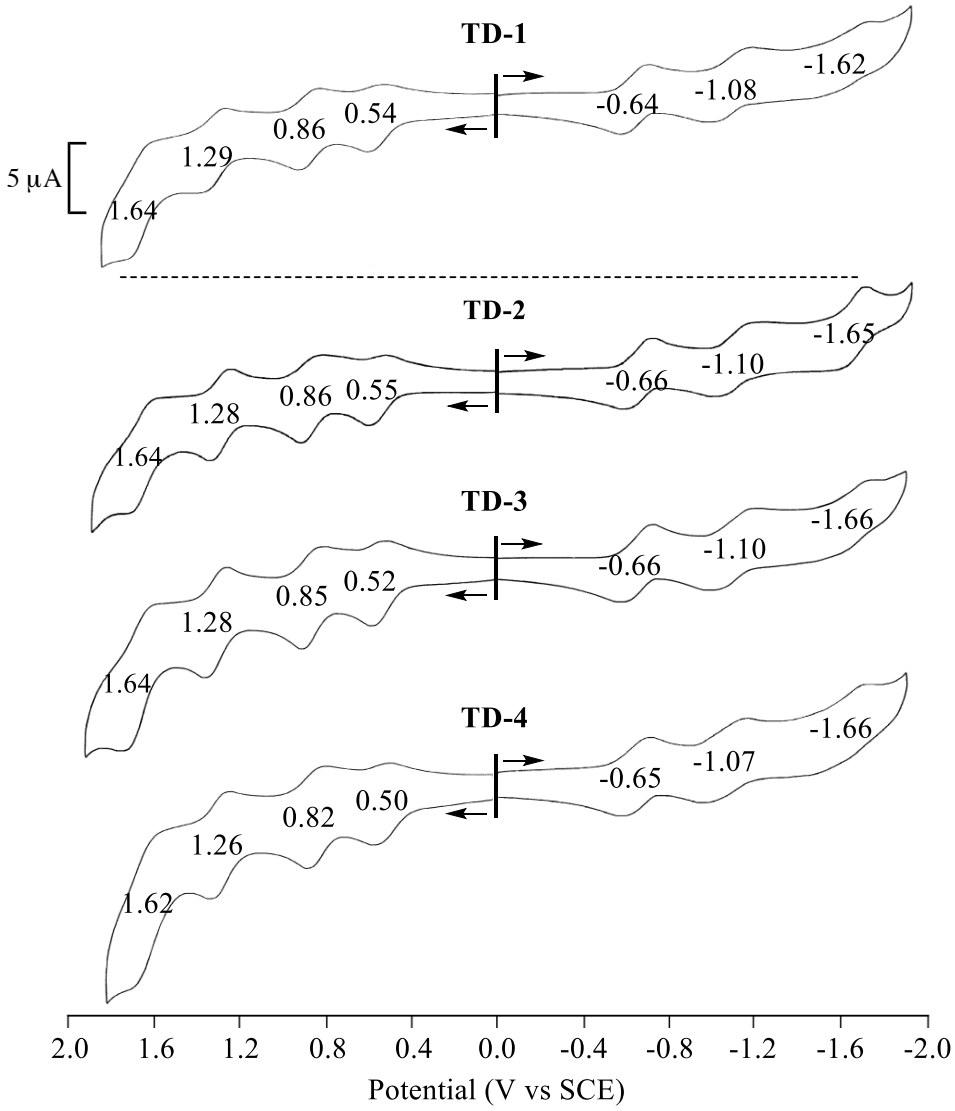

Figure 8-3. Cyclic voltammograms of triple-decker complexes **TD-1** to **TD-4** in PhCN, 0.1 M TBAP.

Table 8-2. Half-wave potentials and assignment of site of electron transfer for reduction and oxidation of **TD-1**-**TD-4** in PhCN and **TD-6**-**TD-14** in CH_2Cl_2 (Data from this work are good to ±10 mV).

		oxidation					**reduction**					
Cpd #	**Compound**	5th	4th	3rd	2nd	1st	1st	2nd	3rd	4th	**H-L gap**	**Ref**
						Pc	**Pc**	**Pc**	**Pc**	**Por**		
TD-1	(Pc)Gd(Pc)Gd(Por)		1.65	1.30	0.86	0.54	-0.64	-1.08		-1.65	**1.18**	*tw*
TD-2	(Pc)Gd(Pc)Gd(Por)		1.63	1.28	0.87	0.54	-0.66	-1.10		-1.65	**1.20**	*tw*
TD-3	(Pc)Tb(Pc)Tb(Por)		1.61	1.26	0.82	0.50	-0.65	-1.06		-1.66	**1.15**	*tw*
TD-4	(Pc)Dy(Pc)Dy(Por)		1.65	1.28	0.85	0.52	-0.66	-1.10		-1.66	**1.18**	*tw*
TD-6	(Pc)Gd(Pc)Gd(Por)	1.93	1.61	1.40	0.93	0.47	-0.64	-1.11	-1.48	-1.70	**1.11**	17
TD-7	(Pc)Tb(Pc)Tb(Por)	1.93	1.61	1.41	0.91	0.44	-0.65	-1.09	-1.52	-1.76	**1.09**	17
TD-8	(Pc)Dy(Pc)Dy(Por)	1.93	1.61	1.42	0.91	0.44	-0.64	-1.09	-1.48	-1.74	**1.08**	17
TD-9	(Pc)Gd(Pc)Gd(Pc)		1.60	1.21	0.67	0.32	-0.71	-1.06	-1.42		**1.03**	18
TD-10	(Pc)Tb(Pc)Tb(Pc)		1.60	1.22	0.66	0.30	-0.70	-1.04	-1.38		**1.00**	18
TD-11	(Pc)Dy(Pc)Dy(Pc)		1.61	1.22	0.64	0.29	-0.68	1.03	-1.38		**0.97**	18
TD-12	$[Eu_2(OEP)_3]$		1.55	1.16	0.59	0.13[a]				-1.68	**1.81**	19
TD-13	$[La_2(OEP)_3]$		1.45	1.10	0.65	0.25[a]				-1.67	**1.92**	19
TD-14	$[Ce_2(OEP)_3]$		1.36	1.06	0.64	0.19[a]				-1.67	**1.86**	19

[a]First reduction is not Pc-based for $[M_2(OEP)_3]$, where M = Eu, La, Ce

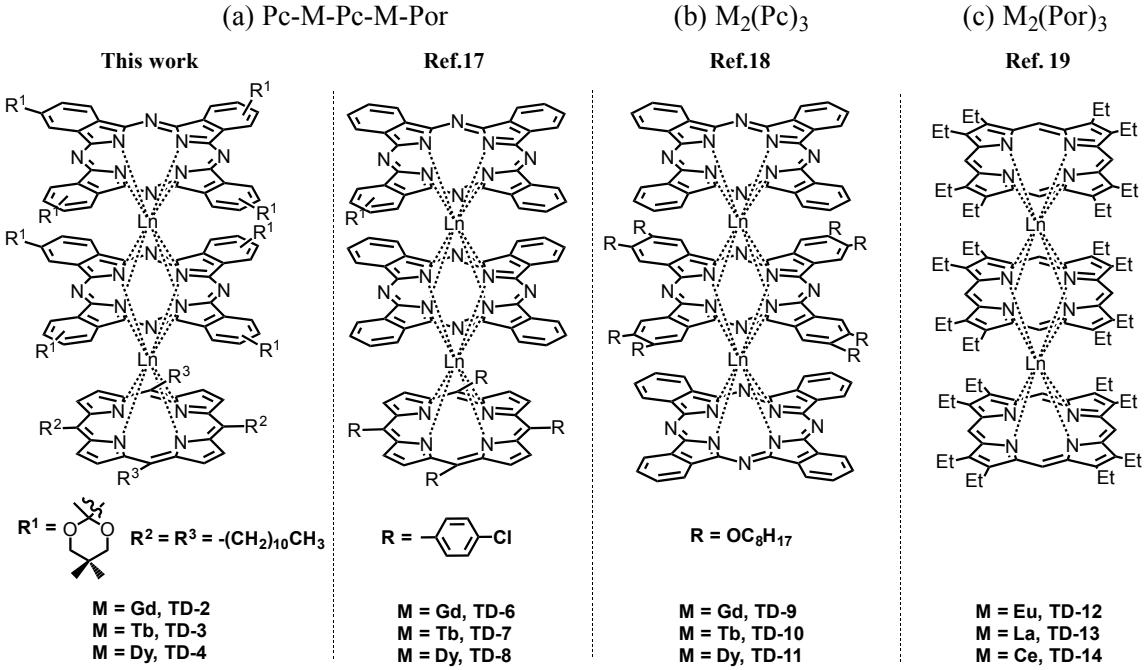

Figure 8-4. Structures for four groups of triple-decker complexes, one from this work and three from the literature. The measured redox potentials are given in Table 8-2.

The reduction of monomeric phthalocyanines[20] is significantly easier than the reduction of monomeric porphyrins[21] having the same central metal ions, and the same trend is observed when comparing compounds in the series of homoleptic triple-deckers, $M_2(Pc)_3$ and $M_2(Por)_3$. For example, the three derivatives of $M_2(OEP)_3$ undergo just a single one-electron reduction in CH_2Cl_2 at $E_{1/2}$ = -1.67 or -1.68 V vs SCE[19], while the three $M_2(Pc)_3$ complexes[14] exhibit three one-electron reductions within the same potential range, the first at $E_{1/2}$ = -1.38 to -1.42 V vs SCE, as seen in Table 8-2.

The first two reductions of $M_2(Pc)_3$ (compounds **TD-9** to **TD-11**) have almost identical $E_{1/2}$ values as the first two reductions of compounds in the two series of Pc-M-Pc-M-Por (**TD-1** to **TD-4** and **TD-6** to **TD-8**) which are reduced at $E_{1/2}$ = -0.64 to -0.66 V in the first step and $E_{1/2}$ = -1.06 to -1.11 V in the second. The potentials for these two reductions are virtually identical in each case, independent of the solvent (PhCN or CH_2Cl_2) or macrocyclic substituents, providing clear evidence for the site of the first two one-electron transfers being located at one or both of the Pc macrocycles in all three series of compounds.

The difference in potentials between the first oxidation of monomeric porphyrins and monomeric phthalocyanines with the same central metal ion is not as great as for reductions and thus one cannot easily assign the site of electron transfer for the first oxidation of the monomeric macrocycles based just on $E_{1/2}$ values alone.[20, 21] The same is true for the triple-decker compounds where the first oxidation of the $M_2(OEP)_3$ derivatives (**TD-12**, **TD-13** and **TD-14**) is much easier than the first oxidation of the $M_2(PC)_3$ species (**TD-9**, **TD-10** and **TD-11**), i.e., 0.13 to 0.25 V vs. 0.29 to 0.32 V. However, smaller differences are observed when comparing $E_{1/2}$ values for the second, third and fourth one-electron abstractions from triple-decker compounds in the series of M_2Pc_3, (**TD-9** to **TD-11**) with those of $M_2(OEP)_3$ (**TD-12** to **TD-14**).

On the other hand, it should be noted that $E_{1/2}$ values for the first oxidation of **TD-1** to **TD-4** are similar to half-wave potentials for the first oxidation of **TD-6**, **TD-7** and **TD-8**, and all

of these values are much more positive than $E_{1/2}$ values for the first oxidation of the three previously investigated $M_2(OEP)_3$ compounds, thus possibly suggesting electron abstraction from the Pc ring of **TD-1** to **TD-8**.

Although no significant differences can be seen between $E_{1/2}$ values for the second oxidation of compounds in the $M_2(OEP)_3$ and $M_2(Pc)_3$ series (where $E_{1/2}$ values range from 0.59 to 0.67 V), these potentials are all more negative than $E_{1/2}$ values for the second oxidation of **TD-1** to **TD-8** where half-wave potentials range from 0.82 to 0.93 V.

Also of importance in the current study is a comparison of compounds in the series **TD-1** to **TD-4** with compounds in the series **TD-6** to **TD-8**. As mentioned above, $E_{1/2}$ values for the first two reductions of compounds in the Pc-M-Pc-M-Por series are almost identical to each other while the $E_{1/2}$ values for first oxidation are only slightly more difficult (more positive potential) in the case of **TD-1** to **TD-4** ($E_{1/2}$ = 0.50 to 0.54 V), as compared to **TD-6** to **TD-8** ($E_{1/2}$ = 0.44 to 0.47 V). This difference in potential could be due to the difference substituents on the Pc and/or Por macrocycles.

Other differences are also observed between the two series Pc-M-Pc-M-Por compounds. As seen in Table 8-2, the earlier studied triple-decker compounds are characterized by four reductions while **TD-1** to **TD-4** undergo only three reductions within the same potential range. The last reduction of **TD-1** to **TD-4** is assigned as occurring primarily on the porphyrin macrocycle by virtue of the half-wave potential for this process which is almost identical to the $E_{1/2}$ value as for the single one-electron reduction of the three $M_2(OEP)_3$ complexes, namely, -1.65 to -1.68 V, as seen in the table. This assignment of a porphyrin-centered reduction in **TD-1** to **TD-4** is consistent with an electron addition to an unreduced porphyrin macrocycle, assuming that the doubly reduced triple-decker compounds contain two Pc macrocyclic ligands.

Finally, it should be noted that half-wave potentials for the fourth oxidation of **TD-1** to **TD-4** are exactly the same as $E_{1/2}$ values for the fourth oxidation of not only **TD-6** to **TD-8**, but

also **TD-8** to **TD-11**, the latter of which must be Pc-based by virtue of the fact that no porphyrin macrocycles are present in the $M_2(Pc)_3$ series of the compounds.

In summary, the above analysis of the electrochemical data is consistent with an initial reduction at one or both of the Pc ligands in **TD-1** to **TD-4** and also with an initial oxidation at one or both of the Pc ligands in the same series of compounds.

In this regard, it should be noted that the experimentally measured HOMO-LUMO gap of **TD-1** to **TD-4** ranges from 1.15 to 1.20 V in PhCN, values which are about 100 mV larger than the HOMO-LUMO gap of **TD-6**, **TD-7** or **TD-8** (1.08 - 1.10 V) and 200 mV larger than the HOMO-LUMO gap for compounds in the $M_2(Pc)_3$ series of compounds **TD-9** to **TD-11**, where $\Delta E_{1/2}$ ranges from 0.97 to 1.03 V, as seen in Table 8-2.

Significantly, however, the HOMO-LUMO gap for the three $M_2(OEP)_3$ compounds (**TD-12** to **TD-14**) ranges from 1.81 to 1.92 V, consistent with a difference in the site of electron transfer between triple-decker derivatives with three OEP macrocycles and those with three Pc macrocycles (**TD-9** to **TD-11**) or with two Pc and one Por macrocycles, as is the case for both series in **TD-1** to **TD-4** and **TD-6** to **TD-8**.

Thin-layer UV-vis spectroelectrochemistry,[22, 23] when combined with assignments of electronic absorption bands for the neutral compounds in the series of complexes (**TD-1** to **TD-4**) was utilized to elucidate and confirm the above-proposed site of electron transfer for the first oxidation and first reduction of the triple-decker compounds. Examples of the spectral changes are given in Figures 8-5 and 8-6 which show UV-vis spectra obtained during the first one-electron oxidation and first one-electron reduction of **TD-2** and **TD-3**, respectively.

For **TD-1**, the band at 406 nm of the neutral compounds is attributed to the porphyrin Soret band, based in part on analysis of electron absorption spectra of the monomeric porphyrin precursor, **7a** or **7b** (Figure 8-2) and in part on previous assignments of the absorption bands in the literature.[24-26] This band in the triple-deckers remained almost unchanged in intensity and position after the first one-electron oxidation at an applied

potential of 0.70 V (Figure 8-5a), which suggested that the first oxidation of **TD-1** is located in large part on one or both of the phthalocyanine macrocycle in the triple-decker compounds. This assignment is also consistent with changes obtained in the phthalocyanine bands of the neutral compound as the reaction proceeds. The bands of the neutral compound at 343, 507 and 578 nm decrease in intensity during the first oxidation, as seen in Figure 8-6a. The Q-band at 626 nm, which is assigned to the Pc macrocycle (see Table 8-1), also decreases significantly in intensity and is replaced by a new band at 667 nm in the one-electron oxidized compound.

Although the porphyrin Soret band of the neutral compound at 406 nm increases slightly in intensity (Figure 8-5b) during reduction, the main spectral changes during the first reduction are attributed to a phthalocyanine-based reaction, based in large part on the fact that the two bands at 343 and 626 nm, which are assigned to the Pc macrocycles, both decrease in intensity. This is consistent with conclusions from the above analysis of the electrochemical data and strongly indicates that one or both phthalocyanine macrocycles are the predominant sites of the first electron addition. Similar spectral changes during the first oxidation and the first reduction are observed for compounds **TD-2** to **TD-4**. One example is given in Figure 8-6 for **TD-2**.

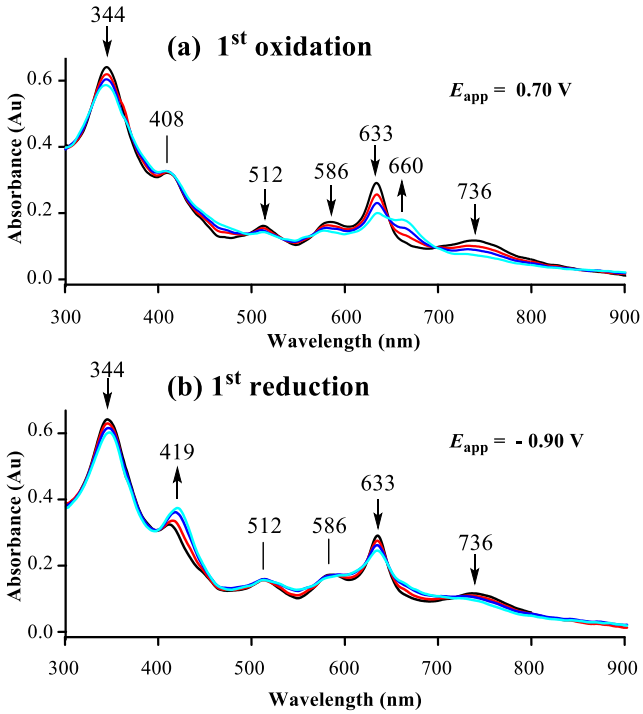

Figure 8-5. UV-vis spectral changes of **TD-2** during controlled potential (a) first oxidation at 0.70 V and (b) first reduction at -0.70 V in PhCN containing 0.1 M TBAP.

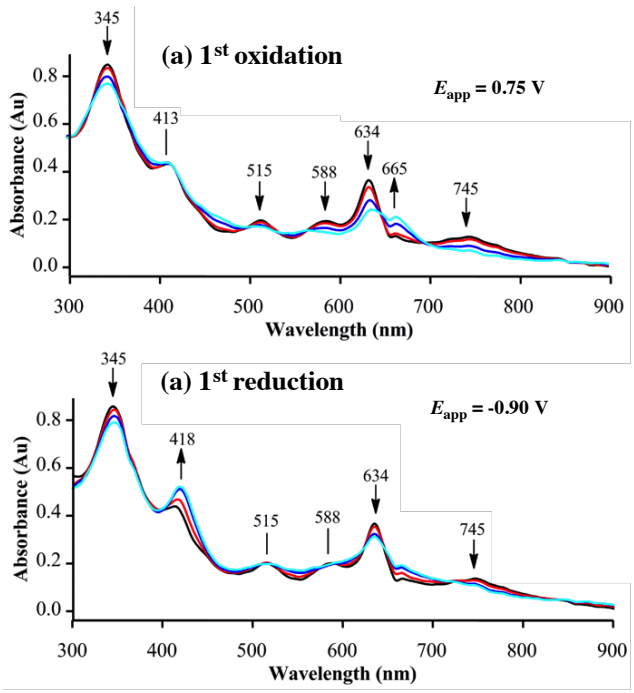

Figure 8-5. UV-vis spectral changes of **TD-3** during controlled potential (a) first oxidation at 0.70 V and (b) first reduction at -0.70 V in PhCN containing 0.1 M TBAP.

In summary, the electrochemical properties of four rare earth heteroleptic porphyrin-phthalocyanine triple-decker complexes with bulky peripheral groups were elucidated by electrochemical and spectroelectrochemical techniques. On the basis of the electronic absorption spectra for the initial compounds and the relative spectral changes during the first oxidation/reduction reaction, the initial site of oxidation or reduction was assigned as porphyrin or phthalocyanine based.

8.3 References

(1) Liu, Z.; Yasseri, A. A.; Lindsey, J. S.; Bocian, D. F. *Science* **2003**, *302*, 1543-1545.

(2) Wei, L.; Padmaja, K.; Youngblood, W. J.; Lysenko, A. B.; Lindsey, J. S.; Bocian, D. F. *J. Org. Chem.* **2004**, *69*, 1461-1469.

(3) Schweikart, K.-H.; Malinovskii, V. L.; Yasseri, A. A.; Li, J.; Lysenko, A. B.; Bocian, D. F.; Lindsey, J. S. *Inorg. Chem.* **2003**, *42*, 7431-7446.

(4) Kong, X.; Zhang, X.; Gao, D.; Qi, D.; Chen, Y.; Jiang, J. *Chem. Sci.* **2015**, *6*, 1967-1972.

(5) Kan, J.; Chen, Y.; Qi, D.; Liu, Y.; Jiang, J. *Adv. Mater.* **2012**, *24*, 1755-1758.

(6) Lu, G.; Chen, Y.; Zhang, Y.; Bao, M.; Bian, Y.; Li, X.; Jiang, J. *JACS.* **2008**, *130*, 11623-11630.

(7) Sakaue, S.; Fuyuhiro, A.; Fukuda, T.; Ishikawa, N. *Chem. Commun.* **2012**, *48*, 5337-5339.

(8) Katoh, K.; Kajiwara, T.; Nakano, M.; Nakazawa, Y.; Wernsdorfer, W.; Ishikawa, N.; Breedlove, B. K.; Yamashita, M. *Chem. Eur. J.* **2011**, *17*, 117-122.

(9) Ishikawa, N.; Iino, T.; Kaizu, Y. *J. Phys. Chem. A* **2003**, *107*, 7879-7884.

(10) Ishikawa, N.; Otsuka, S.; Kaizu, Y. *Angew. Chem. Int. Ed.* **2005**, *44*, 731-733.

(11) Holmberg, R. J.; Polovkova, M. A.; Martynov, A. G.; Gorbunova, Y. G.; Murugesu, M. *Dalton Trans.* **2016**, *45*, 9320-9327.

(12) Schweikart, K.-H.; Malinovskii, V. L.; Diers, J. R.; Yasseri, A. A.; Bocian, D. F.; Kuhr, W. G.; Lindsey, J. S. *J. Mater. Chem.* **2002**, *12*, 808-828.

(13) Lu, J.; Deng, Y.; Zhang, X.; Kobayashi, N.; Jiang, J. *Inorg. Chem.* **2011**, *50*, 2562-2567.

(14) Lu, G.; Li, J.; Jiang, X.; Ou, Z.; Kadish, K. M. *Inorg. Chem.* **2015,** *54*, 9211-9222.

(15) Jin, H.-G.; Balaban, M. C.; Chevallier-Michaud, S.; Righezza, M.; Balaban, T. S. *Chem.Commun.* **2015**, *51*, 11884-11887.

(16) Lu, F.-L.; Mao, Y.-J.; Wang, W.-D.; Xiao, C. *Dyes and Pigments* **2013**, *99*, 686-692.

(17) Sun, X.; Li, R.; Wang, D.; Dou, J.; Zhu, P.; Lu, F.; Ma, C.; Choi, C.-F.; Cheng, D. Y. Y.; Ng, D. K. P.; Kobayashi, N.; Jiang, J. Eur. J. *Inorg. Chem.* **2004**, *19*, 3806-3813.

(18) Zhu, P.; Pan, N.; Li, R.; Dou, J.; Zhang, Y.; Cheng, D. Y.; Wang, D.; Ng, D. K.; Jiang, J. *Chem. Eur. J.* **2005**, *11*, 1425-1432.

(19) Duchowski, J. K.; Bocian, D. F. *J. Am. Chem. Soc.* **1990**, *112*, 8807-8811.

(20) Leznoff, C. C.; Lever, A. B. P. *The Phthalocyanines: Properties and Applications* **1993**; Vol. 3, 1-305.

(21) Kadish, K. M.; Smith, K. M.; Guilard, R.; Editors. *The Porphyrin Handbook*: Vol. 8, Electron Transfer. Academic Press: **2000**; 1-205.

(22) Kaim, W.; Fiedler, J. *Chem. Soc. Rev.* **2009**, *38*, 3373-3382.

(23) Lu, G.; Li, J.; Jiang, X.; Ou, Z.; Kadish, K. M. *Inorg. Chem.* **2015**, *54*, 9211-9222.

(24) Ma, P.; Chen, Y.; Sheng, N.; Bian, Y.; Jiang, J. *Eur. J. Inorg. Chem.* **2009**, *7*, 954-960.

(25) Jiang, J.; Liu,W.; Law, W.-F.; Ng, D. K. P. *Inorg. Chim. Acta.* **1998**, *268*, 49-53.

(26) Zhu, P.; Zhang, X.; Wang, H.; Zhang, Y.; Bian, Y.; Jiang, J. *Inorg. Chem.* **2012**, *51*, 5651-5659.